

ABSTRACT

Title of Thesis: A Methodology for Flammability Diagrams
Joseph Panagiotou, M.S., 2004

Thesis Directed By: Professor James G. Quintiere
Department of Fire Protection Engineering

The current state of fire safety regulations in the United States Department of Transportation is examined, along with some of the associated flammability test methods. The applicability and overall usefulness of these tests is evaluated along with their ability to accurately capture and describe fire performance. Theoretical relationships are shown for the fire phenomena ignition, energy release and flame spread in terms of incident flux to demonstrate the ability to extract meaningful data from calorimetry and flame spread tests. This is done for sample materials to obtain a general overview of their fire performance. This general overview is presented in the form of a Flammability Diagram. A Flammability Diagram is a single plot showing the energy release rate, time to ignition and flame spread rates for a material all as a function of the incident heat flux. Effects of melting, dripping, thickness, sooting and other factors may not be fully described, but the experimental framework captures the overall result of such effects. This study shows the feasibility of developing a measurement methodology that can be followed for the creation of Flammability Diagrams, providing a clear picture of a material's fire performance.

A Methodology for Flammability Diagrams

By

Joseph Panagiotou

Thesis submitted to the Faculty of the Graduate School of the
University of Maryland, College Park, in partial fulfillment
of the requirements for the degree of
Master of Science
2004

Advisory Committee:
Professor James G. Quintiere, Chair
Assistant Professor Andre Marshall
Associate Professor Frederick Mowrer

© Copyright by
Joseph Panagiotou
2004

Acknowledgements

I would like to express my deepest thanks to my advisor Dr. James Quinitere whose help and guidance has been instrumental in this study, and throughout my career as a graduate student at the University of Maryland. In fact without the encouragement from Dr. Quinitere I may not have gotten to this point at all.

I would also like to express my thanks to Dr. Joseph Kolly and the National Transportation Safety Board for supporting me and giving me the opportunity to follow through with the graduate program

Also I would like to thank Dr. Richard Lyons and the Federal Aviation Administration for their generous donation of the materials used in the study. Besides providing materials Dr. Richard Lyons has also always been willing to entertain discussions regarding the project.

I would like to express my thanks to my lab mate Xin Liu for her indispensable help during the development of our “modified” cone calorimeter and the theory behind it.

Last but not least I would like to thank Dr. Frederick Mowrer and Dr. Andre Marshall for being on my committee, and providing me with enlightenment throughout the years of our acquaintance.

Table of Contents

Acknowledgements.....	ii
Table of Contents.....	iii
List of Figures.....	v
Nomenclature.....	ix
Chapter 1: Introduction.....	1
1.1 Background.....	1
1.2 Examples of current flammability test methods.	3
1.3 Objective.....	7
Chapter 2: Experimental Methods and Procedure.....	1
2.1 Sample Materials.	1
2.2 The Cone calorimeter.....	2
2.2.1 Overview of the apparatus and differences from the standard.	2
2.2.2 Sample preparation and test procedure.	5
2.3 The Radiant Heater Apparatus for Flame Spread.....	7
2.3.1 Overview of the apparatus.....	7
2.3.2 Sample preparation and test procedure.....	8
Chapter 3: Physical Observations from Experiment.....	10
3.1 Poly (methyl methacrylate) (PMMA).....	10
3.2 Polyoxymethelene (POM).....	11
3.3 Acrylonitrile butadiene styrene (ABS).....	12
3.4 Polyamide 6,6 (Nylon).....	13
3.5 Polyphenylene sulfide (PPS).....	16
3.6 Polyvinyl Chloride (PVC).....	18
3.7 High-Impact Polystyrene (HIPS).....	18
3.8 High-Density Polyethylene (HDPE).....	19
3.9 Polyvinylidene Fluoride (PVDF).....	20
3.10 Polycarbonate (PC).....	21
3.11 Polyetherimide (PEI).....	22
3.12 Summary of Observations.....	23
Chapter 4: Data Analysis Techniques.....	26
4.1 Cone data analysis.....	26
4.1.1 Time to ignition & Critical Heat Flux.....	26
4.1.2 Energy release rate (\dot{Q}'') & 80% Peak average energy release rate ($\bar{Q}_{80\%}''$)	
.....	27
4.1.3 Mass Loss Rate (\dot{m}'').....	29
4.1.4 Heat of Combustion (Δh_c).....	30
4.1.5 Heat of Gasification (L).....	31

4.1.6 Mass flux at ignition.....	32
4.1.7 Critical Heat Flux for Sustained Burning.....	32
4.2 Flame spread data analysis.....	33
4.2.1 Flame spread velocity.....	35
Chapter 5: Results and Flammability Diagrams.....	37
5.1 Results.....	37
5.2 Flammability Diagrams.....	37
Chapter 6: Conclusions.....	43
Appendix A: Theory of Energy Release Rate.....	46
Appendix B: Test Results for Individual Materials.....	53
B.1 HIPS.....	53
B.2 ABS.....	57
B.3 HDPE.....	61
B.4 PC.....	65
B.5 Nylon.....	68
B.6 PMMA.....	72
B.7 PVC.....	76
B.7 POM.....	80
References.....	84

List of Figures

<u>Figure 1.1.1</u> (Cross modal application of flammability test methods)	2
Figure 1.2.1 (FAA Bunsen burner test)	4
<u>Figure 1.2.2</u> (UL-94 Ratings).....	4
Figure 1.2.3 (ASTM E-162 Radiant panel test).....	6
<u>Figure 1.2.4</u> (ASTM E-648 Flooring radiant panel test)	7
<u>Figure 2.2.1.1</u> (modified Cone calorimeter)	3
<u>Figure 2.2.1.2</u> (Difference in calibration coefficient calculation)	4
<u>Figure 2.2.1.3</u> (The coefficients α and β).....	4
<u>Figure 2.2.2.1</u> (Sample holder, shown with a Lexan sample after a low heat flux test)5	
<u>Figure 2.3.1.1</u> (Flame spread apparatus, shown with heat flux measurement panel in place).....	7
<u>Figure 2.3.2.1</u> (Sample holder for flame spread apparatus, shown with POM sample)9	
<u>Figure 2.3.2.2</u> (Sample ignition for downward flame spread test)	9
<u>Figure 3.1.1</u> (PMMA showing flaming drops and “flowing” flame spread)	11
<u>Figure 3.2.1</u> (POM burning with no external heat flux)	12
<u>Figure 3.2.2</u> (POM showing the effect of flowing in downward flame spread).....	12
<u>Figure 3.3.1</u> (ABS showing increased sooting at lower heat flux levels).....	13
<u>Figure 3.4.1</u> (Nylon skin and bubble formation)	14
<u>Figure 3.4.2</u> (Textured Nylon sample).....	15
<u>Figure 3.4.3</u> (Attempted Nylon test in flame spread apparatus).....	15
<u>Figure 3.5.1</u> (PPS showing the beginning of the bubble formation)	16

<u>Figure 3.5.2</u> (PPS with bubble removed).....	17
<u>Figure 3.5.3</u> (PPS samples exposed to increasing levels of heat flux)	17
<u>Figure 3.5.4</u> (Attempted PPS sample test in the flame spread apparatus)	17
<u>Figure 3.7.1</u> (HIPS showing heavy sooting during upward flame spread).....	19
<u>Figure 3.7.2</u> (HIPS, flowing flame spread seen in downward spread test).....	19
<u>Figure 3.9.1</u> (PVDF original sample and sample from test stopped during flashing period).....	20
<u>Figure 3.9.2</u> (PVDF after long time exposure and charring)	21
<u>Figure 3.10.1</u> (PC showing the formation of a large bubble from testing at $20 \frac{kW}{m^2}$) ...	22
<u>Figure 3.10.2</u> (PC sample manually extinguished during steady burning).....	22
<u>Figure 3.10.3</u> (PC sample after burn out)	22
<u>Figure 3.11.1</u> (PEI after tests at increasing levels of heat flux).....	23
<u>Figure 3.11.2</u> (PEI from unsuccessful flame spread testing).....	23
<u>Figure 3.12.1</u> (Lexan Burning at increasing levels of Heat Flux)	24
<u>Figure 4.1.1</u> (ABS ignition times and critical heat flux).....	27
<u>Figure 4.1.2</u> (Area used to evaluate 80% peak ERR)	28
<u>Figure 4.1.3</u> (Data used in the calculation of an 80% peak average mass loss rate) ..	30
<u>Figure 4.1.5</u> (example calculation of heat of gasification)	31
<u>Figure 4.1.6</u> (location for measurement of mass flux at ignition)	32
<u>Figure 4.2.1</u> (Graphical determination of t^* and $F(t)$)	34
<u>Figure 4.2.2</u> (Correlation of flame spread data to long time heating).....	35
<u>Figure 4.2.3</u> (Example of Flame Spread Velocity Plot).....	36
<u>Figure A.2</u> (Control volume used in energy release rate analysis).....	46

<u>Figure A.2</u> (Parameter α as a function of carbon to hydrogen ratio)	50
<u>Figure A.3</u> (Parameter β as a function of carbon to hydrogen ratio)	50
<u>Figure B.1</u> (Mass loss rate results for HIPS)	54
<u>Figure B.2</u> (Mass loss results for HIPS)	55
<u>Figure B.3</u> (Energy Release Rate results for HIPS).....	56
<u>Figure B.4</u> (Mass loss rate results for ABS)	58
<u>Figure B.5</u> (Mass loss results for ABS)	59
<u>Figure B.6</u> (Energy Release Rate results for ABS).....	60
<u>Figure B.7</u> (Mass Loss Rate results for HDPE).....	62
<u>Figure B.8</u> (Mass Loss results for HDPE)	63
<u>Figure B.9</u> (Energy Release Rate results for HDPE).....	64
<u>Figure B.10</u> (Mass Loss Rate results for PC)	66
<u>Figure B.11</u> (Mass Loss results for PC).....	66
<u>Figure B.12</u> (Energy Release Rate results for PC)	67
<u>Figure B.13</u> (Mass Loss Rate results for Nylon)	69
<u>Figure B.14</u> (Mass Loss results for Nylon).....	70
<u>Figure B.15</u> (Energy Release Rate results for Nylon)	71
<u>Figure B.16</u> (Mass Loss Rate results for PMMA)	73
<u>Figure B.17</u> (Mass Loss results for PMMA)	74
<u>Figure B.18</u> (Energy Release Rate results for PMMA)	75
<u>Figure B.19</u> (Mass Loss Rate results for PVC)	77
<u>Figure B.20</u> (Mass Loss results for PVC).....	78
<u>Figure B.21</u> (Energy Release Rate results for PVC).....	79

<u>Figure B.22</u> (Mass Loss Rate results for POM).....	81
<u>Figure B.23</u> (Mass Loss results for POM).....	82
<u>Figure B.24</u> (Energy Release Rate results for POM).....	83

Nomenclature

I_s	Flame spread index used in ASTM E-162
F_s	Flame spread parameter used in ASTM E-162
Q_s	Heat release parameter used in ASTM E-162
t_{ig}	Time to ignition (assume piloted unless indicated otherwise)
$k\rho c$	Thermal inertia (effective property)
T_{ig}	Surface temperature at ignition
T_o	Initial surface temperature
T_s	Surface temperature
h_t	linearized heat transfer coefficient
\dot{q}_e''	External radiant heat flux
\dot{m}''	Mass flux per unit area
L	Heat of gasification
\dot{Q}''	Energy release rate per unit area
Δh_c	Heat of combustion
δ_f	Difference in flame front position
$\dot{q}_{o,ig}''$	Critical heat flux for ignition
t^*	Time to reach steady state
\dot{q}_∞''	Effective incident heat flux
$F(t)$	Thermal response function
$\dot{m}_{o,ig}''$	Mass flux at ignition
$\bar{Q}_{80\%}''$	80% peak average energy release rate per unit area
$\bar{m}_{80\%}''$	80% peak average mass loss rate per unit area
C	Calibration coefficient used in ASTM E-1354
ΔP	Differential pressure
T_e	Exhaust gas temperature
$X_{O_2}^0$	Baseline oxygen concentration
X_{O_2}	Oxygen concentration

Chapter 1: Introduction

1.1 Background

When selecting new or alternative materials for applications in the built environment a material's fire performance is a necessary consideration. In the event a material becomes exposed to an ignition source or a fire environment, what will be the extent of the material's involvement and contribution to the outcome of the fire? Will the material ignite and be a factor in the spread of fire, or will its involvement be insignificant? Aside from being a consideration for the initial selection of a material, understanding fire performance is also a key issue for any post fire analysis. The role of materials in the development and survivability of fires has long been recognised and for this reason it is required that the materials selected for use must comply with certain measures of fire performance appropriate for the application. To determine this fire performance materials are put through certain tests, called "Flammability tests". This name is generally accepted by industry, regulatory agencies and most persons in the field with regard to these tests. Strangely, it seems that each industry or regulatory agency requires a different set of tests to evaluate a material's fire performance, so there is a multitude of "Flammability test methods". The reason behind this is that there has been no clear definition of what properties or parameters govern a material's fire performance and consequently there are many different test methods, each one measuring something different. There is no established methodology to give a general description of the material's fire performance under conditions representative of those encountered in a fire. It is ultimately up to the various regulatory agencies to prescribe certain test methods and set the limiting performance criteria for their fire safety regulations. These tests can generally be described as small scale (with a few large scale) screening tests. The general nature of most flammability tests is to benchmark or screen a material's performance under a given exposure condition. The performance criteria are typically determined by adopting the test results of a material chosen to give the measure of acceptable

performance. The results of these tests either classify a material’s performance as belonging to a certain group of materials or they provide some sort of index based result. It should be noted that these results are dependent on the test conditions and generally do not relate to all the exposure conditions that could be encountered in a fire. These singular test results do not give an adequate description of a materials fire performance and in very few cases do they provide parameters that could be used for engineering calculations.

Reviewing the requirements and regulations of the different agencies in the United States Department of Transportation (DOT) it is found that there are approximately 23 different tests used [1,2,3,4], all to assess material flammability (Figure 1.1.1). The number is approximate because one could also include international regulations and test methods to the domain of the US Coast Guard. On the regulatory side of fire safety, the general trend is to attempt to unify or “harmonize” the test methods used among organisations. While this may simplify things from a regulatory standpoint it does not necessarily provide for any improvement in understanding the impact of a material on fire safety. The real issue is what governs fire performance? And are the available tests capable of quantifying this? Do they provide a useful tool for assessing fire performance? Can something else more meaningful be done?

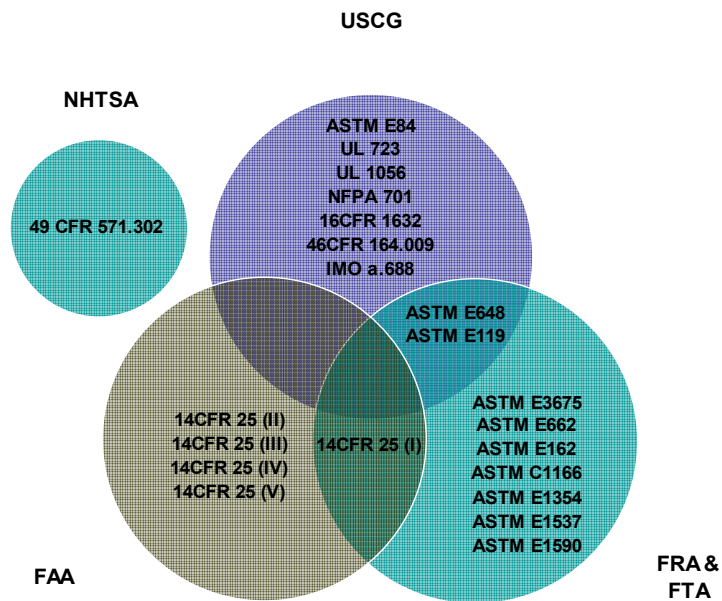


Figure 1.1.1 (Cross modal application of flammability test methods)

Table 1.1.1 (Description of DOT flammability test methods)

Test Name	Description
49 CFR 571.302	Flammability of Interior Materials
46 CFR 164.009	Noncombustible Materials Test
16 CFR 1632	Department of Commerce Standard for Mattress Flammability
14 CFR 25 Part I	Bunsen Burner Tests (Vertical, Horizontal, 45°,60°) for Cabin and Cargo Compartment Materials
14 CFR 25 Part II	Oil Burner Test for Seat Cushions
14 CFR 25 Part III	Oil Burner Test for Cargo Liner
14 CFR 25 Part IV	Modified OSU E-906 Heat Release Rate Apparatus
14 CFR 25 Part V	Smoke Test for Cabin Materials
ASTM E-84	Test Method for Surface Burning Characteristics of Building Materials
ASTM E-648	Test Method for Critical Radiant Flux of Floor-Covering Systems Using a Radiant Heat Energy Source
ASTM E-119	Test Methods for Fire Tests of Building Construction and Materials
ASTM E-3675	Surface Flammability of Materials Using a Radiant Heat Energy Source
ASTM E-662	Test Method for Specific Optical Density of Smoke Generated by Solid Materials
ASTM E-162	Test Method for Surface Flammability of Materials Using a Radiant Heat Energy Source
ASTM C-1166	Test Method for Flame Propagation of Dense and Cellular Elastomeric Gaskets and Accessories
ASTM E-1354	Test Method for Heat and Visible Smoke Release Rates for Materials and Products using an Oxygen Consumption Calorimeter
ASTM E-1537	Test Method for Fire Testing of Upholstered Furniture
ASTM E-1590	Test Method for Fire Testing of Mattresses
IMO a.688	Fire Test Procedures for Ignitability of Bedding Components
UL 723	Surface burning Characteristics of Building Materials
UL 1056	Fire Test for Upholstered Furniture

1.2 Examples of current flammability test methods.

A prime example of the limitations of the standard tests is the family of Bunsen burner tests (Figure 1.2.1). In these tests a sample material is suspended from a holder inside a draft proof chamber and temporarily exposed to a small flame source.

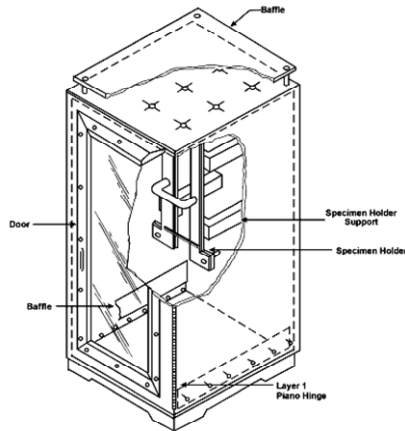


Figure 1-1. Sketch of Vertical Bunsen Burner Test Cabinet

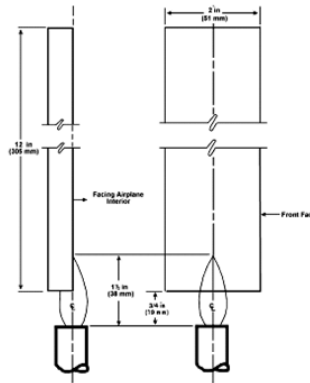


Figure 1-5. Flame Position on Vertical Specimens

Figure 1.2.1 (FAA Bunsen burner test)

There are different variations of the test in which the orientation of the sample or the duration of flame exposure is changed. For example the sample can be vertical, horizontal or inclined on an angle. In all of the cases there is no external heating being applied to the sample. The results given by these tests are in the form of classifications (Figure 1.2.2). Each classification is related to factors such as the distance the flame spread on the sample, the time for the flame to self extinguish after removal of the burner flame, and/or if flaming drips formed.

SURFACE BURN	VERTICAL BURN	HORIZONTAL BURN
Doesn't Ignite Under Hotter Flame	Self Extinguishing	Slow Burn Rating
UL 94 5VA	UL 94 V-0 (Best)	Takes more than
UL 94 5VB	UL 94 V-1 (Good)	3 min. to burn
	UL 94 V-2 (Drips)	4 inches

Figure 1.2.2 (UL-94 Ratings)

The results from these types of tests do not provide a complete description the material's performance and are of little use in an engineering analysis. These tests may determine ignition resistance to a small flame source under ambient conditions, but give no insight to the material's behaviour under any other conditions. Despite this, these tests are used extensively and sometimes exclusively to regulate material

usage. For example, the National Highway Traffic Safety Administration (NHTSA) which is the authority that sets minimum safety standards for new motor vehicles and highway equipment has regulations specifying the usage of the FMVSS 571.302 [5] standard for all materials used inside the passenger compartment of a vehicle. This standard is a horizontal variation of the Bunsen burner test. NHTSA requires all materials in the passenger compartment to have a burning rate of less than 102 mm per minute as determined by the standard. This test just like all other Bunsen burner tests is done without the presence of an external heat flux. The standard says, “The purpose of this standard is to reduce the deaths and injuries to motor vehicle occupants caused by vehicle fires, especially those originating in the interior of the vehicle from sources such as matches or cigarettes” [5]. This test does provide an ignition resistance assessment for a material in ambient conditions exposed to a small ignition source such as matches or a cigarette. The deaths and injuries though generally occur in vehicle crash fires when occupants are trapped inside the vehicle and a fire originates in the engine compartment or in the rear. In these situations there is a developing fire impinging on the passenger compartment and the materials within. This situation is not represented or measurable by the standard test method. The ignition resistance test can give a false sense of safety and be misleading in how the material will react when exposed to a severe fire scenario. NHTSA is not the only organisation using this type of test to qualify materials. The Federal Aviation Administration (FAA) has its own versions of these tests as described in the Code of Federal Regulations [1] (14 CFR 25 Part I). This is not the only test used by the FAA but it is the applicable test for all interior compartment materials. The Federal Railway Administration and Federal Transit Administration [2,3] also use the FAA’s version (14 CFR 25 Part I) of the Bunsen burner test.

Another widely used small scale test method is The ASTM E-162 [6] radiant panel test (Figure 1.2.3).

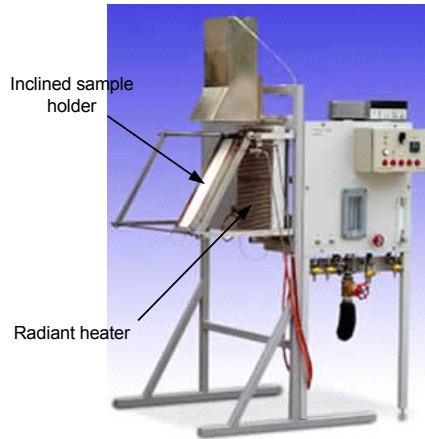


Figure 1.2.3 (ASTM E-162 Radiant panel test)

The intention of this test is to measure material flammability in terms of flame spread. This test uses a radiant panel facing an inclined test specimen. In this configuration the specimen's surface is exposed to a decreasing (from top to bottom) gradient of heat flux. The sample is ignited at the top and the distance and time for the flame front to travel down the sample is measured. From this a flame spread factor F_s is calculated, which is an average flame spread rate down the sample's surface. A heat release factor Q_s is also calculated, which is intended to represent a measure of the peak energy release rate (ERR). With these two factors a flame spread index I_s is generated for the sample.

$$I_s = F_s Q_s \quad (1.1)$$

This result can only rank a material and does not give a useful description of its fire performance. This index can not be used to facilitate any calculation. The test intends to measure fire performance of a material while exposed to an external heat flux and could give insight to the material's behaviour. The end result though is not of much use. More useful data could be obtained from the test apparatus if for example critical flux for upward and downward spread would be measured. Upward and downward flame spread rates as functions of external flux could also be measured with this apparatus. All these things put together could present a more objective or generalized description of the materials fire performance than what is offered by the standard procedure.

Similar to the E-162 test is the ASTM E-648 [7] test for flooring materials. It also uses a radiant panel like the E-162 test but in the horizontal configuration (Figure 1.2.4). The sample is ignited at the high heat flux end and the flame front travels towards the low heat flux end. The point at which the flame spread ceases corresponds to a minimum or critical heat flux for flame spread. Although this measurement does not provide a complete description of the material's fire behaviour, it does provide a sound engineering parameter. This result can be applied to engineering calculations and is not a relic of the test itself. Other such engineering parameters can be found using some of the other existing test methods.

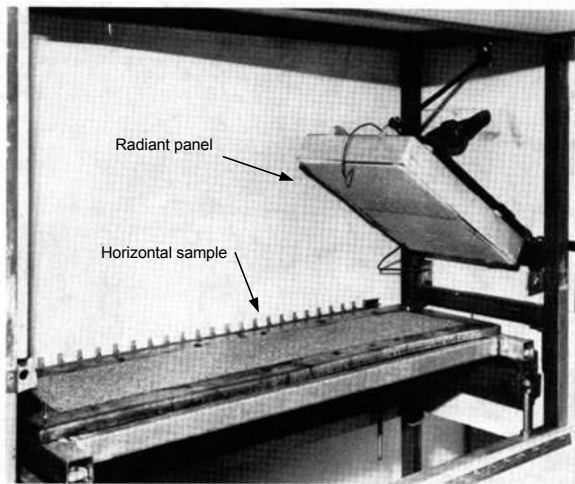


FIG. 2 Flooring Radiant Panel Test Showing Carpet Specimen and Gas Fueled Panel

Figure 1.2.4 (ASTM E-648 Flooring radiant panel test)

1.3 Objective

One would think that the characteristics that would define the flammability of a material should be universal, the multitude of different test methods would indicate otherwise. In spite of the vast number of tests that are available no one test gives a complete picture of the fire performance of the material. Some of the tests are in part a result of the difficulty in having one test that can handle all the physical challenges presented by the diverse materials now in use (ex. melting, deformation, de-

lamination etc). Despite this, fire performance should be measurable in a consistent manner providing there is understanding of what the critical parameters are which drive fire performance. The goal is to demonstrate a framework of flammability testing that would expose in general terms the fire performance of a material.

Because in the initial stages of a fire the most influential parameter is the incident heat flux, it seems logical that the most relevant description of a materials fire performance should be given in terms of incident heat flux.

- Ignition $t_{ig} = \frac{\pi}{4} k \rho c \left(\frac{T_{ig} - T_o}{\dot{q}_{net}''} \right)^2$
- Burning rate $\dot{m}'' = \frac{\dot{q}_{net}''}{L}$
- Energy Release Rate $\dot{Q}'' = \dot{m}'' \Delta h_c = \frac{\dot{q}_{net}''}{L} \Delta h_c$
- Flame spread $v = \frac{\delta_f}{t_{ig}}$

With information like time to ignition, flame spread rate, and energy release rate as functions of heat flux, and along with parameters such as the critical heat fluxes for the ignition and burning processes, flammability diagrams can be drawn to give a more complete picture of a material's fire behaviour. These diagrams show the complete behaviour of a material as a function of heat flux. Previously such diagrams with limited information have been drawn by Quintiere [16]. This approach will also lead to the calculation of properties and parameters that are essential to an engineering analysis. With the availability of these parameters, fire scenarios can be more readily analysed. Some of these parameters are the heat of combustion (Δh_c), thermal inertia ($k\rho c$), and the heat of gasification (L).

The framework for gathering the data necessary to determine a material's flammability will rely on the usage of a Cone calorimeter and a radiant heater apparatus designed to measure flame spread. Since it is possible to vary the level of incident heat flux with both of the apparatuses, multiple data points can be generated for each sample material giving the opportunity to see trends and changes in the

measured parameters. With the exception of flame spread, the Cone is capable of making most of the measurements necessary to evaluate material flammability.

To gain a complete picture of the materials fire behavior, information is also needed about the flame spread rate as a function of heat flux. Experiments to measure flame spread can be done with the ASTM E-1321 [8] “LIFT” apparatus for lateral opposed flow flame spread and the ASTM E-162 [6] apparatus for vertical concurrent and opposed flow flame spread. Both test methods would need slight modification in order to provide a uniform heat flux to the sample’s surface instead of the gradient they are set up to deliver. The uniform heat flux is necessary since the sample needs to reach a steady state, representative of long time heating. Instead of modifying an existing apparatus one was constructed specifically for the tests.

Chapter 2: Experimental Methods and Procedure

2.1 Sample Materials.

The materials used in this study are mainly thermoplastic polymers. The reasoning behind this selection was for the most part availability. The FAA has been conducting a research project involving plastic polymers and generously provided some of their materials for use in this study. Also, the fact that at an increasing rate the built environment contains components made out of such plastics adds to the appeal of using them in the study. These materials can exhibit challenging thermo physical behaviours that make obvious the potential pitfalls of some testing approaches. Such difficulties became immediately apparent while using the Cone calorimeter and also with the flame spread apparatus. For the flame spread apparatus these difficulties made testing all of the available materials not practicable.

The materials used for the study were obtained in sheet form and were cut to the desired sample sizes for each of the two tests. Eleven different plastics (Table 2.1.1) were used for the study, but due to the difficulty encountered with the flame spread apparatus only a few of them were also tested for flame spread. These materials will be the ones with which complete flammability diagrams can be constructed. These materials are listed in table (Table 2.1.2).

Table 2.1.1 (Materials available for the study)

Polymer	Thickness (mm)
Polyphenylene sulfide [PPS]	6.5
Polyvinyl chloride [PVC]	6.1
Polyamide 6,6 [PA66]	6.73
High-Impact Polystyrene [HIPS]	6.14
High-Density Polyethylene [HDPE]	6.35
Polyvinylidene fluoride [PVDF]	6.63
Polyoxymethylene [POM]	6.75
Polycarbonate [PC]	5.35
Poly(methyl methacrylate) [PMMA]	5.35
Acrylonitrile butadiene styrene [ABS]	6.35
Polyetherimide [PEI]	6.85

Table 2.1.2 (Materials used in both the Cone and flame spread apparatus)

Materials	Heat of Combustion (kJ/g)	Critical Heat Flux (kW/m ²)
High Impact Polystyrene [HIPS]	28.8	16
Polyoxymethylene [POM]	13.5	8
Poly(methyl methacrylate) [PMMA]	23.3	8
Acrylonitrile butadiene styrene [ABS]	28.2	12

* values in this table are from the results of this study.

2.2 The Cone calorimeter

The Cone calorimeter, as mentioned in the introduction, was selected as one of the test methods to be used in this study. The Cone calorimeter is an apparatus used primarily to measure the energy release rate of a burning sample material. This is generally done under the influence of an external heat flux provided by a conical heater located just above the sample. The energy release rate is measured by monitoring the amount of oxygen being consumed by the burning sample. The measured oxygen consumption rate is then related to an energy release rate, using a mean heat of combustion per unit mass of oxygen. This mean heat of combustion per unit mass of oxygen has been found to be nearly constant for most materials and so it is used in the measurement of unknown samples also. The oxygen heat of combustion is approximately $13.1 \frac{MJ}{kg_{O_2}}$. The design and use of the Cone calorimeter has been standardized by ASTM in the E-1354 standard [9].

2.2.1 Overview of the apparatus and differences from the standard.

The Cone calorimeter used in this study was a “modified” Cone calorimeter. It was originally an ASTM E-1354 Standard Cone calorimeter [9] made by Atlas/CSI and donated to the University by Bell core in 1995. It has been modified, ultimately in order to put it back into service, but also in an effort to end up with an overall simpler apparatus. The major modification has been to replace all the original wiring and circuitry with a simpler layout and to provide a user interface based on

LabView® and a Fluke® NetDaq® data acquisition system. Physically the Cone has also changed a bit, now that most of the internal circuit boards have been removed and the apparatus has an open frame (Figure 2.2.1.1). Other physical changes are the relocation of the load cell to reduce vibrations and gain signal clarity.



Figure 2.2.1.1 (modified Cone calorimeter)

None of the physical changes have made this Cone cease to comply with the standard's specifications. The calibration and calculation methods are also still in compliance with the standard. There is though one distinction between the standard and the procedure we follow and it has to do with the calibration coefficient. The difference is in the formula used to calculate the calibration coefficient. This is illustrated in Figure 2.2.1.2. The reason for this difference is that the constants indicated in the figure are fuel dependent (Figure 2.2.1.3), and just as we use the heat of combustion specific to methane we should also use the constants that are specific to methane. These constants are the following.

$$\alpha = 1.058 \quad \beta = 1.375 \quad (2.2.1.1)$$

$$\begin{array}{ccc}
 \text{Standard} & & \text{UMD} \\
 \dot{Q} = \frac{\Delta h_c}{r_{O_2}} \left(C \sqrt{\frac{\Delta P}{T_e}} \right) 1.10 \left(\frac{X_{O_2}^o - X_{O_2}}{1.105 - 1.5 X_{O_2}} \right) & & \dot{Q} = \frac{\Delta h_c}{r_{O_2}} \left(C \sqrt{\frac{\Delta P}{T_e}} \right) 1.10 \left(\frac{X_{O_2}^o - X_{O_2}}{1.058 - 1.375 X_{O_2}} \right) \\
 & \swarrow \text{difference} \searrow & \\
 \frac{\Delta h_c}{r_{O_2}} = 12.54 \frac{kJ}{g} \quad (\text{For Methane}) & &
 \end{array}$$

Figure 2.2.1.2 (Difference in calibration coefficient calculation)

$$\begin{array}{c}
 \dot{Q} = \frac{\Delta hc}{r_{O_2}} \left(C \sqrt{\frac{\Delta P}{T_e}} \right) 1.10 \left(\frac{X_{O_2}^o - X_{O_2}}{\alpha - \beta X_{O_2}} \right) \\
 \begin{array}{l}
 r_x \rightarrow \text{Stoichiometric} \\
 \text{ratio of species} \\
 x
 \end{array}
 \begin{array}{l}
 \rightarrow \beta = \frac{r_{CO_2} + r_{H_2O}}{r_{O_2}} \left(\frac{M_{O_2}}{M_{air}} \right) \\
 \rightarrow \alpha = 1 + \frac{Y_{O_2, \infty}}{r_{O_2}}
 \end{array}
 \end{array}$$

Figure 2.2.1.3 (The coefficients α and β)

The ASTM standard [9] uses average values for these constants during calibration and also when testing an unknown sample. For unknown samples we also used the average values indicated by the standard.

Additionally we use a Meeker burner, adjusted to a short premixed flame, for calibration instead of the standard's diffusion burner. The reasoning behind this is to ensure the complete combustion of all the fuel delivered and thus justify using the $50 \frac{kJ}{g}$ heat of combustion for methane as suggested by the standard. This distinction is made because the standard's diffusion burner may not be getting the 100% efficiency implied by using the specified heat of combustion. From Tewarson's chapter in the SFPE Handbook [10] it is seen that the total heat of combustion is $50.1 \frac{kJ}{g}$ and that the chemical heat of combustion is $49.6 \frac{kJ}{g}$. The lower of the two would be more applicable to the standard's diffusion burner. A more detailed account of the

rebuilding and modifications to the cone along with the derivation of the energy release equation and constants therein can be found in Appendix A.

2.2.2 Sample preparation and test procedure.

The samples tested with the Cone calorimeter were cut from bulk sheet to a size of 76mm x 76mm with a nominal thickness of 6.3mm. The exact thicknesses are listed in Table 2.1.1. No sample conditioning was performed since these polymers do not take on moisture from the environment and consequently no drying or special preparation is needed. The samples were stored in the lab at room temperature until the time they were tested.

A sample holder was constructed from 252mm thick Kaowool® refractory ceramic fiber board (Type M). A square piece 15cm x 15cm was used by hollowing out a foot print the size of the sample on the surface of the insulation board. This way the sample would sit in the depression and be flush with the surface of the holder (Figure 2.2.2.1). In order to be able to re use the sample holder, a piece of aluminum foil would be inserted between the holder and the sample as illustrated in the figure.

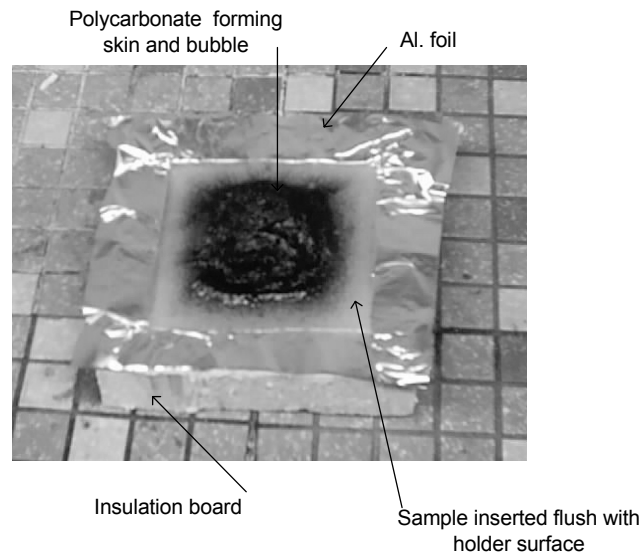


Figure 2.2.2.1 (Sample holder, shown with a Lexan sample after a low heat flux test)

The test procedure's objective was to gather data for each material over a wide range of external heat flux and to determine the critical heat flux for piloted ignition. This began by first testing all the materials over a wide range of external heat flux. The range was from $20 \frac{kW}{m^2}$ to $60 \frac{kW}{m^2}$ in increments of approximately $10 \frac{kW}{m^2}$. With the results of these tests as a guide, each material was then further tested until its critical heat flux for ignition was determined. The cut off point to declare a test as a non ignition was 25 minutes of exposure with no ignition and no indication of imminent change. Ignition also needs to be defined since during the tests, phenomena, such as flashing, temporary ignition or the need for the constant presence of the spark igniter to sustain the flame were sometimes observed. This became problematic especially in the case of materials with fire retardant chemicals (PVDF, PVC) where there were multiple temporary ignitions which could be a few seconds to a minute long. The ignition time was defined to be the time of the ignition which would sustain until burn out of the material. The times that temporary ignitions occurred were also recorded but the sustained ignition time is what was considered time to ignition (t_{ig}).

The information gathered using the Cone is:

1. Time to ignition as a function of incident heat flux $t_{ig} (s)$
2. Critical heat flux for ignition $\dot{q}''_{o,ig} \left(\frac{kW}{m^2} \right)$
3. Peak energy release rate per unit area as a function of heat flux $\dot{Q}'' \left(\frac{kW}{m^2} \right)$
4. Heat of combustion $\Delta h_c \left(\frac{kJ}{g} \right)$
5. Heat of gasification $L \left(\frac{kJ}{g} \right)$

2.3 The Radiant Heater Apparatus for Flame Spread

The apparatus we constructed to measure flame spread as a function of incident heat flux was designed to test in the vertical orientation. With this apparatus upward and downward flame spread rate can be measured.

2.3.1 Overview of the apparatus

The flame spread apparatus uses two propane fuelled, infrared radiant heaters to deliver the incident heat flux to the test sample (Figure 2.3.1.1). The heaters are held fixed in place with a frame and oriented so that the irradiance on the sample is uniform from top to bottom. The sample holder hangs vertically in front of the heaters and can be translated along a track keeping it alignment and maintaining the uniform heat flux. This was verified by inserting a mock up of the sample holder with two Gardon type heat flux gauges embedded in it, one at the top and one at the bottom, into position where the sample holder would go. This was used to both give measure of the magnitude of the incident heat flux at and to verify the uniformity of the incident heat flux distribution. To adjust the incident heat flux either the fuel flow to the heaters was adjusted or the sample holder was moved.

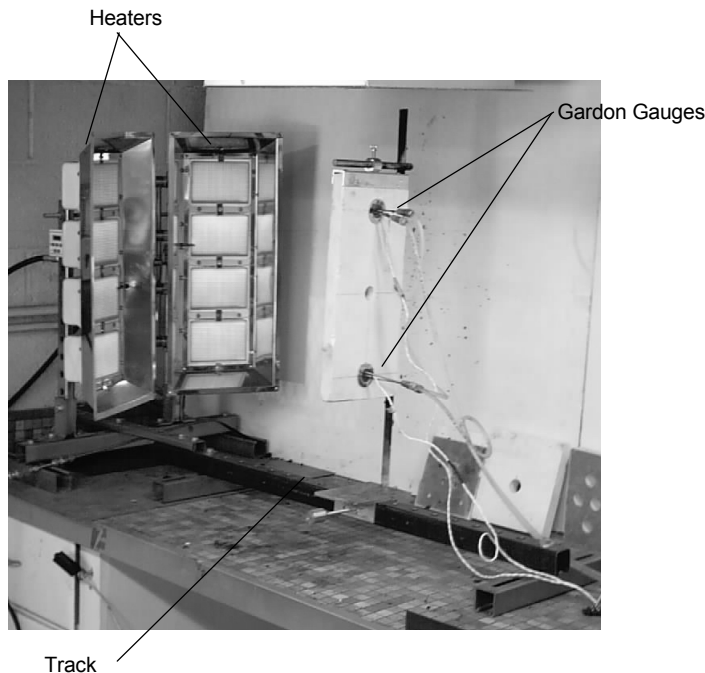


Figure 2.3.1.1 (Flame spread apparatus, shown with heat flux measurement panel in place)

2.3.2 Sample preparation and test procedure.

The sample holder consists of 252mm thick Kaowool® refractory ceramic fiber board (Type M) held by an aluminum frame with a hinged front cover (Figure 2.3.2.1). The front cover is a thin piece of sheet metal with an opening cut out in it. It is held in place in front of the sample, to both secure the sample in place and cover its edges. The opening leaves an exposed sample area of 76mm by 280mm. Along the edge of the sample holder there are marks every 2 cm to aid in recording the flame spread rate. It was attempted to get discrete data for the spread rate but in most instances, especially in upward spread, it was only practical to measure the time to reach the half way mark and the end point. The flame front is the location where the base material is pyrolyzing.

The procedure was to set a certain heat flux level using the Gardon gauges and then to place the sample holder into position in front of the heaters. The sample was left in place to preheat so the surface would reach a steady state temperature. The time required to reach steady state was determined using the ignition data gathered in the Cone calorimeter. This will be explained in the analysis, but overall it involves determining the thermal response of the material to get a measure of the time it takes to reach steady state (t^*). For most of the thermoplastics, leaving them to preheat until steady state resulted in the materials becoming too soft to stay in place for the test. For this reason the samples were heated for a time less than t^* and then the incident heat flux was correlated using the thermal response function for the material (equation 2.3.2). This approach is also described in the ASTM E-1321 standard [8].

$$\dot{q}_{\infty}'' = \dot{q}'' F(t) \quad (2.3.2)$$

After leaving the material in place to heat up for a time as close to t^* as possible it would then be ignited either from the top or bottom depending on the test. The igniter we used was constructed to be like a small ribbon burner so that the whole edge of the sample would be ignited at once (Figure 2.3.2.2). The time and position of the flame front was then recorded using a stop watch and visually noting the flame front position.

The information gathered using this apparatus is:

1. Upward flame spread rate as a function of heat flux (FSR_U)
2. Downward flame spread rate as a function of heat flux (FSR_D)

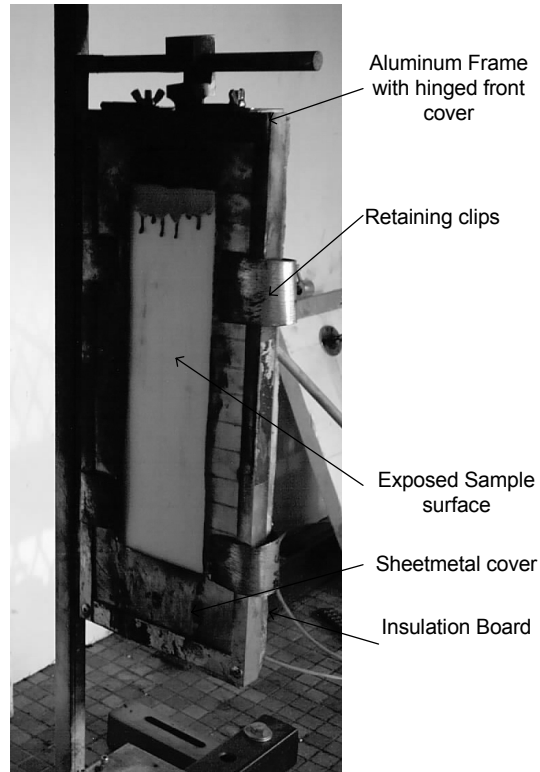


Figure 2.3.2.1 (Sample holder for flame spread apparatus, shown with POM sample)



Figure 2.3.2.2 (Sample ignition for downward flame spread test)

Chapter 3: Physical Observations from Experiment

All of the materials available for the study (Table 2.1.1) were able to be tested in the Cone calorimeter. In the Cone the sample is in the horizontal position, so even if it becomes molten it stays in place. On the contrary in our flame spread apparatus the sample is oriented vertically, and if the sample becomes soft and fluid before decomposition into ignitable gases the experiment can not be carried out. For this reason there is substantially more Cone data than flame spread data gathered in this study. The various polymers used in these tests exhibited some interesting physical behavior that may suggest they undergo different stages of decomposition during the heating and later combustion process. Each one of the materials will be discussed individually in the following subsections.

3.1 Poly (methyl methacrylate) (PMMA)

The PMMA samples did not pose any particular difficulties or display any unexpected behavior when tested in the Cone. When exposed to an external heat flux the sample's surface begins to produce multiple tiny bubbles which start to break releasing fuel vapor. After ignition the burning process continues along the same lines with an increased rate of bubbling. The bubbling covers the entire surface of the sample and resembles a boiling liquid. No residue is left over after burnout.

In the flame spread apparatus where the sample is in the vertical position, PMMA can be difficult to test. After it is preheated and forced to ignite it begins to sag and flow. This accelerates downward spread by causing a molten river of PMMA to flow down the sample's surface carrying the flame along with it. This process is being referred to as "flowing" flame spread. At times this molten PMMA will detach from the surface and form a flaming droplet which falls into the catch pan below (Figure 3.1.1). At times this flowing flame spread behavior can make measuring the location of the flame front difficult. As discussed in the experimental procedure for

the flame spread apparatus, the flame front is considered the location where the base material is also involved.



Figure 3.1.1 (PMMA showing flaming drops and “flowing” flame spread)

3.2 Polyoxymethelene (POM)

The POM samples were also fairly straight forward with a behavior similar to PMMA. Just prior to ignition the entire surface of the sample will erupt with numerous tiny bubbles. With additional heating these bubbles begin to break, releasing fuel and in the presence of the spark igniter ignition follows. The distinguishing characteristic of POM is its short blue flame with virtually no smoke being produced (Figure 3.2.1). Additionally it was the most difficult material in the study to extinguish. When extinguished the vapors coming off of the material are extremely irritating to the eyes and respiratory system.

In the flame spread apparatus POM also tends to melt and drip producing flaming droplets and flowing flame spread. The melt produced by POM appeared to be of very low viscosity. This has the same effect as in the case of PMMA, where in the downwards direction it accelerates the spread rate, and in the upward direction it may slow it down (Figure 3.2.2). The slow down in the upward direction could be attributed to a flow of heat (the molten material) in the direction opposite to the flame spread.



Figure 3.2.1 (POM burning with no external heat flux)



Figure 3.2.2 (POM showing the effect of flowing in downward flame spread)

3.3 Acrylonitrile butadiene styrene (ABS)

ABS was easy to work with in the Cone calorimeter. While being heated the surface color darkens and small bubbles form prior to ignition. These bubbles begin to break which then leads to ignition. ABS burns with a tall bright yellow flame and produces a lot of soot. There was no formation of a “skin” on the surface as with some of the other plastics that will be discussed.

In the flame spread apparatus the behavior of ABS was more troublesome because the soot noticed in the Cone tests now was collecting on the sample's surface during upward flame spread (Figure 3.3.1). In a test with no external heat flux, flame spread stopped in the upward direction because the soot collecting on the sample's surface, above the flame, effectively shielded the uninvolved material. Due to the shielding effect once the area that was forced to ignite at the beginning of the test burnt out, the fire self extinguished. This sample is shown on the left in Figure 3.3.1. Each one of the other samples tested had an external heat flux applied and managed to spread the fire to the top of the sample. At the higher heat flux levels the flame spread rate outruns the soot deposition rate and flame spread does not seem to be affected.

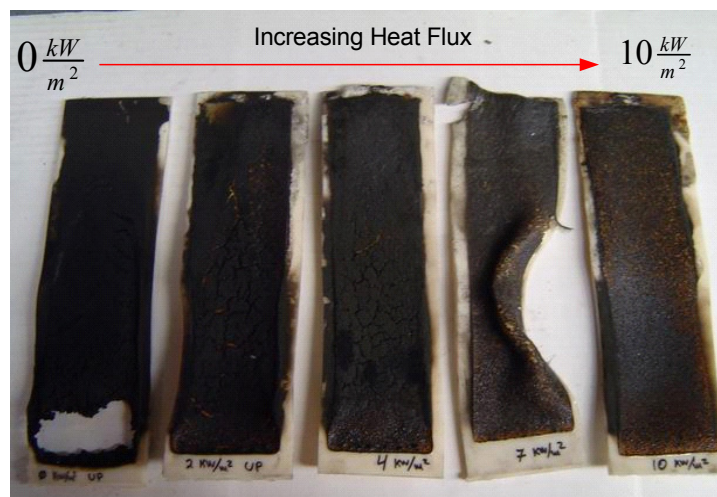


Figure 3.3.1 (ABS showing increased sooting at lower heat flux levels)

3.4 Polyamide 6,6 (Nylon)

Nylon was difficult to test as far as the ignition time and critical heat flux for ignition are concerned. The difficulty with nylon is that during the heating process a skin begins to form over the sample's surface. This skin contains the gases that would be leaving from the sample's surface and results in the formation of a large bubble (Figure 3.4.1). If you were to manually rip the bubble the escaping gases cause ignition in the presence of the spark igniter. In other words if not for the skin, piloted ignition would occur at this time. If you do not tamper with the bubble it

continues to grow until at some point it rips and fuel is vented like a small jet. The bubble does not pop like a balloon, instead a small rip occurs and pressure is relieved. If the igniter happens to be near the location of the vent, ignition occurs. The small flame at the vent either erodes the skin enough to sustain the ignition and slowly spread or the skin reseals itself extinguishing the flame. From this behavior it is hard to justify what exactly the time to ignition should be. It should also be noted that the formation of the skin is dependent on the heating rate of the sample. At high heat flux exposure the skin does not form fast enough and does not impact the ignition process. In the high heat flux case the material begins to outgas combustible fuel before the skin has a chance to fully cover the surface. As the exposure becomes less and less severe the skin begins to have an effect on the ignition. In the low heat flux case the skin forms before any combustible gases begin to evolve so when they are finally produced they become trapped underneath the skin forming a bubble. To see if this skin formation was in part dependent on the surface being smooth we machined a few samples so that the surface had features (Figure 3.4.2). This did not stop the skin from forming over the entire surface of the sample.

When tested in the flame spread apparatus, it was not possible to get a sustained ignition. At the highest level of incident heat flux and with the igniter impinging on the sample it was possible to ignite, but upon removal of the igniter the flame would extinguish. Also the material being forced to ignite would quickly melt and flow down the sample's surface. Again a skin was seen to form (Figure 3.4.3)

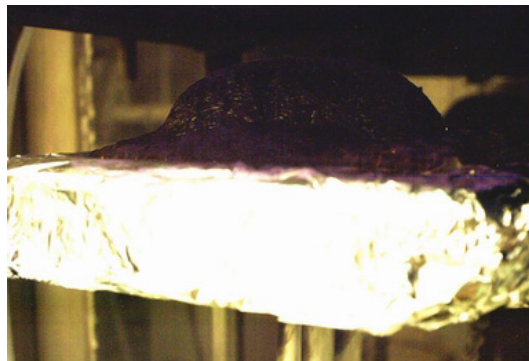


Figure 3.4.1 (Nylon skin and bubble formation)

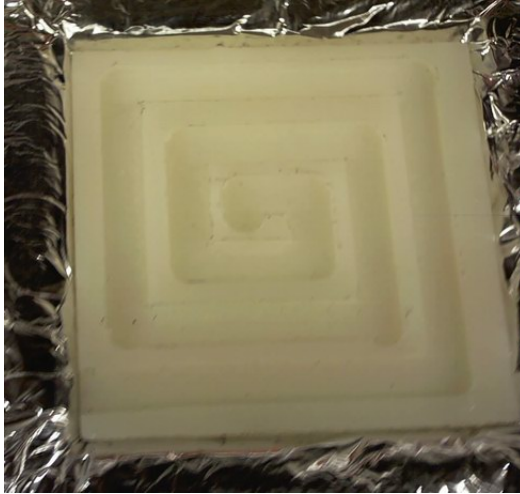


Figure 3.4.2 (Textured Nylon sample)



Figure 3.4.3 (Attempted Nylon test in flame spread apparatus)

3.5 Polyphenylene sulfide (PPS)

PPS was also one of the skin and bubble forming materials. This plastic forms a skin during the heating process. This skin is most likely the result of an oxidation process taking place at the samples surface. This skin formation delays ignition by containing the combustible gases. When the bubble “vents” it is possible to ignite the escaping vapors. For example during a test at $30 \frac{kW}{m^2}$ a bubble formed and began to vent around 9 minutes into the test. These small jets of fuel vapor were temporarily ignitable. The bubble would vent around its base so as it would shrink the vent would seal up. At 19 minutes into the test the gases inside the bubble became so hot that when the bubble would vent the jets of fuel would auto ignite. When the sample became fully involved it resulted in a bubbling and splattering fire, with a smell similar to tar. The molten PPS would essentially boil under the skin and pop expelling flaming droplets.

It was not possible to test PPS in the flame spread apparatus. This was not surprising and was indicated from its performance in the Cone, where PPS was seen to become entirely molten well before any ignition would take place. In the flame spread test after prolonged exposure to the igniter the sample would slump and fall away without any sign of ignition (Figure 3.5.1.4).

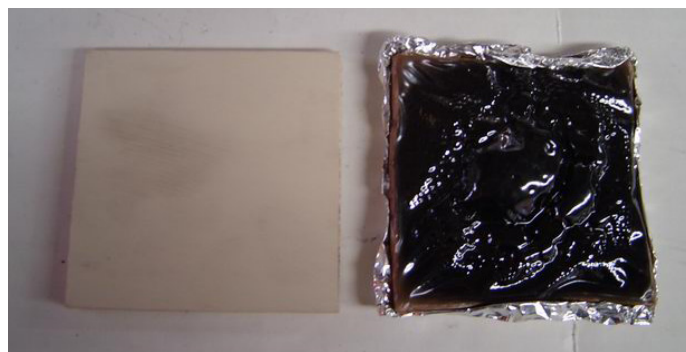


Figure 3.5.1 (PPS showing the beginning of the bubble formation)

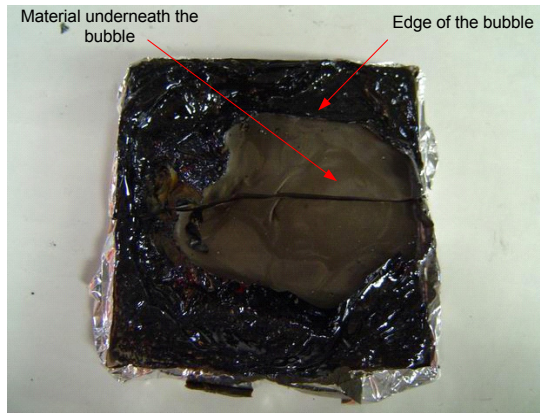


Figure 3.5.2 (PPS with bubble removed)



Figure 3.5.3 (PPS samples exposed to increasing levels of heat flux)



Figure 3.5.4 (Attempted PPS sample test in the flame spread apparatus)

3.6 Polyvinyl Chloride (PVC)

PVC was rather difficult to test in the cone due to the fire retardant nature of the material and its physical behavior. Ignition was very difficult to maintain and of short duration when it occurred. It was sometimes possible to ignite the gases above the sample but, difficult for the flame to attach to the surface. The sample would go through a flaming period but it would last about 30 seconds. Then it would return to the flashing phase. PVC begins to deform rather rapidly in tests above $30 \frac{kW}{m^2}$. This deformation was in the form of an expansion towards the heater. The sample goes from being a flat slab of 6.1mm thick, to almost the shape of a cube. I did not get a picture of this but it is similar to what is shown in Figure 3.10.3 for polycarbonate. This structure has a porous appearance. At the point in a test when the material has become a porous cube, a glowing or charring combustion process takes over. This condition persists for a considerable amount of time until it extinguishes.

3.7 High-Impact Polystyrene (HIPS)

HIPS behaves in a similar manner as ABS. There were no particular difficulties to be noted. Prior to ignition the sample's surface begins to darken in color followed by the formation of numerous tiny bubbles. The bubbles begin to break releasing fuel which leads to ignition. No skin was observed to form at the surface. HIPS generates a tall orange flame with a considerable amount of soot.

The similarity of HIPS and ABS was not limited to the Cone. A very similar behavior was observed including the sooting phenomenon (Figure 3.7.1) when tested in the flame spread apparatus. Again, the sooting played a role in the flame spread rate at low heat flux levels only. The thickness of the soot layer was found to be approximately 1mm at the locations measured. At high heat flux levels HIPS exhibited flowing flame spread as shown in figure 3.7.2 when tested in the downward spread configuration.



Figure 3.7.1 (HIPS showing heavy sooting during upward flame spread)

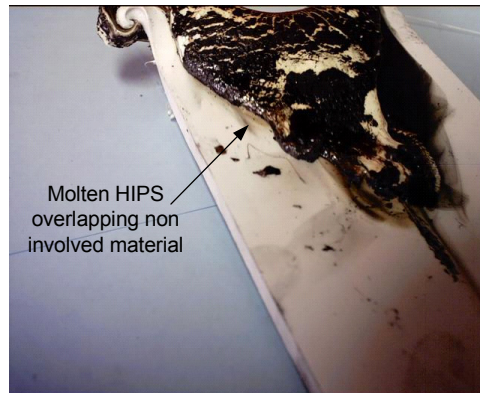


Figure 3.7.2 (HIPS, flowing flame spread seen in downward spread test)

3.8 High-Density Polyethylene (HDPE)

HDPE did not pose any difficulties in the Cone tests. The material quickly melts and begins to vaporize. After ignition of the vapor, the flame quickly spreads over the entire surface of the sample. The sample's surface becomes entirely liquid and boiling begins. HDPE burns with a tall bright yellow flame. The material burns to completion leaving behind only a wax like residue. HDPE has a very large peak

energy release rate and was not tested at $60 \frac{kW}{m^2}$ since at $50 \frac{kW}{m^2}$ the burning sample managed to bring the temperature in the Cone's exhaust up to 250 °C.

HDPE did not work in the flame spread apparatus because it becomes soft and melts too easily.

3.9 Polyvinylidene Fluoride (PVDF)

PVDF displayed some unexpected behavior. The sample begins as an opaque material and as it is heated it abruptly turns optically clear. This occurs as it approaches 170 °C and results in the once opaque sample becoming clear. This is probably an indication of some chemical change taking place in the polymer. Additional heating of the material makes it take on an amber hue before starting to bubble and vaporize. The vapors can be ignited with the Cone's spark igniter but flames do not attach to the sample's surface. As soon as the igniter is removed the flames extinguish. This flashing condition is very similar to that observed with PVC. At high heat flux levels and at the beginning of the test, the flames may attach momentarily to the surface of the sample. This last for about 30s to 1 minute and then flashing may continue. After prolonged exposure to the incident heat flux the sample expands slightly and becomes porous (Figure 3.9.2). At this point a glowing/charring process takes over which appears to be throughout the volume of the sample. It was not possible to test PVDF in the flame spread apparatus.



Figure 3.9.1 (PVDF original sample and sample from test stopped during flashing period)



Figure 3.9.2 (PVDF after long time exposure and charring)

3.10 Polycarbonate (PC)

PC was an overall difficult material to burn. While being heated it appears that small bubbles begin to form inside the material and spread towards the surface. The surface darkens and forms a skin which leads to a large bubble, similar to the other skin forming plastics. At $20 \frac{kW}{m^2}$ the test sample did not ignite after 25 minutes. That sample (Figure 3.10.1) clearly shows the bubble formation that is typical of the skin forming plastics. At higher heat flux levels it was possible to ignite vapors being vented from small rips in the skin. These small ignitions would gradually spread, but not over the sample's entire surface. The large bubble which formed prior to ignition remains but begins to take on a char like appearance (Figure 3.10.2). Towards the end of test the sample goes into the glowing/charring phase leaving behind a brittle, cube shaped porous structure (Figure 3.10.3).

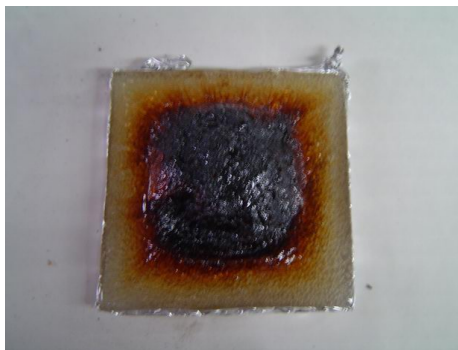


Figure 3.10.1 (PC showing the formation of a large bubble from testing at $20 \frac{kW}{m^2}$)



Figure 3.10.2 (PC sample manually extinguished during steady burning)



Figure 3.10.3 (PC sample after burn out)

3.11 Polyetherimide (PEI)

PEI is also one of the skin forming plastics. In the Cone calorimeter it formed a skin leading to the typical bubble trapping the gases given off by the material. Upon rupture of the skin and ignition of the venting fuel, ignition could be sustained at the

sample's surface. This ignition would gradually spread to other ruptures in the skin. The fire never became very large and resembled multiple point sources, like small volcanoes (Figure 3.11.1).

It was not possible to ignite PEI in the flame spread test even after the sample had been preheated to the point of forming bubbles on the surface (Figure 3.11.2).



Figure 3.11.1 (PEI after tests at increasing levels of heat flux)



Figure 3.11.2 (PEI from unsuccessful flame spread testing)

3.12 Summary of Observations

As a general observation all these materials have a complex behavior during decomposition and likely go through different stages both before and after ignition.

An example of this may be seen with polycarbonate where consistently there is a short lived spike in energy release rate followed by a charring period (Figure 3.12.1). Curiously the increase in external heat flux has more of an effect on the charring period than on the brief peak at ignition. Overall the plastics tested exhibited various peculiar behaviors but the most common and influential on the materials performance are the skin forming as seen in the Cone tests and the sooting and flowing flame spread seen in the flame spread apparatus. A short summary of these observations is presented in Table 3.12.1

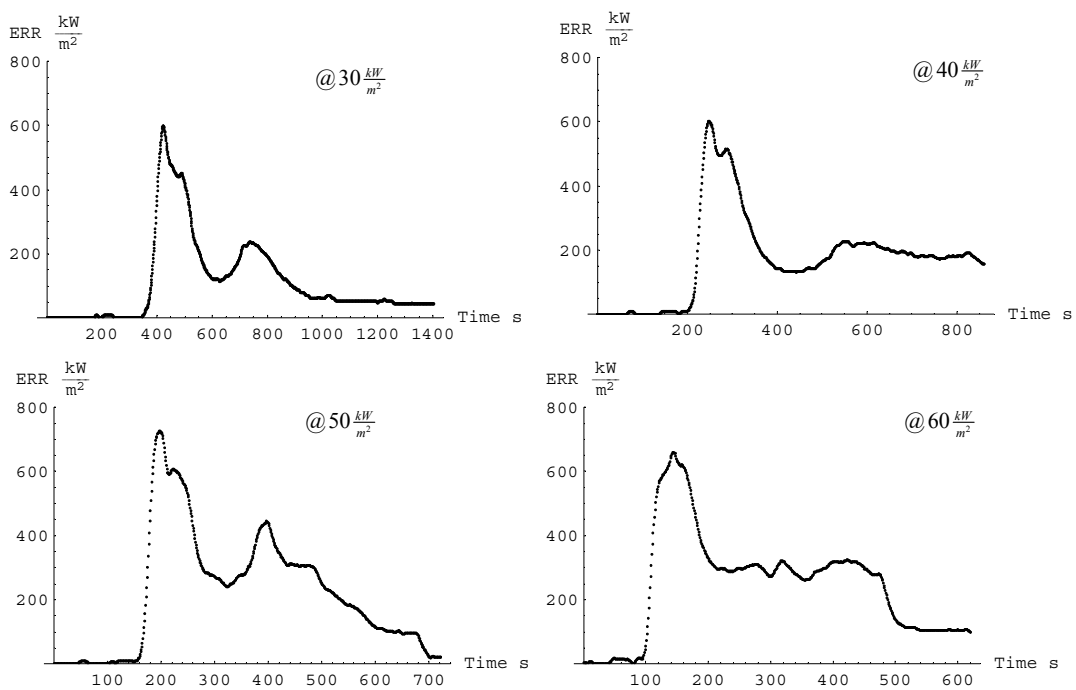


Figure 3.12.1 (Lexan Burning at increasing levels of Heat Flux)

Polymer Name	Increases Downward Flame Spread Rate		Decreases Upward Flame Spread Rate		Increases Ignition Time, Decreases Burning Rate		Porous Structure
	Flaming drops	Melt Flow	Sooting	Skin formation			
Polyphenylene sulfide [PPS]	N.A	N.A	N.A	x			
Polyvinyl chloride [PVC]	N.A	N.A	N.A				x
Polyamide 6,6 [PA66]	N.A	N.A	N.A	x			
High-Impact Polystyrene [HIPS]	x	x					
High-Density Polyethylene [HDPE]		x					
Polyvinylidene fluoride [PVDF]	N.A	N.A	N.A				x
Polyoxymethylene [POM]	x	x					
Polycarbonate [PC]	N.A	N.A	N.A	x			x
Poly(methyl methacrylate) [PMMA]	x	x					
Acrylonitrile butadiene styrene [ABS]		x	x				
Polyetherimide [PEI]	N.A	N.A	N.A				x

* N.A is for tests that were not possible

Table 3.12.1 (Overview of material behavior)

Chapter 4: Data Analysis Techniques

This chapter describes the data reduction procedures followed for the Cone calorimeter and the flame spread experiments. The Cone data analysis is presented first because information from these tests was necessary in order to analyze the flame spread data.

4.1 Cone data analysis

The measurements we made with the Cone calorimeter include time to ignition (t_{ig}), energy release rate (\dot{Q}''), mass loss rate (\dot{m}''), heat of combustion (Δh_c), heat of gasification (L), and in some cases mass flux at ignition ($\dot{m}''_{o,ig}$). After completing a series of tests with different levels of incident heat flux additional measurements can be made including critical heat flux for ignition ($\dot{q}''_{o,ig}$).

4.1.1 Time to ignition & Critical Heat Flux

The time to ignition was measured manually by using a stop watch. There is no data reduction for this measurement. The data is plotted as time to ignition vs. incident heat flux. By plotting the ignition data in this manner, it clearly shows the critical heat flux for the material. For example in the case of ABS the sample would ignite at $13 \frac{kW}{m^2}$ but not at $11 \frac{kW}{m^2}$. The critical heat flux for ignition then would be expected to be approximately $12 \frac{kW}{m^2}$. In the Plot (Figure 4.1.1) the critical heat flux represents an asymptote to the ignition time.

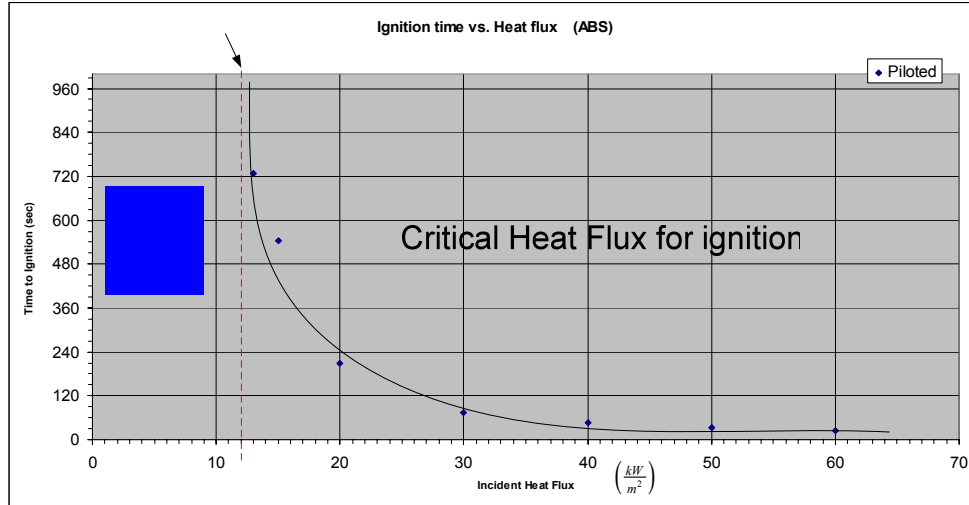


Figure 4.1.1 (ABS ignition times and critical heat flux)

Table 4.1.1 (Critical Heat Flux values for the materials tested)

Polymer Name	Critical Heat Flux ($\frac{kW}{m^2}$)
Polyphenylene sulfide [PPS]	38
Polyvinyl chloride [PVC]	20
Polyamide 6,6 [PA66]	18
High-Impact Polystyrene [HIPS]	16
High-Density Polyethylene [HDPE]	16
Polyvinylidene fluoride [PVDF]	38
Polyoxymethylene [POM]	8
Polycarbonate [PC]	28
Poly(methyl methacrylate) [PMMA]	8
Acrylonitrile butadiene styrene [ABS]	12
Polyetherimide [PEI]	38

4.1.2 Energy release rate (\dot{Q}'') & 80% Peak average energy release rate ($\bar{\dot{Q}}''_{80\%}$)

For the calculation of the energy release rate, the equation given by the ASTM oxygen calorimetry standard [9] was used.

$$\dot{Q} = 13100 \left(C \sqrt{\frac{\Delta P}{T_e}} \right) 1.10 \left(\frac{X_{O_2}^0 - X_{O_2}}{1.105 - 1.5X_{O_2}} \right) \quad (4.1)$$

$X_{O_2}^0$ Ambient oxygen concentration (%)

X_{O_2} Oxygen concentration at the current time step (%)

- ΔP Differential pressure across the mass flow meter (Pa)
- T_e Temperature of the gases at the location of the mass flow meter (K)
- C Cone's calibration coefficient
- \dot{Q} Energy release rate (kW)

To get the energy release rate per unit area, the energy release rate is divided by the sample's surface area ($.0058m^2$)

Since the test samples were not very thick ($\sim 6.5mm$) the fires in the Cone rarely reached a sustained peak burning rate and sometimes displayed narrow peaks in energy release rate. To obtain a more consistent and representative energy release rate, an 80% peak average was computed. This was done in the following manner. Once the actual peak was found the points on the energy release rate curve corresponding to 80% of that peak were found. This was done by plotting the energy release rate along with a straight line corresponding to 80% of the peak value (Figure 4.1.2). The energy release rate was then integrated between the intersecting points and divided by the time interval as shown in equation 4.2

$$\bar{Q}_{80\%}'' = \frac{\int \dot{Q}'' dt}{\Delta t} \quad (4.2)$$

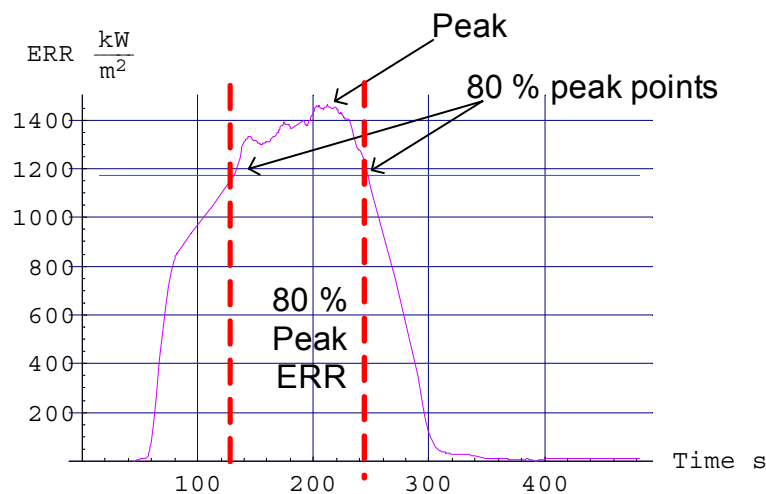


Figure 4.1.2 (Area used to evaluate 80% peak ERR)

Before performing the calculation with the raw data, an eight point moving average was first applied to these data. This was in an effort to smooth out the noise in the signals. The calculations were carried out using Mathematica to automate the process.

4.1.3 Mass Loss Rate (\dot{m}'')

To calculate the mass loss rate it is necessary to differentiate the mass loss signal. As was previously mentioned, all of the signals are subject to an eight point moving average before any of the calculations are done. This smoothing effect was adequate for most of the signals, but since we were calculating the derivative of the mass loss signal, additional smoothing was needed. This was done by calculating the derivative using a three point interpolation formula [11].

$$\dot{m}_i = \frac{dm_i}{dt} = \frac{1}{t}(-.5m_{i+2} + 2m_{i+1} - 1.5m_i) \quad (4.3)$$

Once the mass loss rate was calculated and the peak value identified, the 80% peak average was calculated (Figure 4.1.3). This was done in the same way as in the calculation of $\bar{Q}_{80\%}''$

$$\bar{m}_{80\%}'' = \frac{\int_{t_2}^{t_1} \dot{m}'' dt}{\Delta t} \quad (4.4)$$

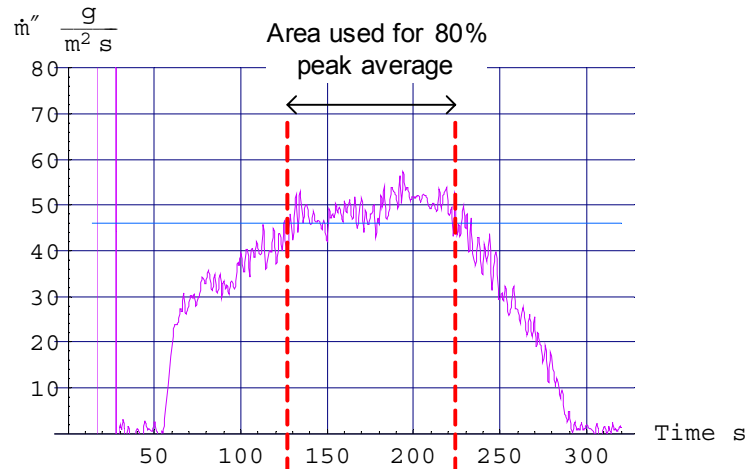


Figure 4.1.3 (Data used in the calculation of an 80% peak average mass loss rate)

4.1.4 Heat of Combustion (Δh_c)

Heat of combustion is the amount of energy released per unit mass of a given substance when it is burned in the presence of oxygen. The ASTM calorimetry standard [9] specifies a time-varying heat of combustion to be calculated as

$$\Delta h_c = \frac{\dot{Q}''(t)}{\dot{m}''(t)} \quad (4.5)$$

$\dot{Q}''(t)$ Heat release rate per unit area (kW/m^2)

$\dot{m}''(t)$ Mass loss rate per unit area ($\text{g/m}^2\text{s}$)

This is the rate of energy produced divided by the rate of sample mass consumed. Instead of calculating this at every time step the heat of combustion was calculated in the same interval that was used to calculate the 80% peak average values for the energy release rate and the mass loss rate.

$$\Delta h_c = \frac{\bar{\dot{Q}}''_{80\%}}{\bar{\dot{m}}''_{80\%}} \quad (4.6)$$

This method seems to give reasonable results since our calculated values for heat of combustion are generally within $\pm 2 \frac{kJ}{g}$ of the values reported by Tewarson in the SFPE handbook [10] for similar materials.

4.1.5 Heat of Gasification (L)

The heat of gasification (or vaporization) is a thermodynamic property for liquids. For solids this is more of an effective property since it does not take into account phenomena such as charring or other steps in the pyrolysis process. The burning rate is proportional to the heat flux received and inversely proportional to the heat of gasification.

$$\dot{m}'' = \frac{\dot{q}_{net}''}{L} \quad (4.7)$$

From this it is apparent that the heat of gasification can be found by plotting the burning rate versus the incident heat flux and taking the slope of the line (Figure 4.1.5).

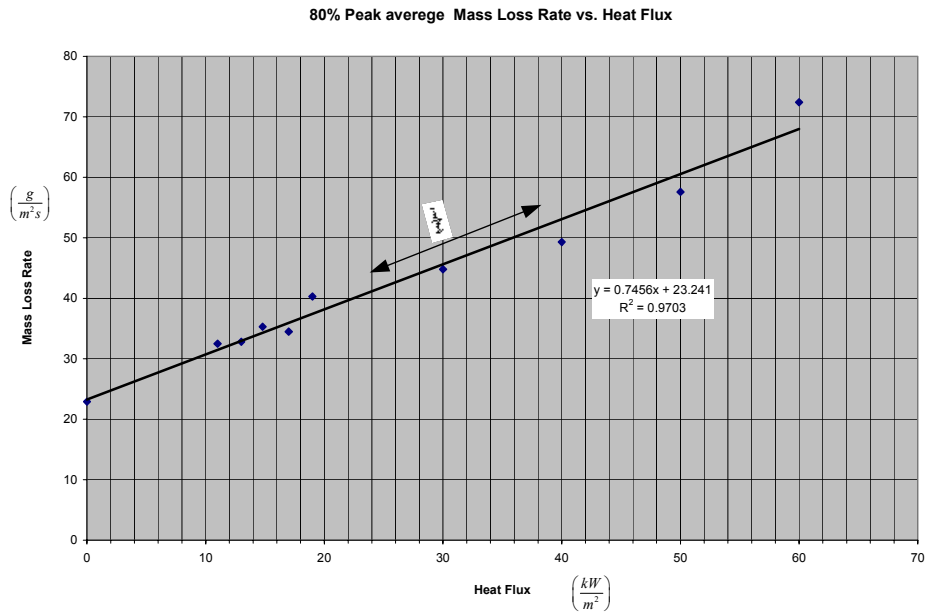


Figure 4.1.5 (example calculation of heat of gasification)

4.1.6 Mass flux at ignition.

A measurement of the mass flux at ignition could be performed in some cases by evaluating the mass loss rate at the instant of ignition. A flaw in this method though is that ignition does not always occur at the instant when the mass flux has reached a critical value. Ignition occurs when the a flammable mixture forms near the spark igniter, so when ignition occurs it does not necessarily coincide with the exact time the mass flux has reached its critical value. I think this delay may have a larger effect at high levels of heat flux where the change in mass loss rate is high and so a delay would make a significant difference in the measured value. At low levels of heat flux this delay would not result in such a large change. To try and correct for this, the critical mass flux was consistently evaluated at a point 5 seconds prior to sustained ignition (Figure 4.1.6). For the materials tested it seems that the mass flux at ignition remains fairly constant over the different levels of heat flux testes. These values turned out slightly lower than those reported by Tewarson for comparable materials [10].

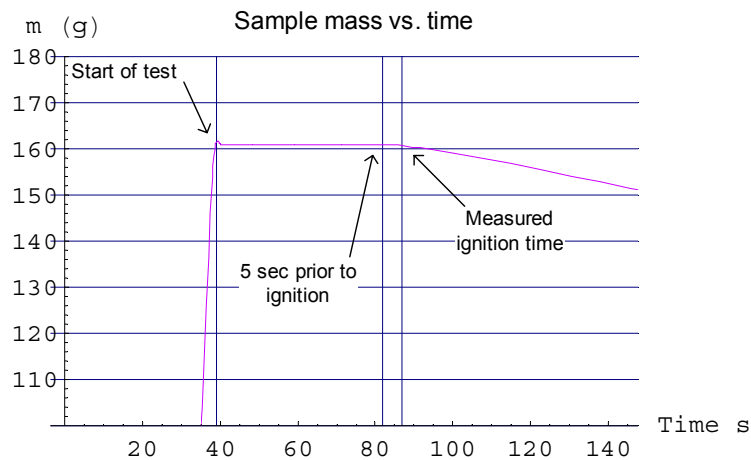


Figure 4.1.6 (location for measurement of mass flux at ignition)

4.1.7 Critical Heat Flux for Sustained Burning.

As an afterthought we tried to see if it would be possible for some of the materials to measure the minimum heat flux required to sustain ignition. For example some of the materials (ABS, POM, PMMA, HIPS, HDPE) that have critical heat flux

levels between 8 and 16 once ignited will burn with no need for external heating. Some of the other materials though require a minimum level of heat flux to remain burning. To try and measure this we did some tests in which the samples were forced to ignite and then placed under the Cone's heater. The heater would be set slightly below the material's critical heat flux for ignition. If burning was sustained the heater temperature was set lower and lower until the point was found where the burning rate began to decrease leading to extinction. The heat flux at this point is the minimum heat flux for sustained ignition.

4.2 Flame spread data analysis

As was mentioned in the procedure (chapter 2), the preheating time in the flame spread experiments was less than that which would be required to reach a steady state. This was due to the thermoplastic nature of the materials. Since it was not possible to leave the samples in place long enough to reach steady state, it was necessary to correlate those results to a steady state condition. To do this the thermal response of the material was evaluated based on the ignition data from the cone calorimeter. Piloted ignition occurs when the surface temperature of a material reaches a threshold value (T_{ig}). At this temperature the material decomposes at a rate which can reach the lower flammable limit for ignition. To reach this ignition temperature the material must be exposed to a sufficient heat source. Formulated as a one dimensional heat transfer problem [8], the surface temperature rise for a thermally thick material exposed to an external radiant flux can be expressed as

$$T_s - T_\infty = \frac{\dot{q}_e''}{h_t} \left(1 - e^{-\tau} \operatorname{erfc}(\sqrt{\tau}) \right) \quad (4.8)$$

$$\tau = \frac{h_t^2 t}{k \rho c} \quad (4.9)$$

At the critical heat flux for ignition, $\dot{q}_{o,ig}''$, it is expected that ignition will occur as $t \rightarrow \infty$. For long time ignition the conductive losses into the material are minimized and the heat loss from the surface balances the imposed external flux.

$$\dot{q}_{o,ig}'' = h_t (T_{ig} - T_\infty) \quad (4.10)$$

Equation 4.8 along with 4.10 can be rewritten for $t = t_{ig}$ and $T_s = T_{ig}$ as follows

$$\frac{\dot{q}_{o,ig}''}{\dot{q}_e''} = \left(1 - e^{-\tau} \operatorname{erfc}(\sqrt{\tau})\right) \quad (4.11)$$

An empirically derived [8] counterpart to this equation is

$$\frac{\dot{q}_{o,ig}''}{\dot{q}_e''} = F(t) = \begin{cases} b\sqrt{t_{ig}}, & t_{ig} < t^* \\ 1, & t_{ig} \geq t^* \end{cases} \quad (4.12)$$

$$b = \frac{2h_t}{\sqrt{\pi k \rho c}} \quad (4.13)$$

The t^* is the time to reach equilibrium or steady state. The ignition data measured in the Cone calorimeter can now be used to determine $F(t)$ from the previous relationship. With the time to ignition measured at various levels of external heat flux, and the critical heat flux for ignition the data for each material can be plotted as

$\frac{\dot{q}_{o,ig}''}{\dot{q}_e''}$ vs. $\sqrt{t_{ig}}$ (Figure 4.2.1)

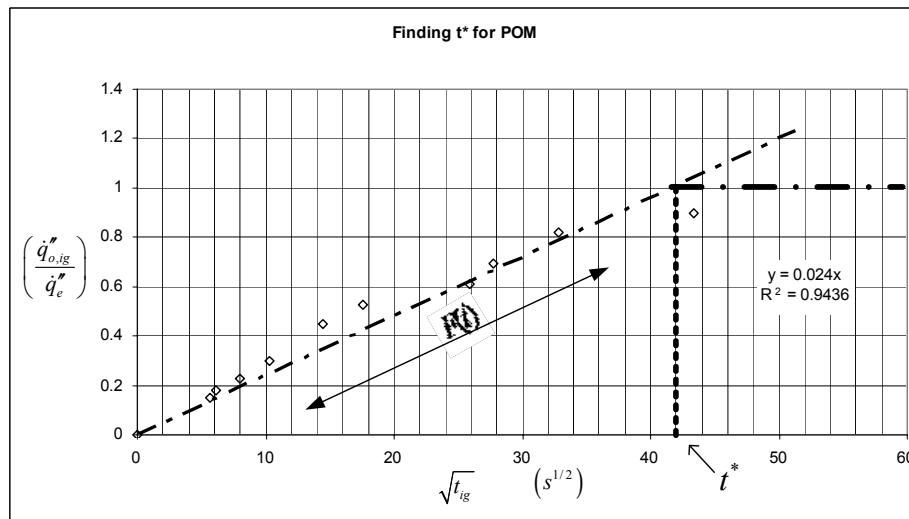


Figure 4.2.1 (Graphical determination of t^* and $F(t)$)

When the external heat flux is equal to the critical heat flux ($\dot{q}_{o,ig}'' / \dot{q}_e'' = 1$) the time to ignition is the thermal response time of the material t^* . To adjust for preheating times less than the thermal response time, the function $F(t)$ is used and the incident flux becomes

$$\dot{q}_{\infty}'' = \dot{q}_e'' F(t) \quad (4.11)$$

Here (\dot{q}_{∞}'') is the effective external flux applied after a long time. For example, in the case of POM we know the critical heat flux for ignition is $8 \frac{kW}{m^2}$. Using Figure 4.2.1, If this material is preheated at $6 \frac{kW}{m^2}$ for 4 minutes in the flame spread test, then the effective “long time” external flux would be found as follows. The preheating time of 4 minutes corresponds to 15.5 on the x axis of Figure 4.2.1. The value of $F(t)$ for $\sqrt{t_{ig}} = 15.5 (s^{1/2})$ is approximately 0.38. This means that the long time, external heat flux that would characterise this test is $\dot{q}_{\infty}'' = 6 \times .38 = 2.3 \frac{kW}{m^2}$. This correction approach adjusts the flame spread data so it is representative of long time heating. An example of the result from this type of correction is shown for the case of ABS in Figure 4.2.2.

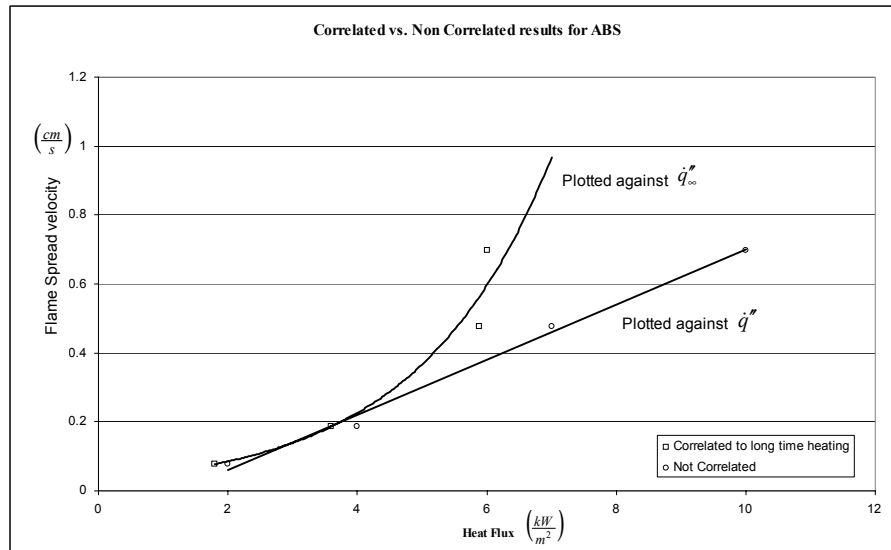


Figure 4.2.2 (Correlation of flame spread data to long time heating)

4.2.1 Flame spread velocity

The flame spread velocity was calculated simply as the change in the flame front position over time. The time to reach the middle and the time to reach the end were used to calculate two velocities which were then averaged to give an overall velocity for the test. Although some acceleration was noted, especially in the upward

flame spread direction, the calculated flame spread rate represents an average value for the entire length of the sample.

$$FSR = \frac{\delta_f}{\Delta t} \quad (4.12)$$

This was done for each of the heat flux levels tested and the data were plotted with their corresponding long time external heat flux (\dot{q}''_{∞}) as shown in figure 4.2.3.

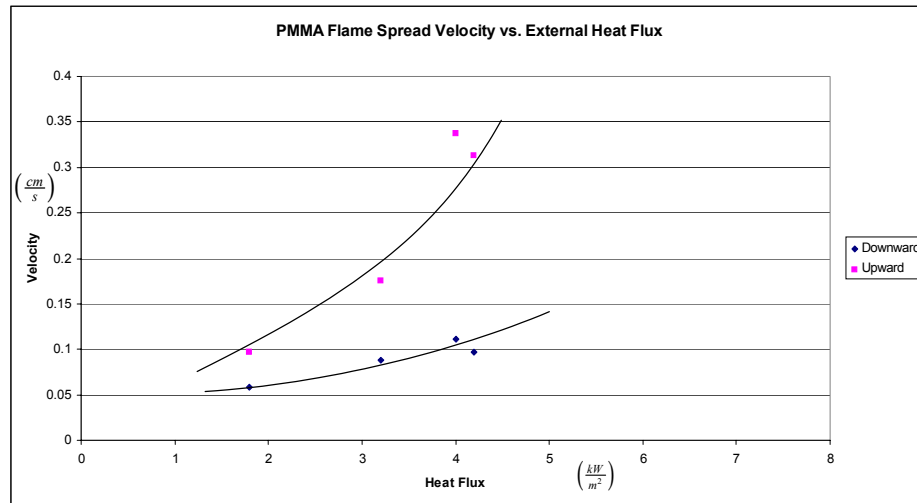


Figure 4.2.3 (Example of Flame Spread Velocity Plot)

Chapter 5: Results and Flammability Diagrams

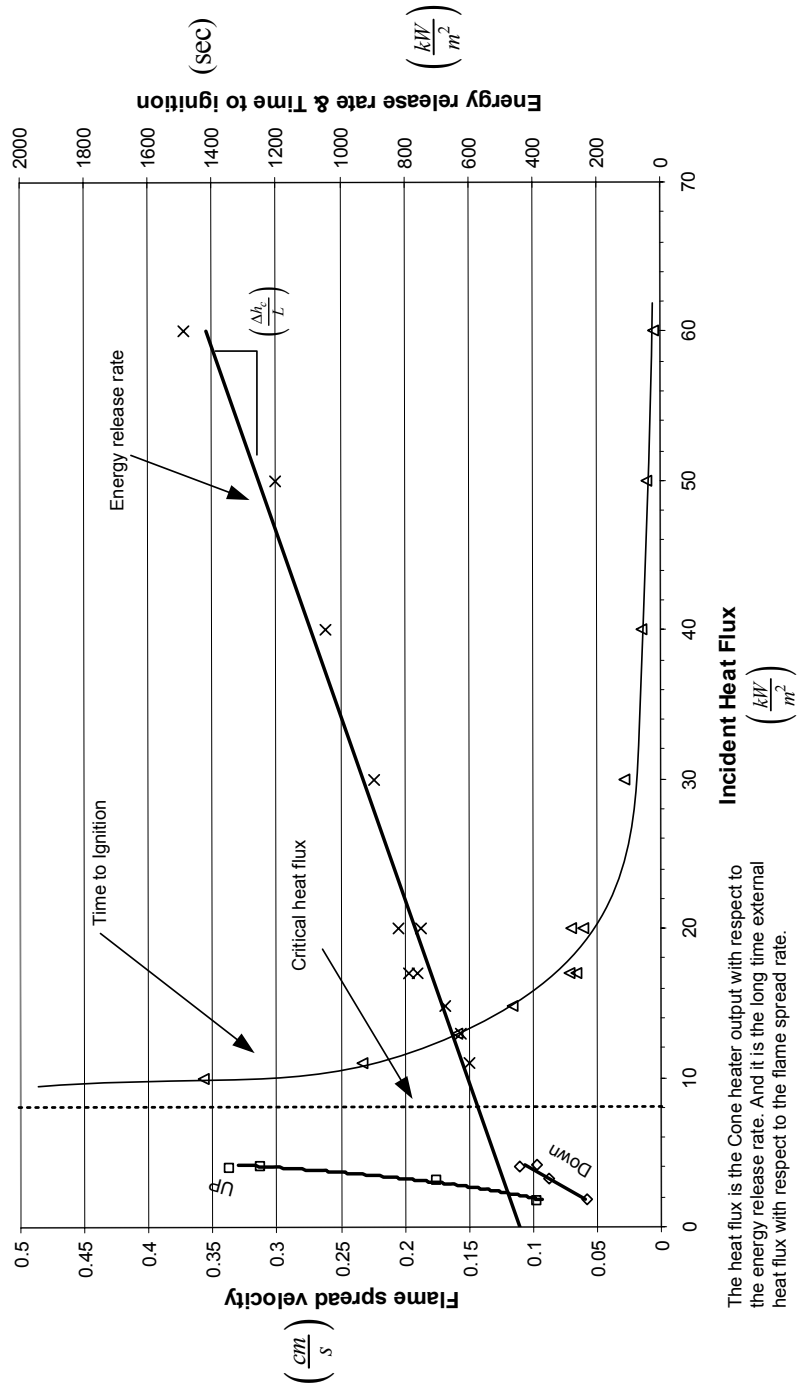
5.1 Results

The calculation methods outlined in the previous chapter were performed with the data gathered from the two tests. The results from the energy release rate, mass loss rate, time to ignition, heat of combustion, critical heat flux and in some cases ignition mass flux, are presented in the tables and graphs of Appendix B for each material.

5.2 Flammability Diagrams

From the trends in the results it is seen that heat flux is the principal factor controlling early fire growth, it is incumbent on the engineer and safety regulator to understand the fire behaviour as a function of heat flux. With the results from the ignition and flame spread data, plots giving a general description of the fire performance of the materials as a function of heat flux can be constructed. These plots are called flammability diagrams. The flammability diagrams show energy release rate, time to ignition, and flame spread rates as functions of heat flux. Having all of this information on the same diagram gives a complete overview of the material's fire performance. In these diagrams the critical heat flux is seen to be both the asymptote of the time to ignition and the flame spread velocity for both upward and downward spread. This is would be expected since at long time ($t_{ig} \rightarrow \infty$) heating under the critical flux, the surface temperature would approach the ignition temperature (T_{ig}). For flame spread when the sample surface is at the ignition temperature (after long time heating at the critical heat flux) the time for ignition approaches zero and the flame spread velocity would approach the limiting value of gas phase flame velocity. This is why both the ignition time and flame spread velocity have the critical heat flux as an asymptote.

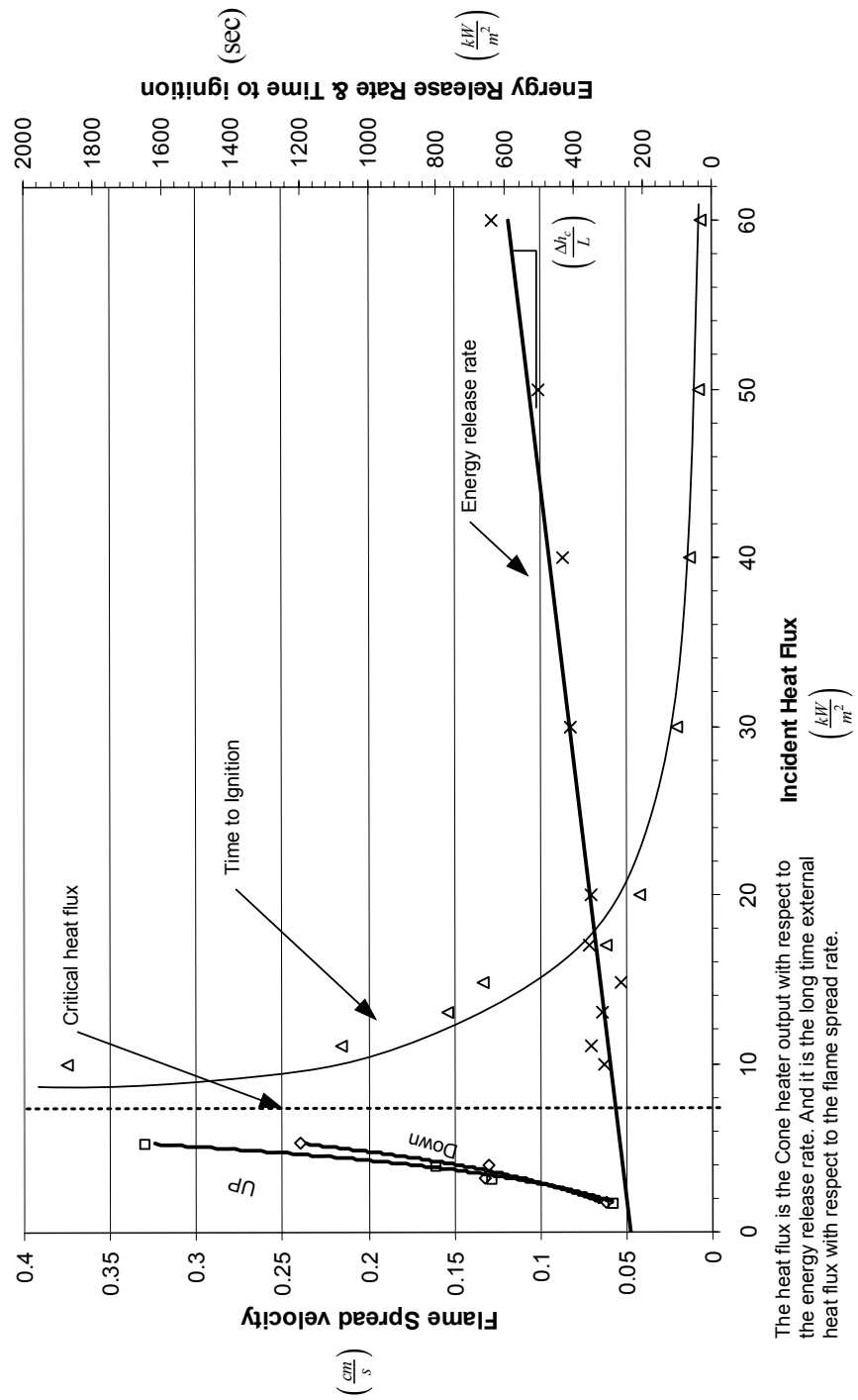
PMMA Flammability Diagram



The heat flux is the Cone heater output with respect to the energy release rate. And it is the long time external heat flux with respect to the flame spread rate.

Figure 5.2.1 (Flammability Diagram for PMMA)

POM Flammability Diagram



The heat flux is the Cone heater output with respect to the energy release rate. And it is the long time external heat flux with respect to the flame spread rate.

Figure 5.2.2 (Flammability Diagram for POM)

HIPS Flammability Diagram

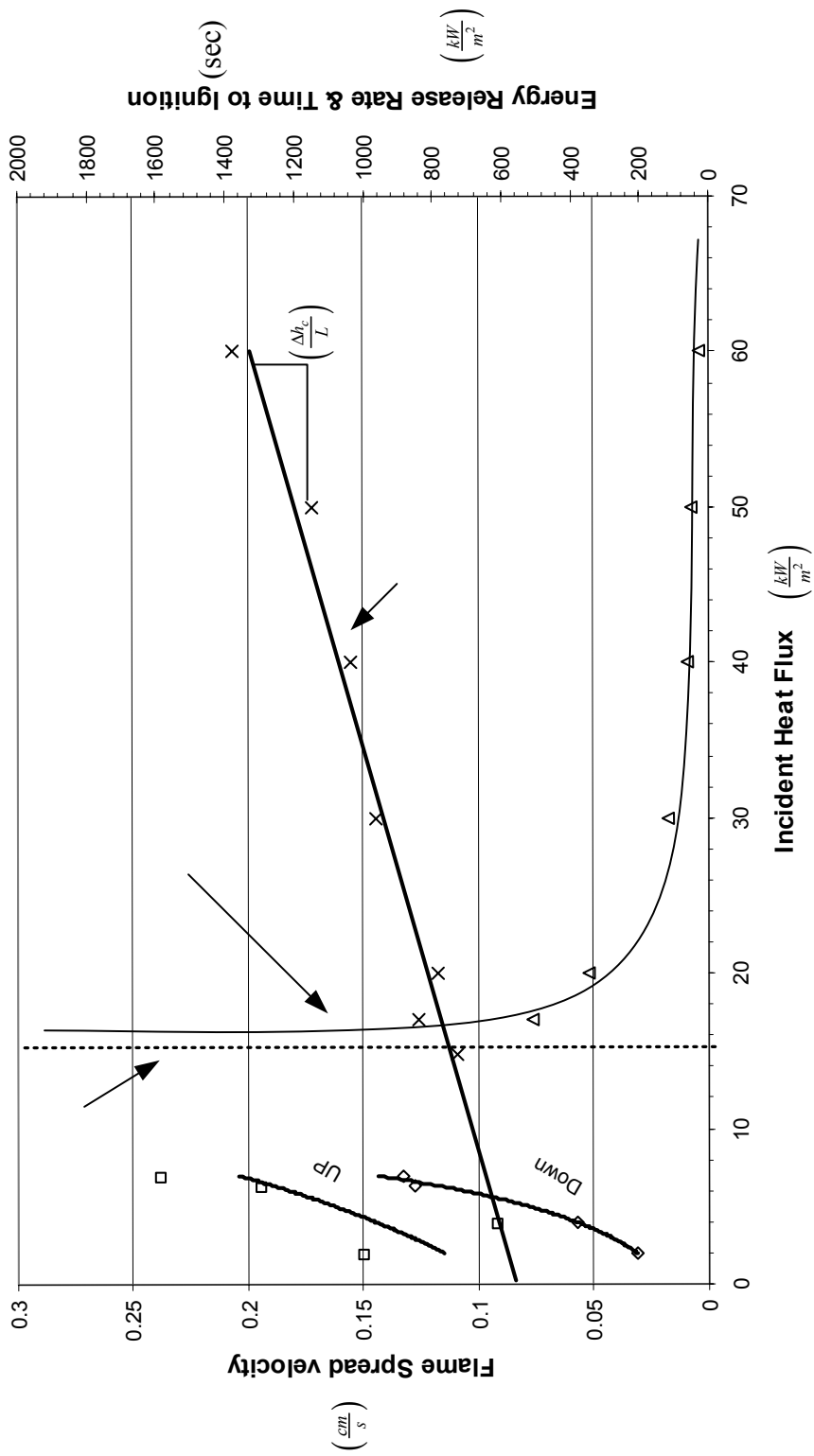


Figure 5.2.3 (Flammability Diagram for HIPS)

ABS Flammability Diagram

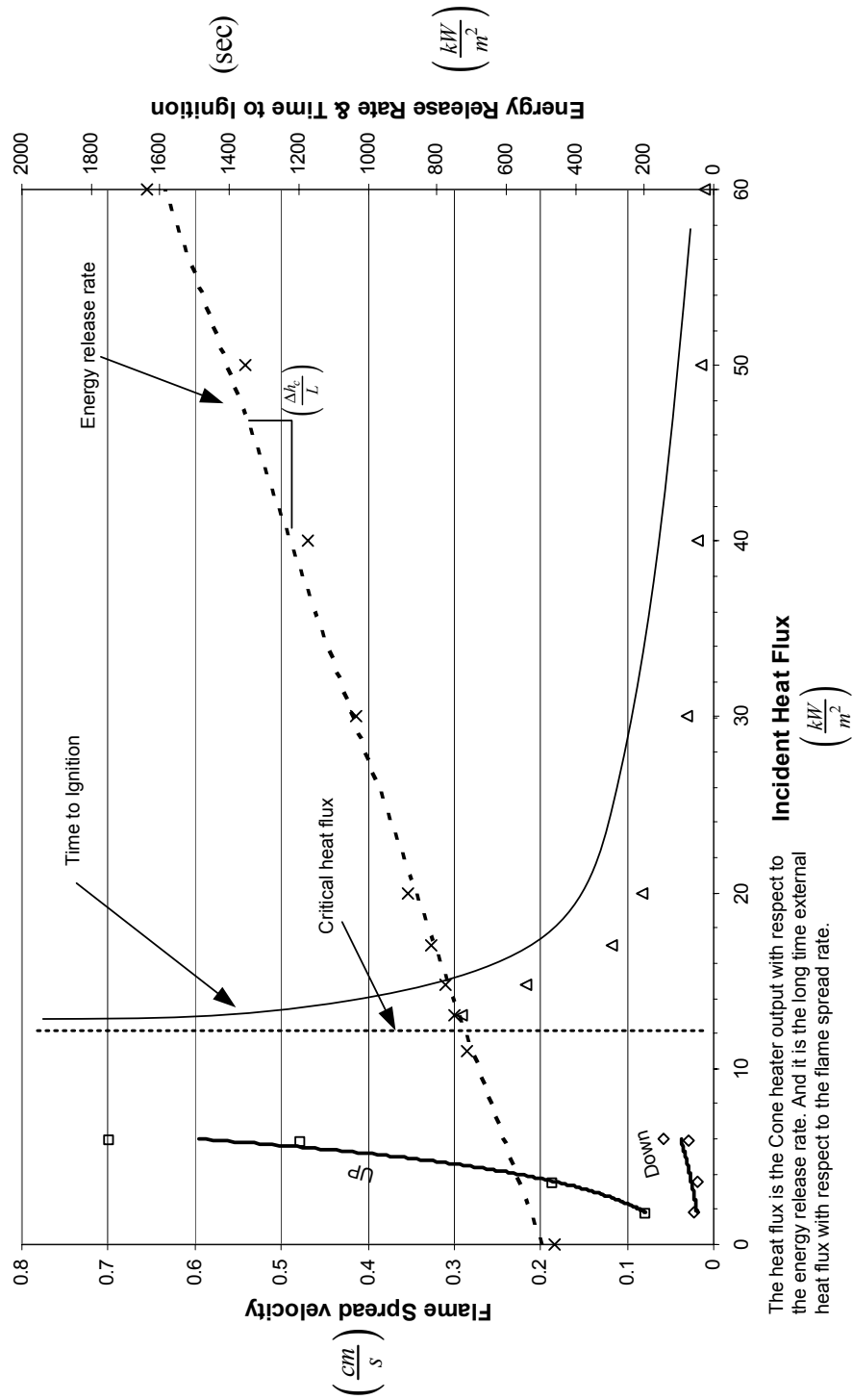


Figure 5.2.4 (Flammability Diagram for ABS)

From the Flammability diagrams it is seen that the fire performance of materials is highly dependent on incident heat flux, which is consistent with theory. The flammability diagrams show a lot of detail which at first may seem distracting. This detail exposes the differences among the materials and allows for direct comparisons to be made. It can be seen that ignition is different from energy release rate, or flame spread rate and that one thing does not necessarily follow the other. It is obvious that a classification provided by a standard test can do little to expose the true nature of these materials. It is not possible to have a test that measures one thing and then tries to predict the entire range of fire performance.

From the flammability diagrams of PMMA (Figure 5.2.1) and POM (figure 5.2.2) you can see that although the two materials have similar ignition times and critical heat flux, PMMA has 2.3 times the peak energy release rate of POM. For the same two materials you will also notice that although they exhibit the same upward flame spread rate, they are dissimilar in the downward rate. Looking back at the observations this difference in downward flame spread rate can be attributed to the flowing flame spread seen more pronounced with the POM samples than with PMMA. This was due to the fact that the melt produced by POM was less viscous than that of PMMA. Another point that is exposed in the flammability diagrams is the slope of the energy release rate versus the incident heat flux. This slope (\dot{Q}'' / \dot{q}_e'') is equivalent to $\frac{\Delta h_c}{L}$, the heat of combustion over the heat of gasification (which happens to be Tewarson's HRP parameter). This parameter effectively controls the burning rate as can be seen from the following equation.

$$\dot{Q}'' = \frac{\dot{q}_{net}''}{L} \Delta h_c \quad (5.1)$$

Even though difficulties such as melting, sooting and the formation of a skin could use special handling, meaningful flammability diagrams could still be produced despite these effects and they show the overall fire response of the material.

Chapter 6: Conclusions

Having obtained a complete picture of a material's flammability through the creation of the flammability diagrams it is worth while to see how this testing framework could relate to regulatory fire safety testing. One could perhaps seek to determine an index or classification based on the fire performance indicated by the flammability diagram. Caution must be used when following such an approach to avoid ending up with a result like those we already have from the standard test methods. As a reminder of the misleading nature such classifications an example of the Bunsen burner classifications is given. The materials PMMA, POM, HIPS, ABS get the same classification of HB (Figure 1.2.2) when tested in the Bunsen burner type tests. Looking back at the flammability diagrams (Figures 5.2.1-4) these materials are not alike and certainly not similar enough to be considered the same. They have differences in critical heat flux for ignition, there are differences in energy release rate and also flame spread rate. This classification does not say much about the material. If a classification is to be used it should be based on parameters that govern the material's fire performance. For example people are always concerned with the energy release rate of a material. This of course depends on the level of incident heat flux, and on its own is not of much use. What is more important and underlies the energy release rate is the heat release parameter already (HRP) previously mentioned [12]. This is not the only useful parameter or property that can be extracted from the information in a flammability diagram. These include a thermal response parameter (TRP), the energy release rate at zero external flux (HRR_0), the critical heat flux for sustained burning ($\dot{q}_{o,b}''$) and the flame heat flux (\dot{q}_f''). With the exception of the critical heat flux for sustained burning, the other parameters are directly extracted from the Cone data. These parameters are in control of fire performance and could serve as indicators with which to classify materials for regulatory purposes.

The HRR_0 can be used to predict the flame spread potential of a material [13]. A limiting value $\sim 100 \frac{kW}{m^2}$ has been proposed to draw the line between materials that

will exhibit flame spread, and those that will self extinguish. Along the same line is the flame heat flux \dot{q}_f'' which gives indication of how much strength the material has to burn on its own.

Additionally with the ratio of the heat release parameter and the time response parameter (HRP/TRP) you can get an idea of how fast fire will spread on a material.

These properties and parameters are readily extracted from the flammability diagrams and are shown in the following table for selected materials. Additionally information such as smoke obscuration and gas species yields could also be incorporated into the Flammability Diagrams. It is noted here that the results for Polycarbonate (Lexan) are not quite representative as result of the calculation method used and the peculiar performance of the material (Figure 2.12.1). This is because of the burning behavior, which consists of a short flaming period followed by a prolonged charring period. The data presented for Lexan is representative of the short flaming period (peak and 80% peak values) and does not capture the effect of charring. The results for most of the other plastics seem to be in keeping with literature values.

Fuel Type	$\dot{Q}''_{30} \left(\frac{\text{kJ}}{\text{m}^2} \right)$	$\dot{Q}''_{60} \left(\frac{\text{kJ}}{\text{m}^2} \right)$	$\Delta h_c \left(\frac{\text{kJ}}{\text{g}} \right)$	$L \left(\frac{\text{kJ}}{\text{g}} \right)$	HRP	TRP	$\dot{q}''_{O,lg} \left(\frac{\text{kJ}}{\text{m}^2} \right)$	$\dot{q}''_{O,b} \left(\frac{\text{kJ}}{\text{m}^2} \right)$	$\dot{q}''_f \left(\frac{\text{kJ}}{\text{m}^2} \right)$	HRR ₀
	1134	1868								
ABS	1134	1868	28.2	1.35	20.9	0.0034	12	0	-25	528
HDPE	1625	2021	40.9	2	20.5	0.0026	16	0	-27	730
HIPS	1050	1489	28.7	2	14.4	0.0032	16	0	-60	700
Lexan (PC)	597	657	19.1	4.76	4.0	0.002	28	12	-169	508
Nylon	1160	1821	29.2	1.53	19.1	0.0025	18	3.5	-20	443
PMMA	962	1635	23.3	2.26	10.3	0.0033	8	0	-29	500
POM	455	703	13.5	2.04	6.6	0.0032	8	0	-42	270
PVC	151	260	8.7	1.47	5.9	0.0039	20	20	2	-9.9

Table 5.1.1 (Overview of selected parameters and properties)

Appendix A: Theory of Energy Release Rate

The following analysis applies to the case where only oxygen (O_2) is measured. In this case, water vapor and carbon dioxide (CO_2) are removed from the sample gas and it is assumed that the sample consists only of nitrogen (N_2) and oxygen. Carbon monoxide (CO) will be assumed negligible. This approach is similar to what is described by Mark Janssens [14,15].

The energy release rate of a fuel during combustion is proportional to the mass loss rate \dot{m}_F of the fuel and the fuel's heat of combustion Δh_c .

$$\dot{Q} = \dot{m}_F \Delta h_c \quad (A.1)$$

Although \dot{m}_F can be measured for an unknown fuel, direct measurement of the energy release rate \dot{Q} is not possible since the fuel's heat of combustion is not known. The energy release rate can be measured indirectly by relating it to the amount of oxygen consumed by the reaction.

$$\dot{Q} = \dot{m}_F \Delta h_c = \dot{m}_{O_2,used} \Delta h_{O_2} \quad (A.2)$$

Where the basic requirement to measure $\dot{m}_{O_2,used}$ is that all of the combustion products are collected and removed through an exhaust duct. This enables a control volume analysis to be performed. The control volume used is depicted in Figure A.1.

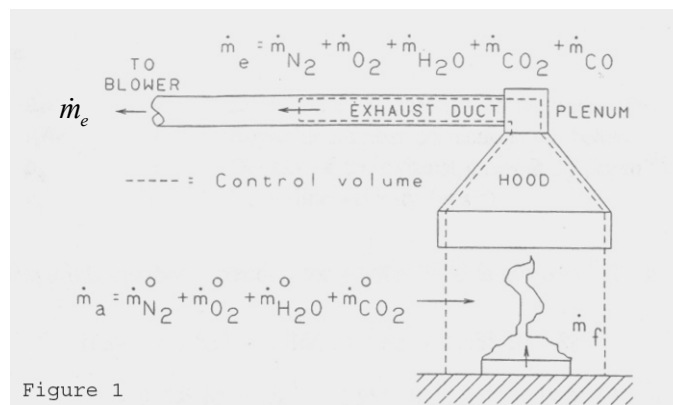


Figure A.2 (Control volume used in energy release rate analysis)

Mass conservation,

$$\dot{m}_e = \dot{m}_a + \dot{m}_F \quad (\text{A.3})$$

Where the quantity we want to measure is $\dot{m}_{O_2,used}$

$$\dot{m}_{O_2,used} = \dot{m}_{O_2}^0 - \dot{m}_{O_2} = \dot{m}_a Y_{O_2,\infty} - \dot{m}_e Y_{O_2} \quad (\text{A.4})$$

$$\dot{m}_{O_2,used} = (\dot{m}_e - \dot{m}_F) Y_{O_2,\infty} - \dot{m}_e Y_{O_2} = \dot{m}_e (Y_{O_2,\infty} - Y_{O_2}) - \dot{m}_F Y_{O_2,\infty} \quad (\text{A.5})$$

Combining equations A.2 and A.5

$$\dot{Q} = [\dot{m}_e (Y_{O_2,\infty} - Y_{O_2}) - \dot{m}_F Y_{O_2,\infty}] \Delta h_{O_2} \quad (\text{A.6})$$

The exhaust mass flow \dot{m}_e is a mixture of gases including CO_2 , H_2O , N_2 , and O_2 .

$$\dot{m}_{CO_2} = \dot{m}_e Y_{CO_2}, \quad \dot{m}_{H_2O} = \dot{m}_e Y_{H_2O} \text{ etc.}$$

Since we remove CO_2 and H_2O before measuring oxygen:

$$\dot{m}_e Y_{O_2} = (\dot{m}_e - \dot{m}_{CO_2} - \dot{m}_{H_2O}) Y'_{O_2} \quad (\text{A.7})$$

Y'_{O_2} Is the mass fraction in the oxygen analyzer after CO_2 and H_2O are removed from the sample gas.

$$Y_{O_2} = (1 - Y_{CO_2} - Y_{H_2O}) Y'_{O_2} \quad (\text{A.8})$$

Substituting this into equation A.6

$$\dot{Q} = [\dot{m}_e Y_{O_2,\infty} - \dot{m}_e (1 - Y_{CO_2} - Y_{H_2O}) Y'_{O_2} - \dot{m}_F Y_{O_2,\infty}] \Delta h_{O_2} \quad (\text{A.9})$$

For stoichiometric oxidation of a fuel in complete combustion



$$\dot{m}_{CO_2} = \dot{m}_e Y_{CO_2} = \frac{\nu_{CO_2} M_{CO_2}}{\nu_F M_F} \dot{m}_F \quad \Rightarrow \quad Y_{CO_2} = \frac{\left(\frac{\nu_{CO_2}}{\nu_F}\right) \left(\frac{M_{CO_2}}{M_F}\right)}{\dot{m}_e} \dot{m}_F \quad (\text{A.11})$$

$$\dot{m}_{H_2O} = \dot{m}_e Y_{H_2O} = \frac{v_{H_2O} M_{H_2O}}{v_F M_F} \dot{m}_F \quad \Rightarrow \quad Y_{H_2O} = \frac{\left(\frac{v_{H_2O}}{v_F}\right) \left(\frac{M_{H_2O}}{M_F}\right)}{\dot{m}_e} \dot{m}_F \quad (\text{A.12})$$

Substituting equations A.11 and A.12 into equation A.9

$$\dot{Q} = [\dot{m}_e (Y_{O_2, \infty} - Y'_{O_2}) + \left(\frac{v_{CO_2}}{v_F}\right) \left(\frac{M_{CO_2}}{M_F}\right) \dot{m}_F Y'_{O_2} + \left(\frac{v_{H_2O}}{v_F}\right) \left(\frac{M_{H_2O}}{M_F}\right) \dot{m}_F Y'_{O_2} - \dot{m}_F Y_{O_2, \infty}] \Delta h_{O_2}$$

With the following substitutions:

$$r_{CO_2} = \frac{v_{CO_2}}{v_F} \frac{M_{CO_2}}{M_F} \quad r_{H_2O} = \frac{v_{H_2O}}{v_F} \frac{M_{H_2O}}{M_F} \quad \Delta h_{O_2} = \frac{\Delta h_c}{r_{O_2}}$$

the equation can be re written as:

$$\dot{Q} = [\dot{m}_e (Y_{O_2, \infty} - Y'_{O_2}) + (r_{CO_2} + r_{H_2O}) \dot{m}_F Y'_{O_2} - \dot{m}_F Y_{O_2, \infty}] \frac{\Delta h_c}{r_{O_2}} \quad (\text{A.13})$$

At this point, the mass fractions will be converted to mole fractions since this is the measurement given by the oxygen analyzer.

$$\dot{Q} = \dot{m}_e \left(\frac{X_{O_2}^0}{M_a} - \frac{X_{O_2}}{M_e} \right) M_{O_2} \frac{\Delta h_c}{r_{O_2}} + \dot{m}_F (r_{CO_2} + r_{H_2O}) \frac{X_{O_2} M_{O_2}}{M_e} \frac{\Delta h_c}{r_{O_2}} - \dot{m}_F Y_{O_2, \infty} \frac{\Delta h_c}{r_{O_2}}$$

Since $\dot{m}_F \Delta h_c = \dot{Q}$ and with the assumption that $M_e \approx M_a$ the previous equation becomes:

$$\dot{Q} = \frac{\Delta h_c}{r_{O_2}} \dot{m}_e \left(\frac{M_{O_2}}{M_a} \right) \frac{X_{O_2}^0 - X_{O_2}}{1 + \frac{Y_{O_2, \infty}}{r_{O_2}} - \frac{r_{CO_2} + r_{H_2O}}{r_{O_2}} \left(\frac{M_{O_2}}{M_a} \right) X_{O_2}} \quad (\text{A.14})$$

This heat release equation can be further simplified with:

$$\frac{M_{O_2}}{M_a} \approx 1.10 \quad \alpha = 1 + \frac{Y_{O_2, \infty}}{r_{O_2}} \quad (\text{A.15}) \quad \beta = \frac{r_{CO_2} + r_{H_2O}}{r_{O_2}} \left(\frac{M_{O_2}}{M_a} \right) \quad (\text{A.16})$$

After simplification

$$\dot{Q} = 1.10 \times \frac{\Delta h_c}{r_{O_2}} \dot{m}_e \frac{X_{O_2}^0 - X_{O_2}}{\alpha - \beta X_{O_2}} \quad (\text{A.17})$$

The exhaust mass flow \dot{m}_e is measured using a thin square edge orifice meter. The differential pressure across the orifice is measured along with the gas temperature, to assess the exhaust mass flow rate. The relation is the following: $\dot{m}_e = C \sqrt{\frac{\Delta P}{T_e}}$ where C is the calibration coefficient. Substituting this into equation A.17 gives the final form of the energy release rate equation.

$$\dot{Q} = 1.10 \times \frac{\Delta h_c}{r_{O_2}} \left(C \sqrt{\frac{\Delta P}{T_e}} \right) \left(\frac{X_{O_2}^0 - X_{O_2}}{\alpha - \beta X_{O_2}} \right) \quad (\text{A.18})$$

The variables $\frac{\Delta h_c}{r_{O_2}}$, α and β are fuel dependent. These values have been calculated for certain types of fuels and can be found in Appendix A. When the fuel type is unknown and these values are not available then $\alpha = 1.105$, $\beta = 1.5$ and $\frac{\Delta h_c}{r_{O_2}} = 13100$ are used making the energy release rate equation become identical to what is prescribed in ASTM E-1354 [9].

$$\dot{Q} = 13100 \left(C \sqrt{\frac{\Delta P}{T_e}} \right) 1.10 \left(\frac{X_{O_2}^0 - X_{O_2}}{1.105 - 1.5 X_{O_2}} \right) \quad (\text{A.19})$$

The values of α and β depend on the stoichiometric ratios r_{CO_2} , r_{H_2O} and r_{O_2} as seen in equations A.15 and A.16 For simple hydrocarbons the values of α and β increase with increasing carbon to hydrogen ratio. For more complex ‘real’ fuels containing other atoms besides just carbon and hydrogen the values for α and β do not seem to be dependent on the carbon to hydrogen ratio. This can be seen below in the Figures A.2 and A.3

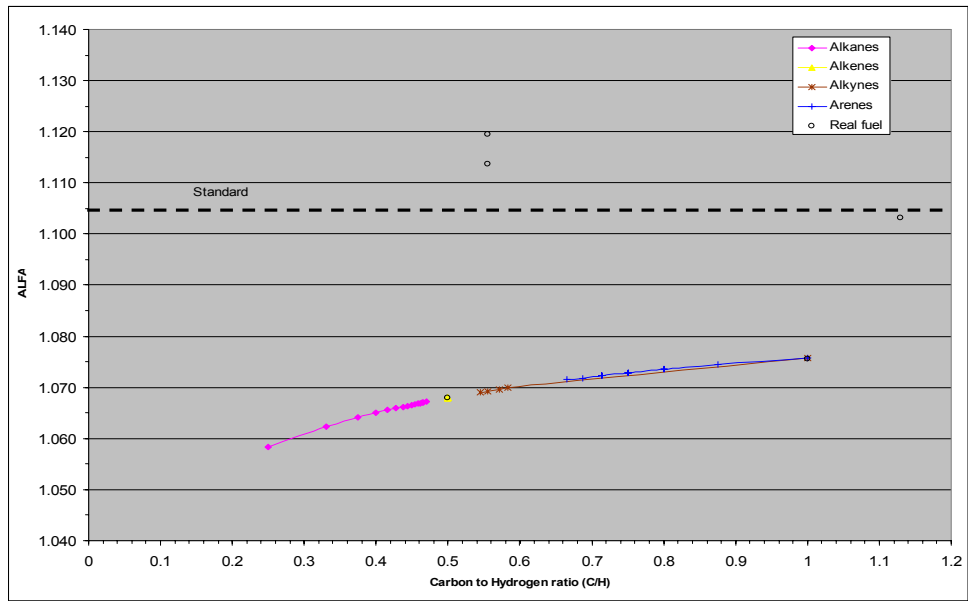


Figure A.2 (Parameter α as a function of carbon to hydrogen ratio)

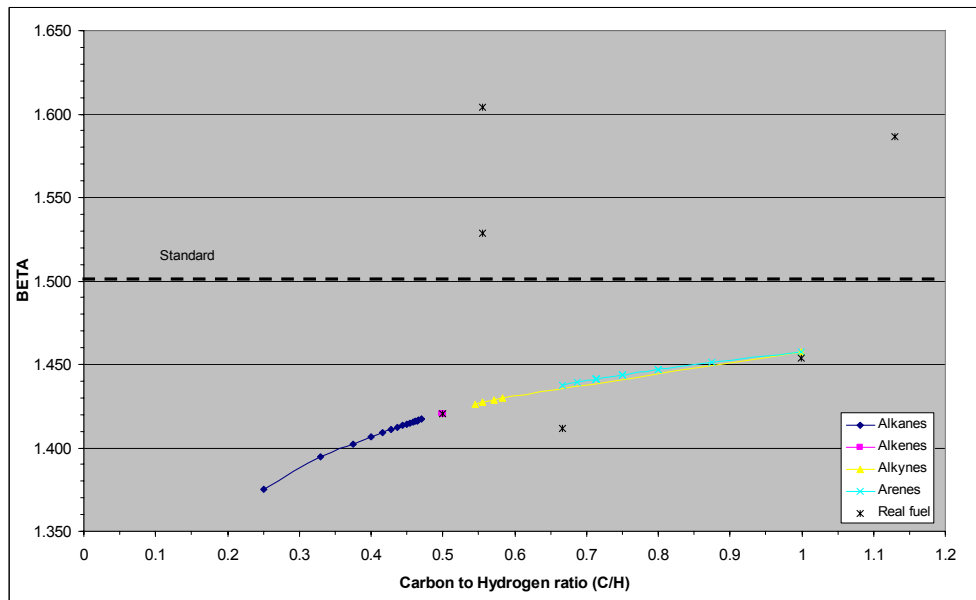


Figure A.3 (Parameter β as a function of carbon to hydrogen ratio)

Table A.1 (Parameters α & β for Alkanes)

Normal Alkanes			
Fuel	Formula	a	b
Methane	CH ₄	1.058	1.375
Ethane	C ₂ H ₆	1.062	1.395
Propane	C ₃ H ₈	1.064	1.403
Butane	C ₄ H ₁₀	1.065	1.407
Pentane	C ₅ H ₁₂	1.066	1.409
Hexane	C ₆ H ₁₄	1.066	1.411
Heptane	C ₇ H ₁₆	1.066	1.413
Octane	C ₈ H ₁₈	1.066	1.414
Nonane	C ₉ H ₂₀	1.067	1.414
Decane	C ₁₀ H ₂₂	1.067	1.415
Undecane	C ₁₁ H ₂₄	1.067	1.415
Dodecane	C ₁₂ H ₂₆	1.067	1.416
Tridecane	C ₁₃ H ₂₈	1.067	1.416
Kerosene	C ₁₄ H ₃₀	1.067	1.417
Hexadecane	C ₁₆ H ₃₄	1.067	1.417
	AVG	1.065	1.409

Table A.2 (Parameters α & β for Alkenes)

Normal Alkenes			
Fuel	Formula	a	b
Ethylene	C ₂ H ₄	1.068	1.421
Propylene	C ₃ H ₆	1.068	1.421
Butylene	C ₄ H ₈	1.068	1.421
Pentene	C ₅ H ₁₀	1.068	1.421
Hexene	C ₆ H ₁₂	1.068	1.421
Heptene	C ₇ H ₁₄	1.068	1.421
Octene	C ₈ H ₁₆	1.068	1.421
Nonene	C ₉ H ₁₈	1.068	1.421
Decene	C ₁₀ H ₂₀	1.068	1.421
Dodecene	C ₁₂ H ₂₄	1.068	1.421
Tridecene	C ₁₃ H ₂₆	1.068	1.421
Tetradecene	C ₁₄ H ₂₈	1.068	1.421
Hexadecene	C ₁₆ H ₃₂	1.068	1.421
Octadecene	C ₁₈ H ₃₆	1.068	1.421
	AVG	1.068	1.421

Table A.3 (Parameters α & β for Alkynes)

Normal Alkynes			
Fuel	Formula	a	b
Acetylene	C2H2	1.076	1.458
Heptyne	C7H12	1.070	1.430
Octyne	C8H14	1.070	1.429
Decyne	C10H18	1.069	1.427
Dodecyne	C12H22	1.069	1.426
	AVG	1.071	1.434

Table A.4 (Parameters α & β for Arenes)

Arenes			
Fuel	Formula	a	b
Benzene	C6H6	1.076	1.458
Toluene	C7H8	1.074	1.451
Ethylbenzene	C8H10	1.074	1.447
Xylene	C8H10	1.074	1.447
Propylbenzene	C9H12	1.073	1.444
Trimethylbenzene	C9H12	1.073	1.444
Cumene	C9H12	1.073	1.444
Butylbenzene	C10H14	1.072	1.441
Diethylbenzene	C10H14	1.072	1.441
p-Cymene	C10H14	1.072	1.441
Pentylbenzene	C11H16	1.072	1.439
Triethylbenzene	C12H18	1.071	1.438
	AVG	1.073	1.445

Table A.5 (Parameters α & β various common fuels)

Various Fuels			
Fuel	Formula	a	b
Polycarbonate	CH0.88O0.19	1.103	1.587
Polypropylene	CH	1.076	1.454
Polyvinylchloride	CH1.5Cl0.50	1.303	1.411
Nylon	CH1.8O0.17N0.17	1.119	1.529
GM21	CH1.8O0.30N0.05	1.114	1.604
Polyethylene	CH2	1.068	1.421

Appendix B: Test Results for Individual Materials

B.1 HIPS

Data File Name	Heat Flux $\frac{kW}{m^2}$	Peak ERR $\frac{kW}{m^2}$	80% Peak ERR $\frac{kW}{m^2}$	Peak MLR $\frac{g}{m^2-s}$	80% Peak MLR $\frac{g}{m^2-s}$	Ignition Mass Flux $\frac{g}{m^2}$	Time to Ignition SEC	Heat of Combustion $\frac{kJ}{g}$	Critical Heat Flux $\frac{kW}{m^2}$
HIPS_freeburn.txt	0	794	633	32	23	-	forced	-	16
HIPS7.txt	14.8	801.7	727.6	33.3	26.4	-	forced	28.6	
HIPS6.txt	17	912.3	839.2	35.45	28.7	1.8	510	29.8	
HIPS1.txt	19	874.8	783.2	34.4	28.7	0.8	350	28.8	
HIPS2.txt	30	1050.1	966	42.3	35.5	3.6	120	28.5	
HIPS3.txt	40	1124.8	1035.7	47	38.5	2.7	63	28.2	
HIPS4.txt	50	1242	1146.3	48.7	40.6	1.9	48	29.2	
HIPS5.txt	60	1489.6	1377.8	63.2	52.1	3.2	28	28.3	

Table B.1 (HIPS Results)

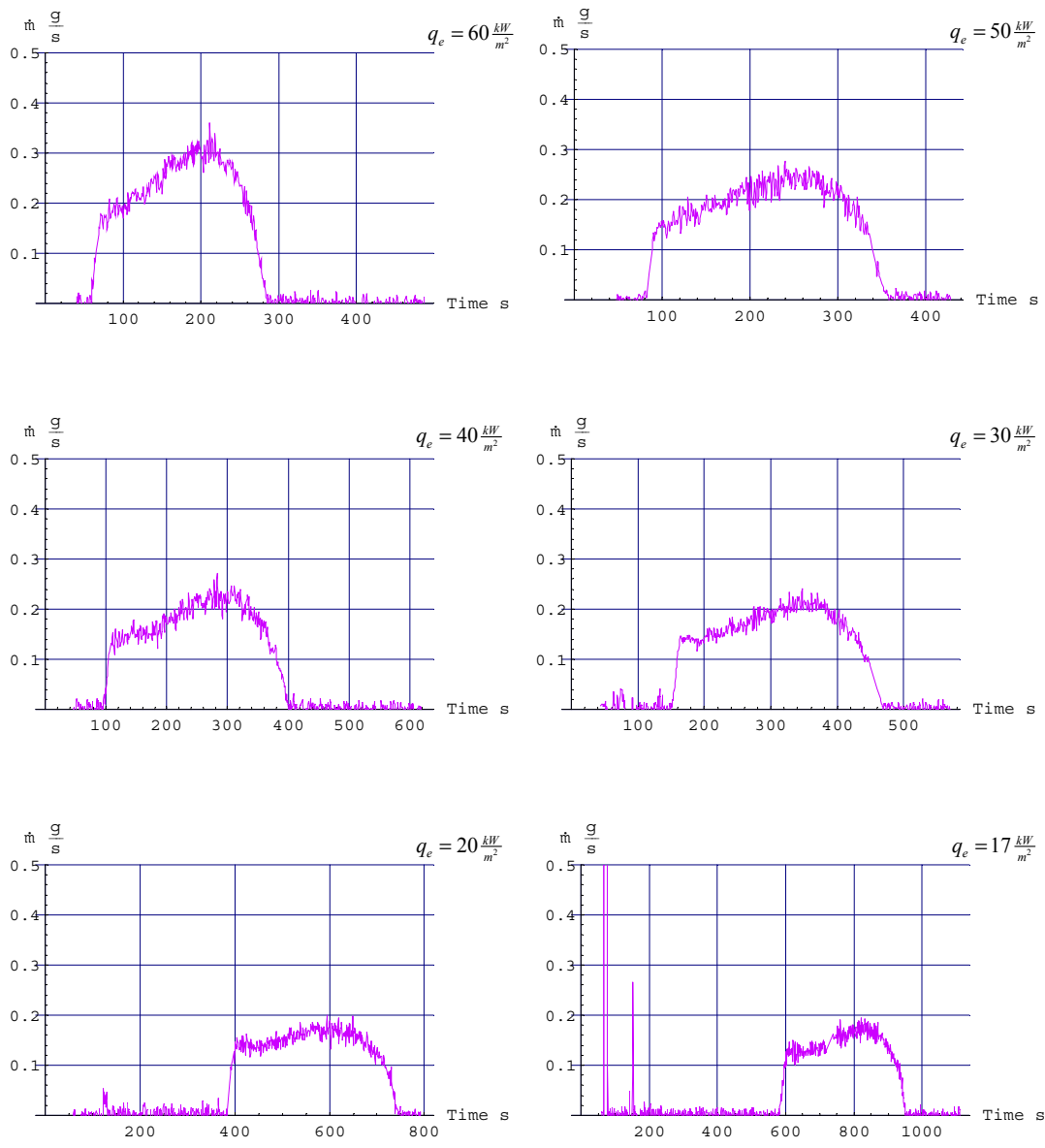


Figure B.1 (Mass loss rate results for HIPS)

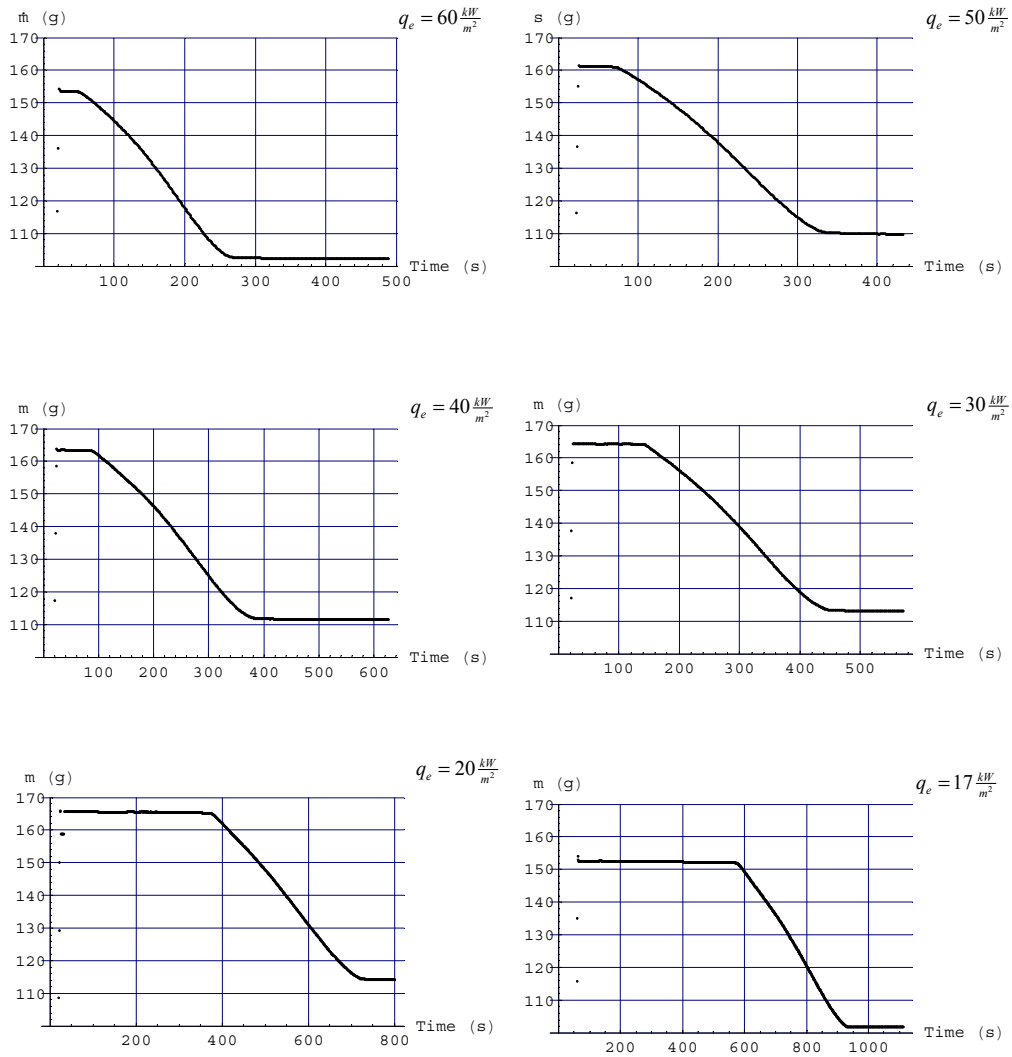


Figure B.2 (Mass loss results for HIPS)

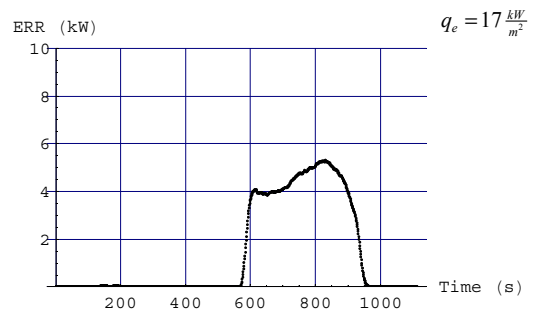
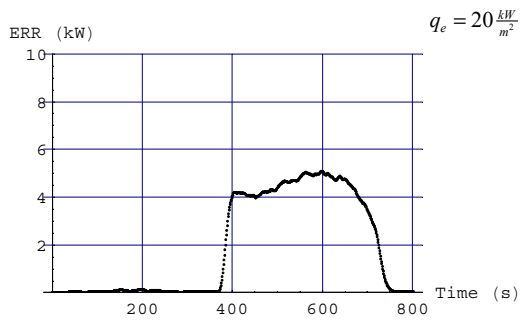
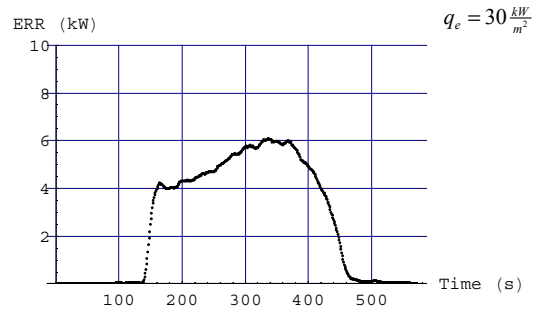
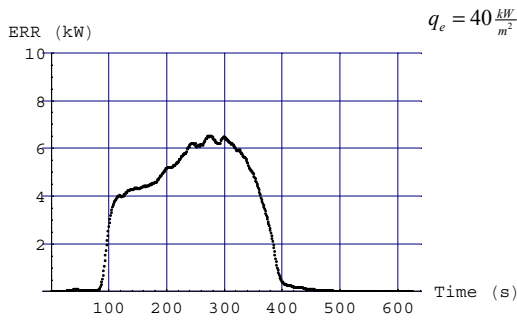
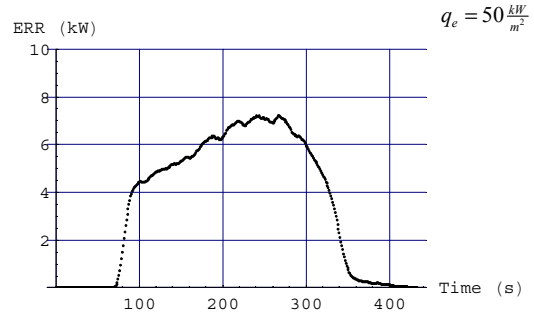
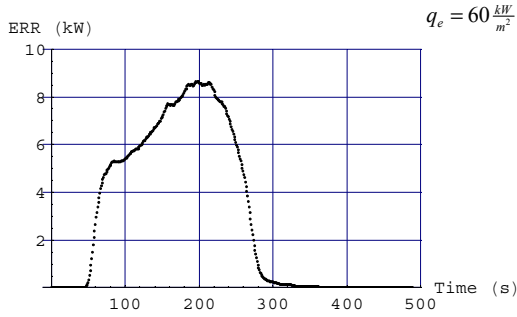


Figure B.3 (Energy Release Rate results for HIPS)

B.2 ABS

Data File Name	Heat Flux $\frac{kW}{m^2}$	Peak ERR $\frac{kW}{m^2}$	80% Peak ERR $\frac{kW}{m^2}$	Peak MLR $\frac{g}{m^2-s}$	80% Peak MLR $\frac{g}{m^2-s}$	Ignition Mass Flux $\frac{g}{m^2}$	Time to Ignition SEC	Heat of Combustion $\frac{kJ}{g}$	Critical Heat Flux $\frac{kW}{m^2}$
ABS forced_noHF.txt	0	503	459	22.9	17.4	-	forced	26.7	12
ABS8.txt	11	797	711	32.5	26.1	-	forced	28.8	
ABS7.txt	13	840	751	32.8	26.4	-	728	28.5	
ABS6.txt	14.8	816	776	35.3	27.3	-	544	28.6	
ABS9.txt	17	856	816	34.5	28.2	0.32	292	29.4	
ABS1.txt	19	962	882	40.3	32.4	2.4	208	28	
ABS2.txt	30	1134	1032	44.8	38	2.6	75	28.2	
ABS3.txt	40	1324	1173	49.3	41	7.7	46	28.1	
ABS4.txt	50	1463	1356	57.6	48.4	8.3	34	27.8	
ABS5.txt	60	1868	1640	72.4	56.5	9.5	26	27.3	

Table B.2 (ABS Results)

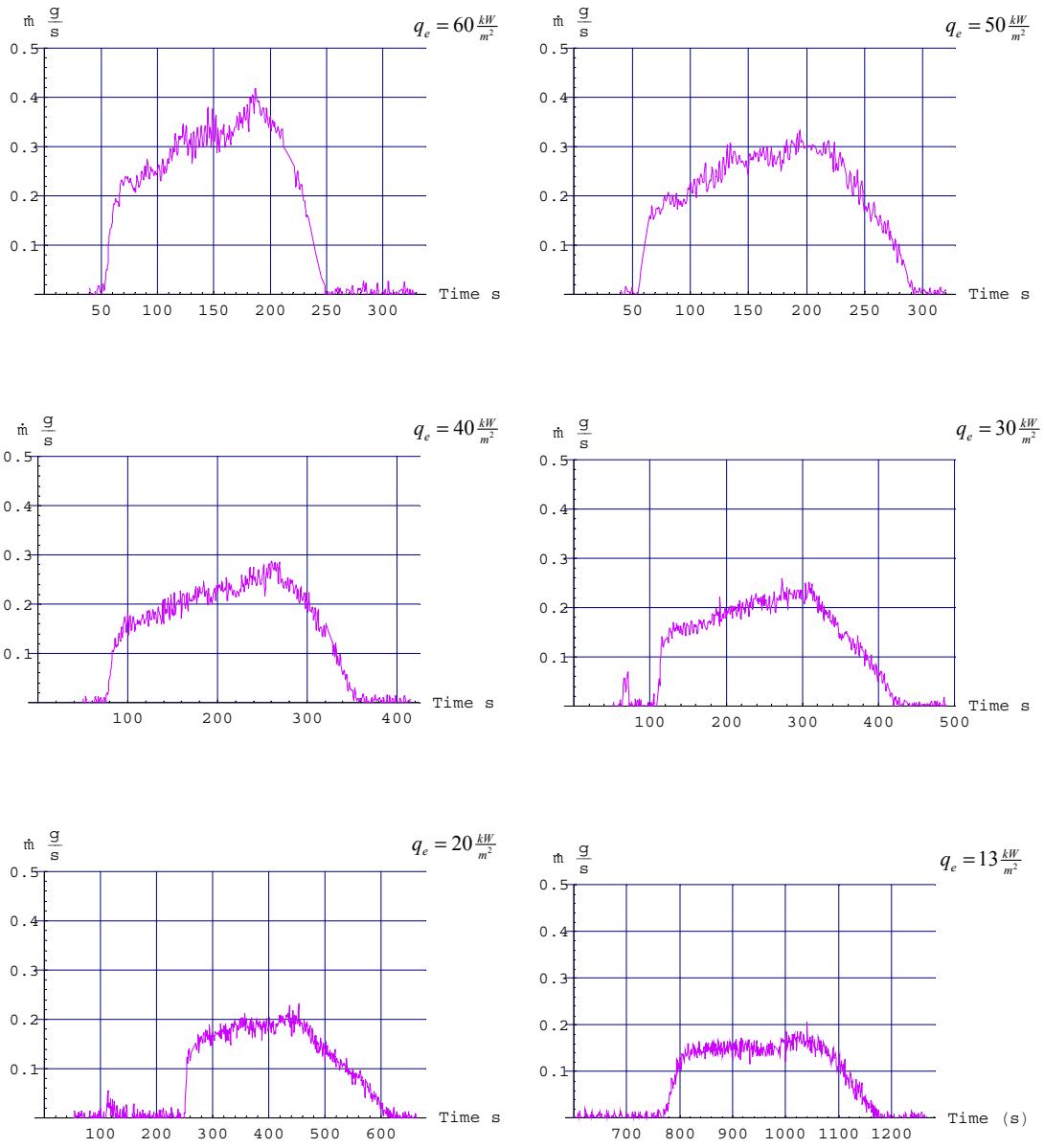


Figure B.4 (Mass loss rate results for ABS)

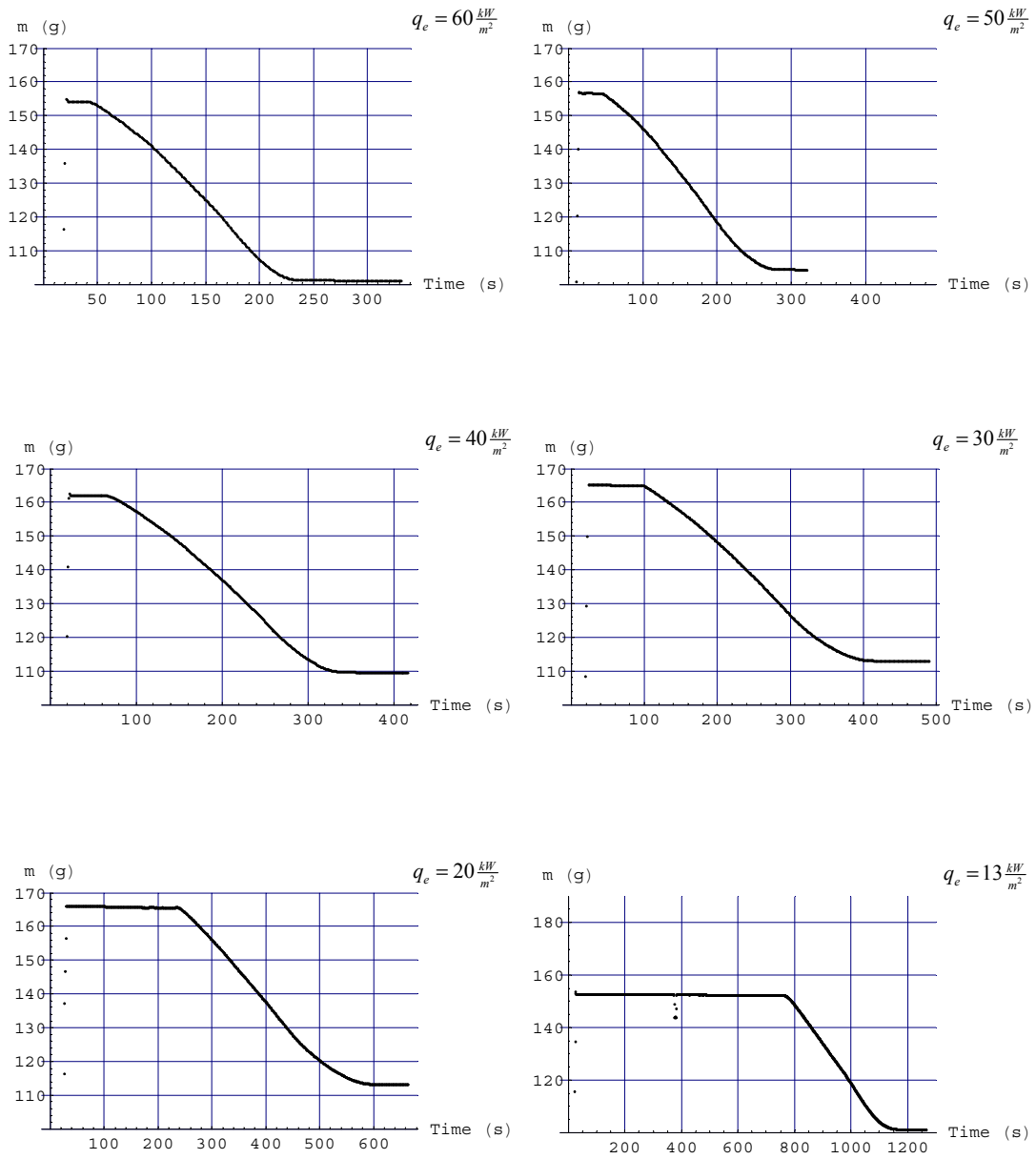


Figure B.5 (Mass loss results for ABS)

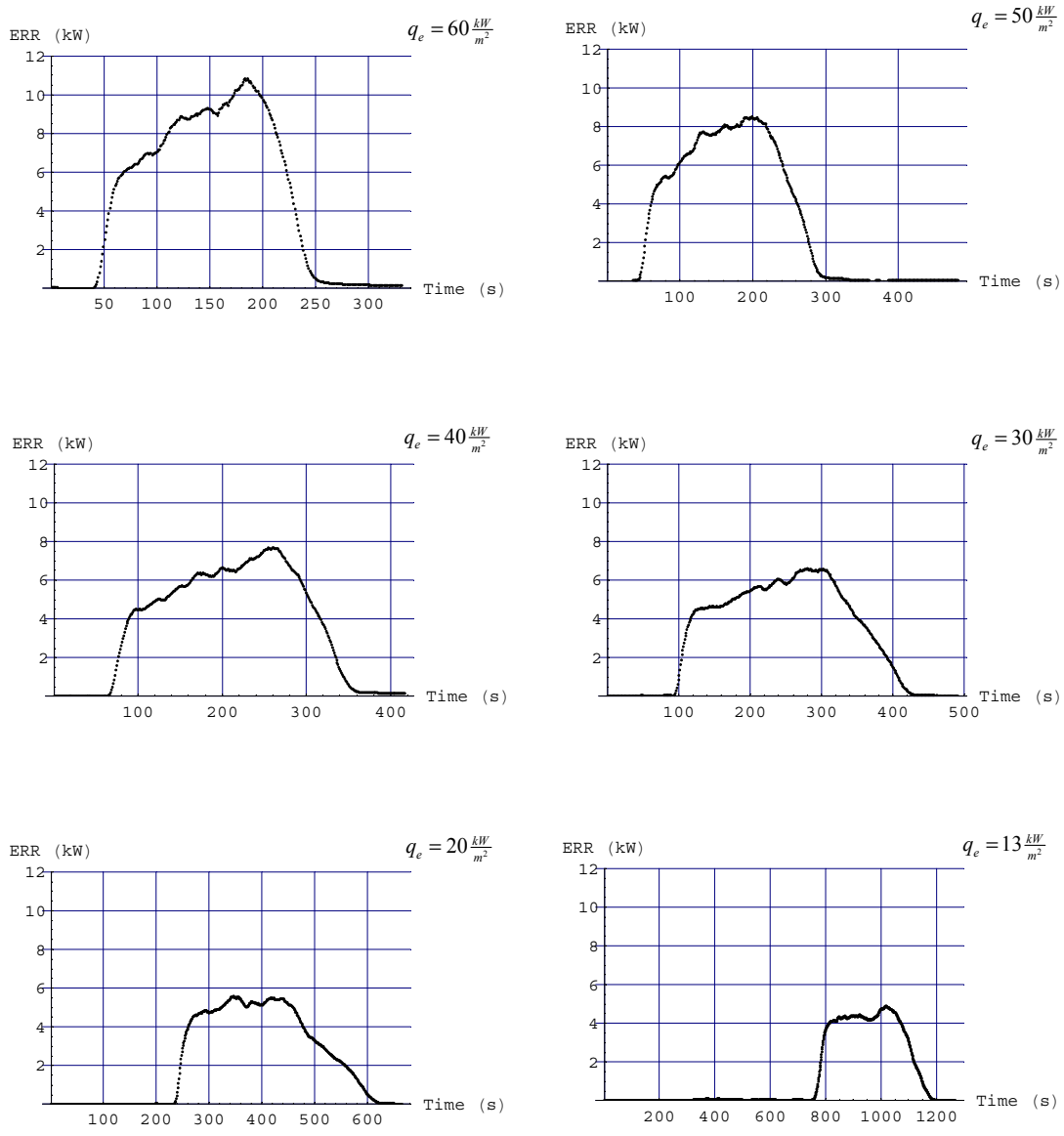


Figure B.6 (Energy Release Rate results for ABS)

B.3 HDPE

	Heat Flux	Peak ERR	80% Peak ERR	Peak MLR	80% Peak MLR	Time to Ignition	Heat of Combustion	Critical Heat Flux
Data File Name	$\frac{kW}{m^2}$	$\frac{kW}{m^2}$	$\frac{kW}{m^2}$	$\frac{g}{m^2-s}$	$\frac{g}{m^2-s}$	SEC	$\frac{kJ}{g}$	$\frac{kW}{m^2}$
HDPE7.txt	14.8	1125	1016	34.5	27.9	no ignition	36.4	16
HDPE6.txt	17	1116	1011	27.8	24.3	907	41.6	
HDPE1.txt	19	1250	1150	32.8	28.8	482	40	
HDPE2.txt	30	1625	1472	40.1	35.5	157	41.4	
HDPE3.txt	40	1819	1657	45.1	38.9	83	42.6	
HDPE4.txt	50	2021	1827	47.8	41.7	71	43.8	

Table B.3 (HDPE Results)

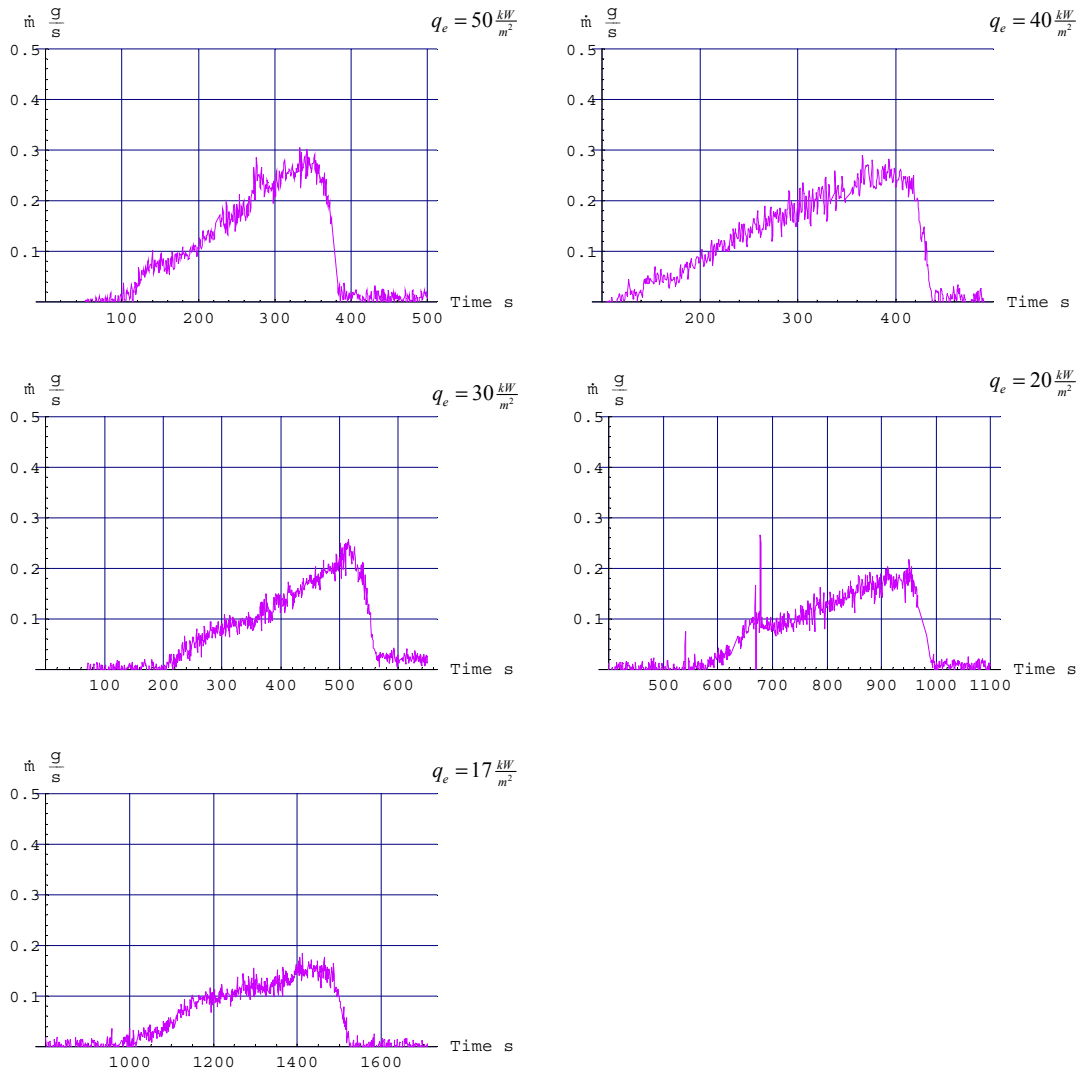


Figure B.7 (Mass Loss Rate results for HDPE)

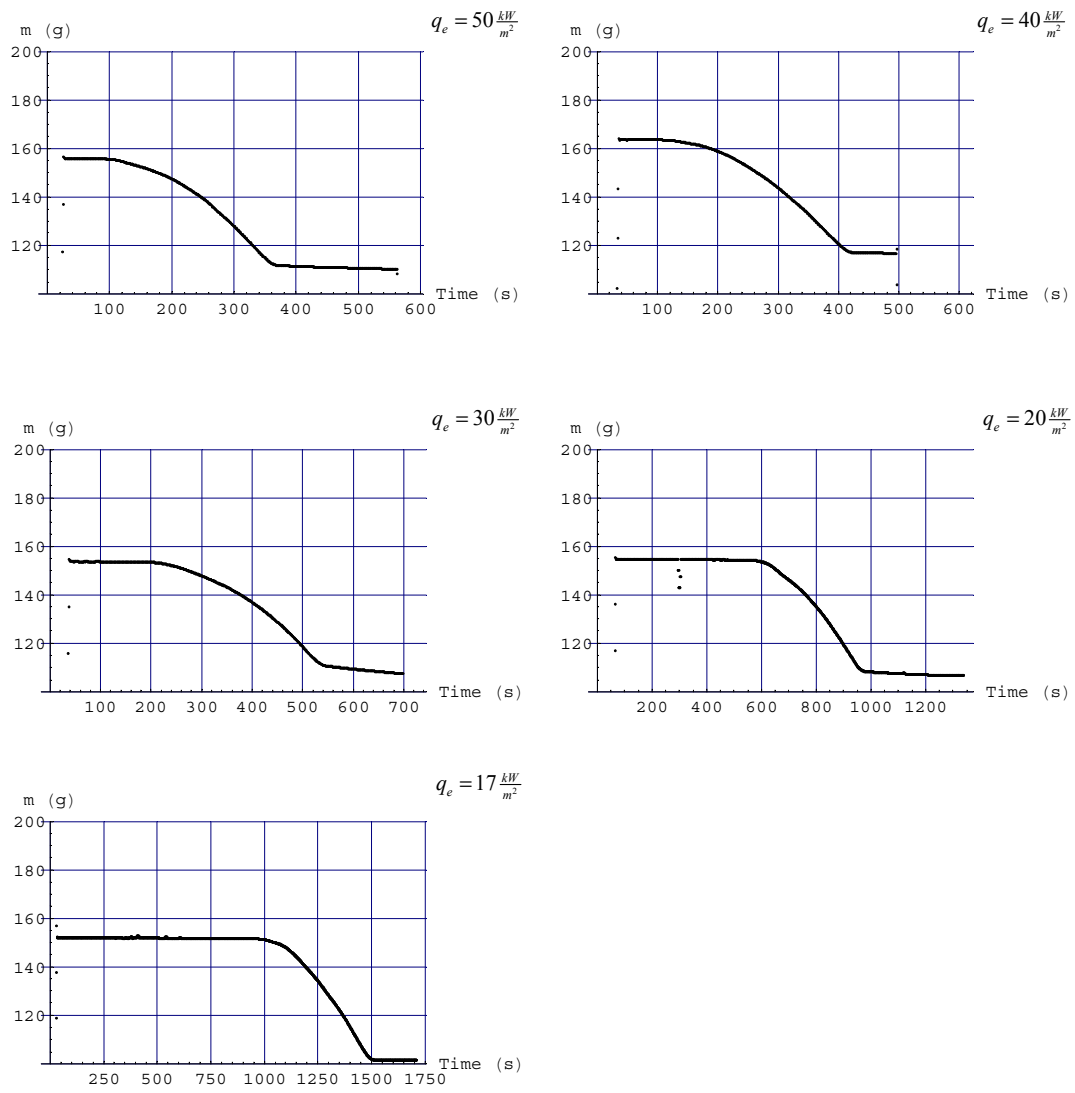


Figure B.8 (Mass Loss results for HDPE)

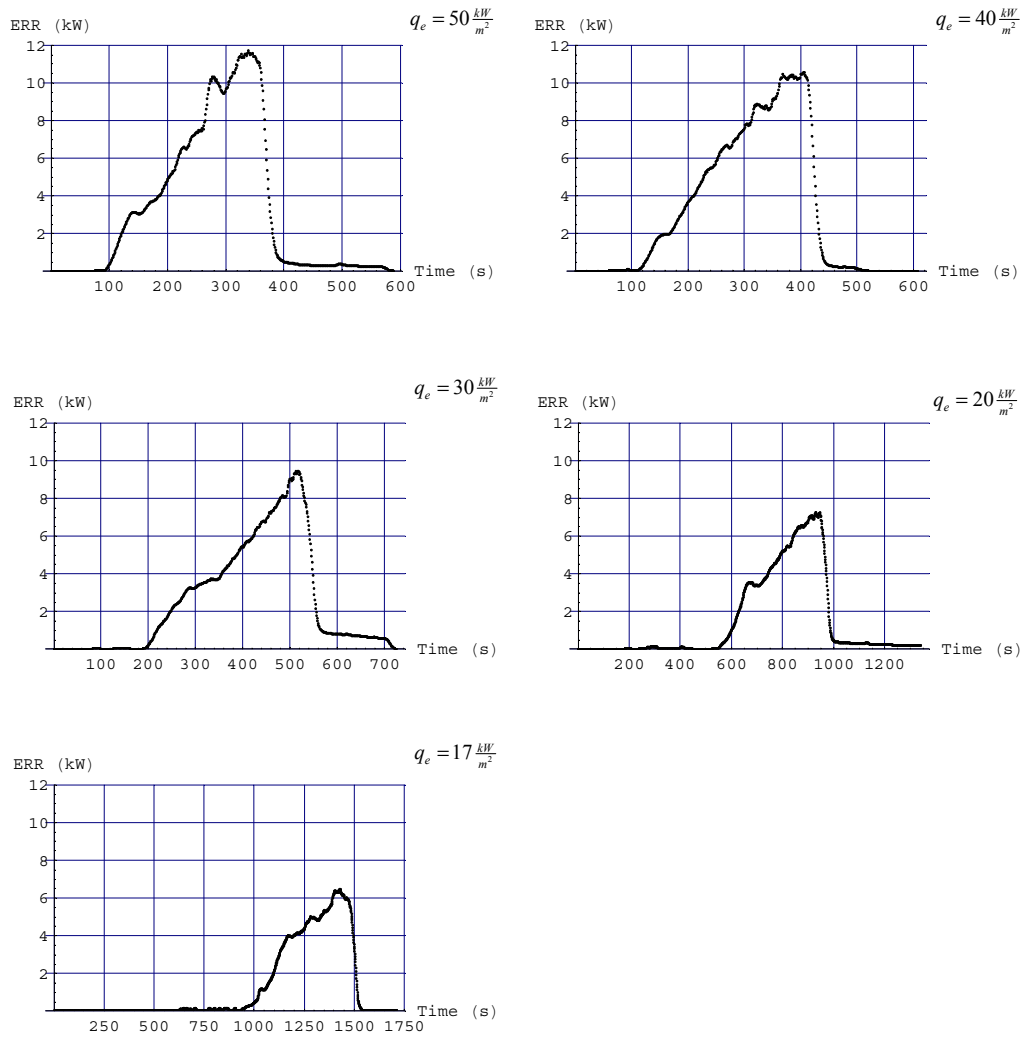


Figure B.9 (Energy Release Rate results for HDPE)

B.4 PC

Data File Name	Heat Flux $\frac{kW}{m^2}$	Peak ERR $\frac{kW}{m^2}$	80% Peak ERR $\frac{kW}{m^2}$	Peak MLR $\frac{g}{m^2-s}$	80% Peak MLR $\frac{g}{m^2-s}$	Time to Ignition SEC	Heat of Combustion $\frac{kJ}{g}$	Critical Heat Flux $\frac{kW}{m^2}$
Lexan1.txt	19					no ignition		28
Lexan6.txt	26					no ignition		
Lexan2.txt	30	597	540	31.4	28.3	300	19	
Lexan3.txt	40	601	529	33.2	27.4	177	19.3	
Lexan4.txt	50	725	642	39	32.8	125	19.5	
Lexan5.txt	60	657	603	36.6	32.3	70	18.7	

Table B4 (PC Results)

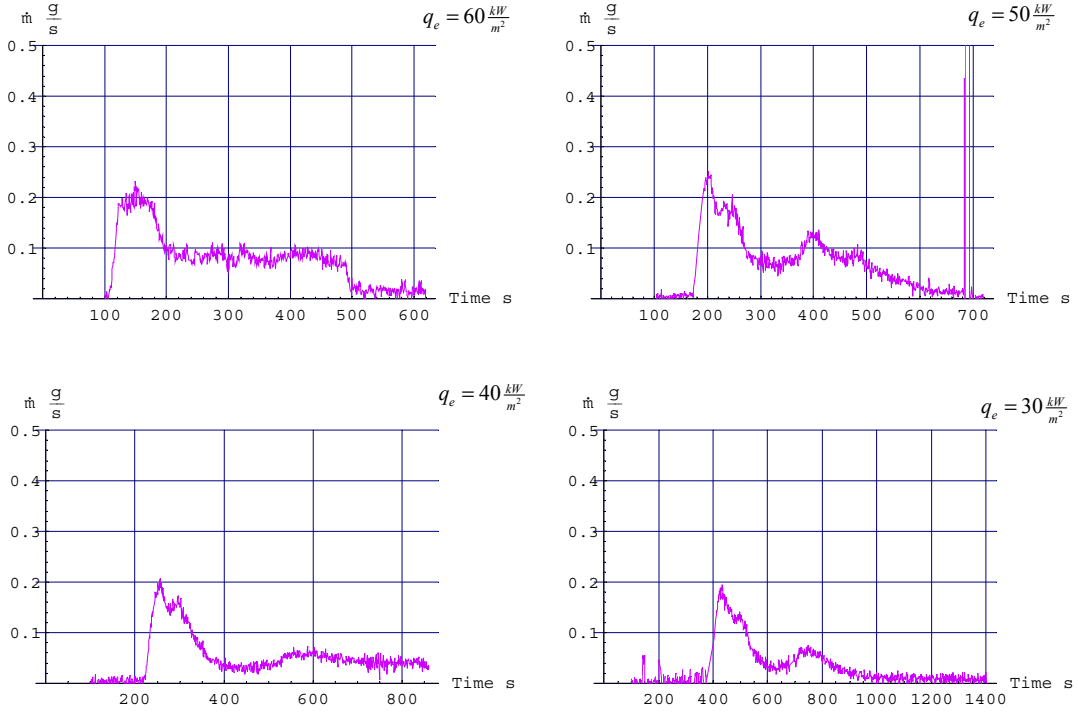


Figure B.10 (Mass Loss Rate results for PC)

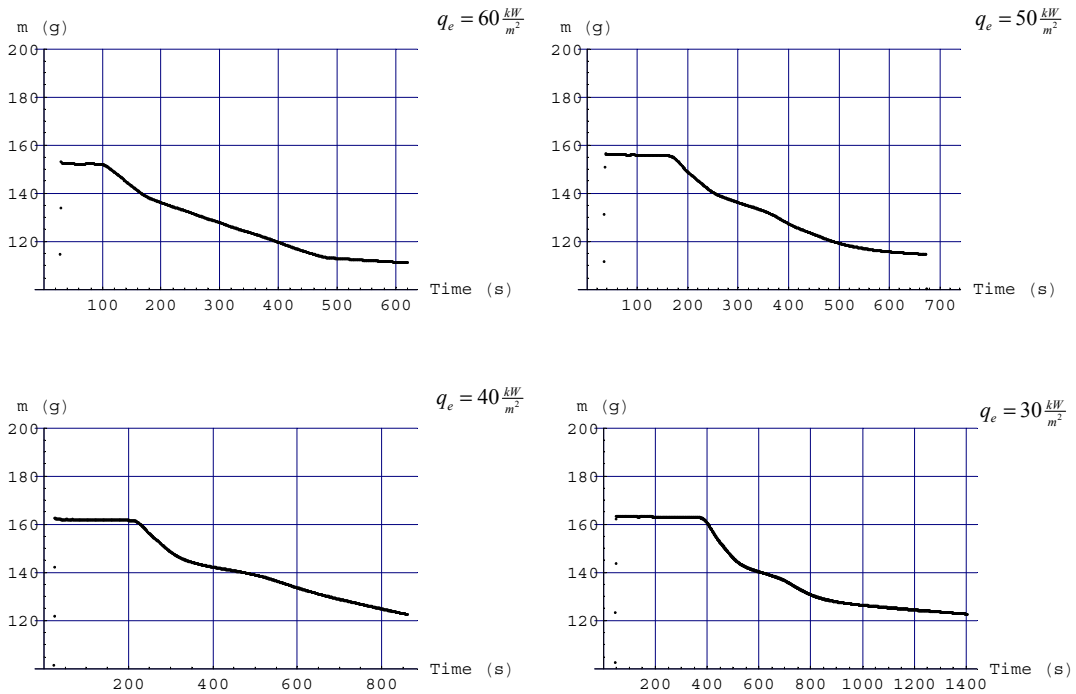


Figure B.11 (Mass Loss results for PC)

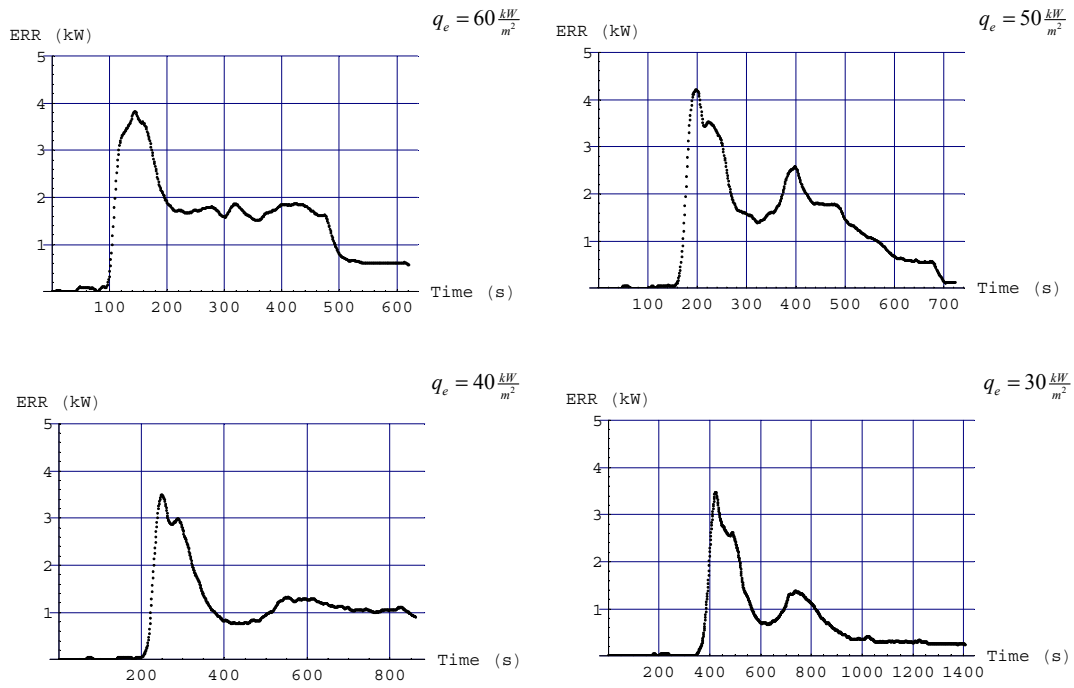


Figure B.12 (Energy Release Rate results for PC)

B.5 Nylon

Data File Name	Heat Flux $\frac{kW}{m^2}$	Peak ERR $\frac{kW}{m^2}$	80% Peak ERR $\frac{kW}{m^2}$	Peak MLR $\frac{g}{m^2-s}$	80% Peak MLR $\frac{g}{m^2-s}$	Time to Ignition SEC	Heat of Combustion $\frac{kJ}{g}$	Critical Heat Flux $\frac{kW}{m^2}$
Nylon6.txt	17					no ignition		18
Nylon1_1.txt	19	773	717	28.6	25	628	28.6	
Nylon1.txt	19	953	875	33.9	30.6	no ignition	28.6	
Nylon2.txt	30	1160	1057	42.4	36.7	372	28.8	
Nylon3.txt	40	1252	1123	43.4	38.5	140	29.2	
Nylon4.txt	50	1489	1369	52.6	46.1	86	29.7	
Nylon5.txt	60	1821	1672	58.8	55.2	51	30.3	

Table B5 (Nylon Results)

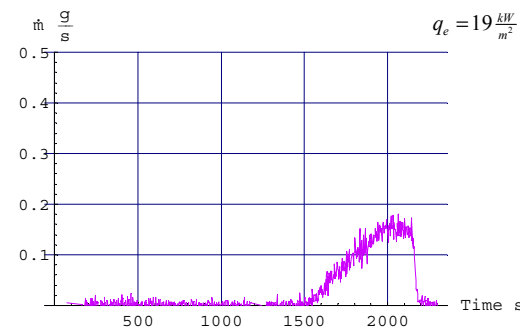
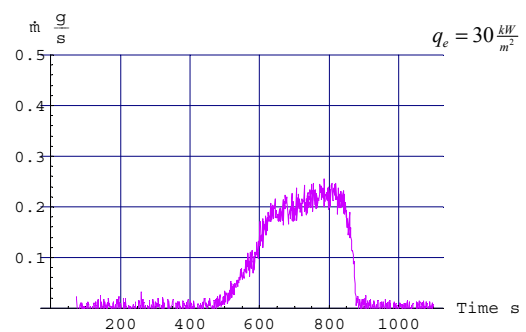
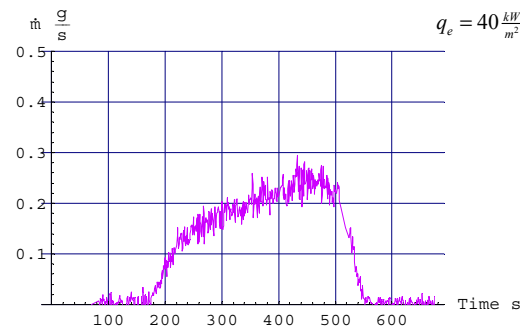
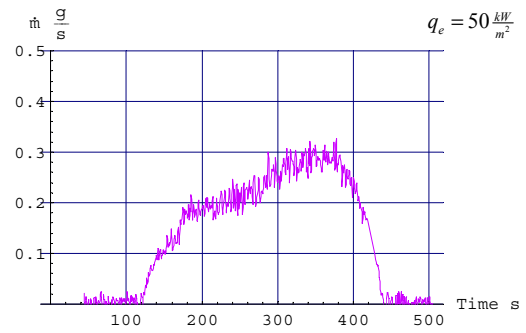
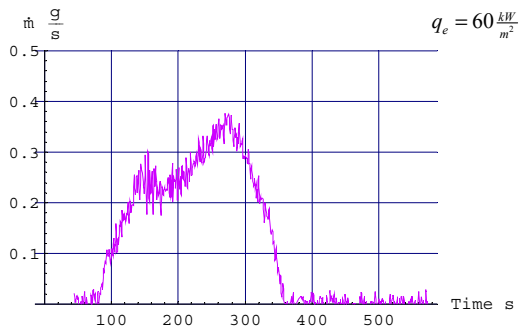


Figure B.13 (Mass Loss Rate results for Nylon)

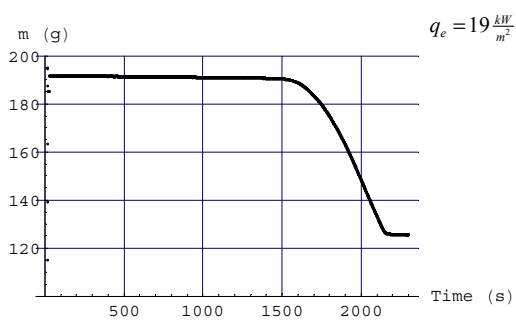
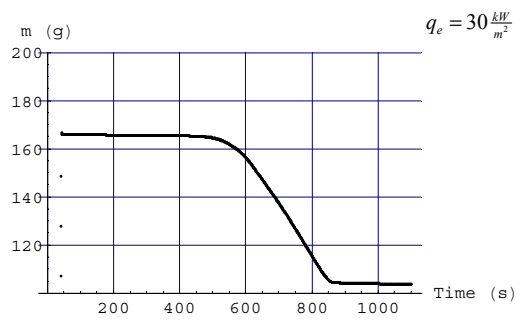
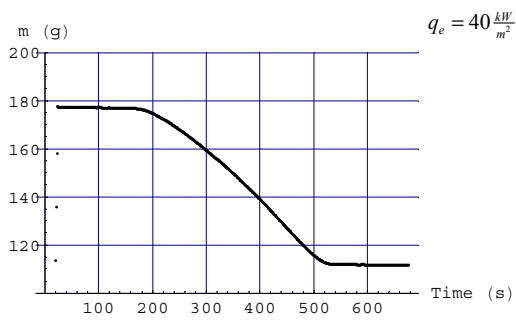
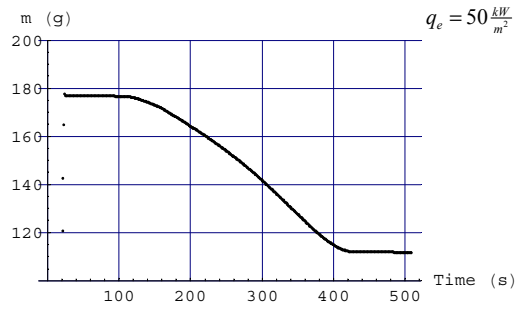
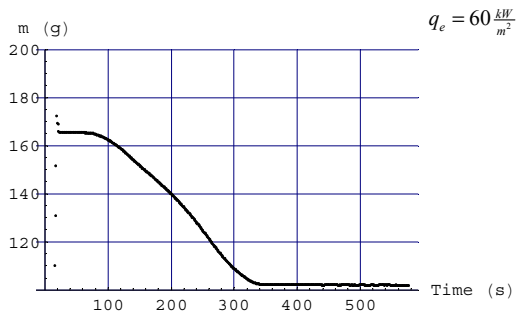


Figure B.14 (Mass Loss results for Nylon)

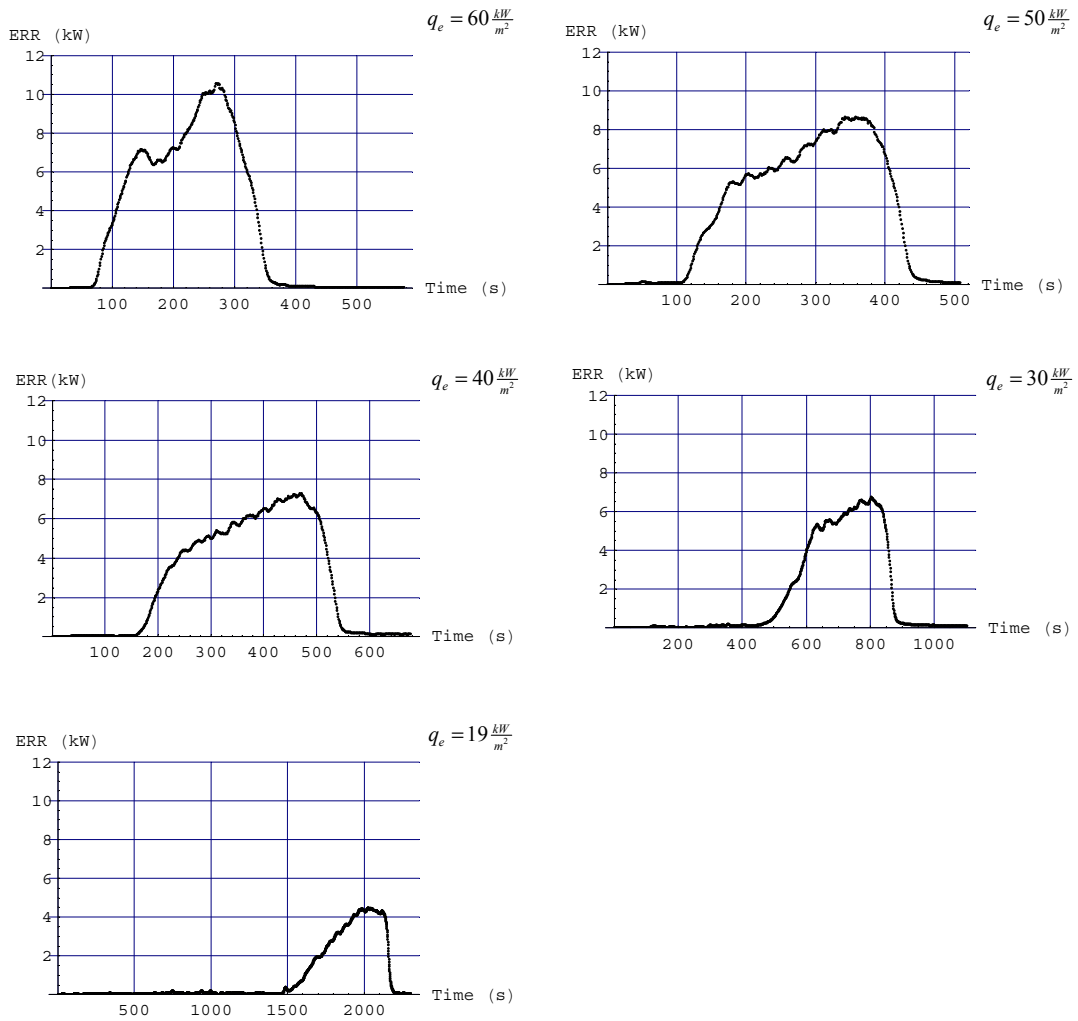


Figure B.15 (Energy Release Rate results for Nylon)

B.6 PMMA

Data File Name	Heat Flux $\frac{kW}{m^2}$	Peak ERR $\frac{kW}{m^2}$	80% Peak ERR $\frac{kW}{m^2}$	Peak MLR $\frac{g}{m^2-s}$	80% Peak MLR $\frac{g}{m^2-s}$	Ignition Mass Flux $\frac{g}{m^2}$	Time to Ignition SEC	Heat of Combustion $\frac{kJ}{g}$	Critical Heat Flux $\frac{kW}{m^2}$
PMMA_freeburn.txt	0	552	508	28.8	23		Forced	22.7	8
PMMA10.txt	10						1427		
PMMA9.txt	11	659	600	32.2	26.1		933	23.3	
PMMA8.txt	13	686	626	34.6	27.8		637	23.5	
PMMA7.txt	14.8	726	672		26		461	24.3	
PMMA6_6.txt	17	820	761	40.4	31.6		285	23	
PMMA6.txt	17	847	786	40.4	33.4	1.4	264	24.2	
PMMA1_1.txt	19	873	821	41	35.2	2.6	245	23.3	
PMMA1.txt	19	808	747	41	33.7		278	22.8	
PMMA2.txt	30	962	894	45.1	39.3	3.5	115	22.6	
PMMA3.txt	40	1131	1044	54.9	44.9	2.1	58	22.8	
PMMA4.txt	50	1306	1203	57.2	50.3	3.3	45	23.1	
PMMA5.txt	60	1635	1489	72.4	63.4	3.5	24	23.3	

Table B6 (PMMA Results)

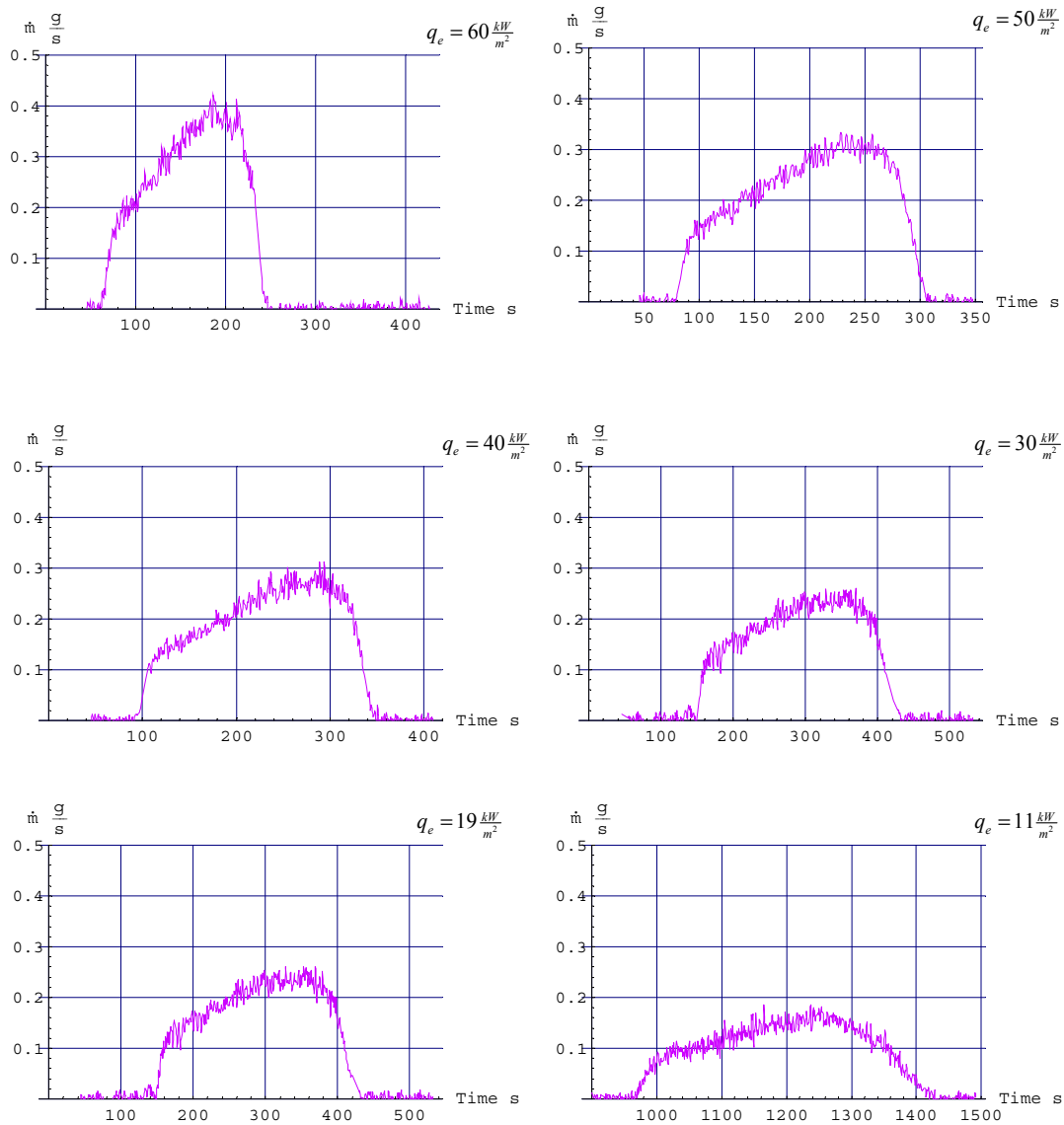


Figure B.16 (Mass Loss Rate results for PMMA)

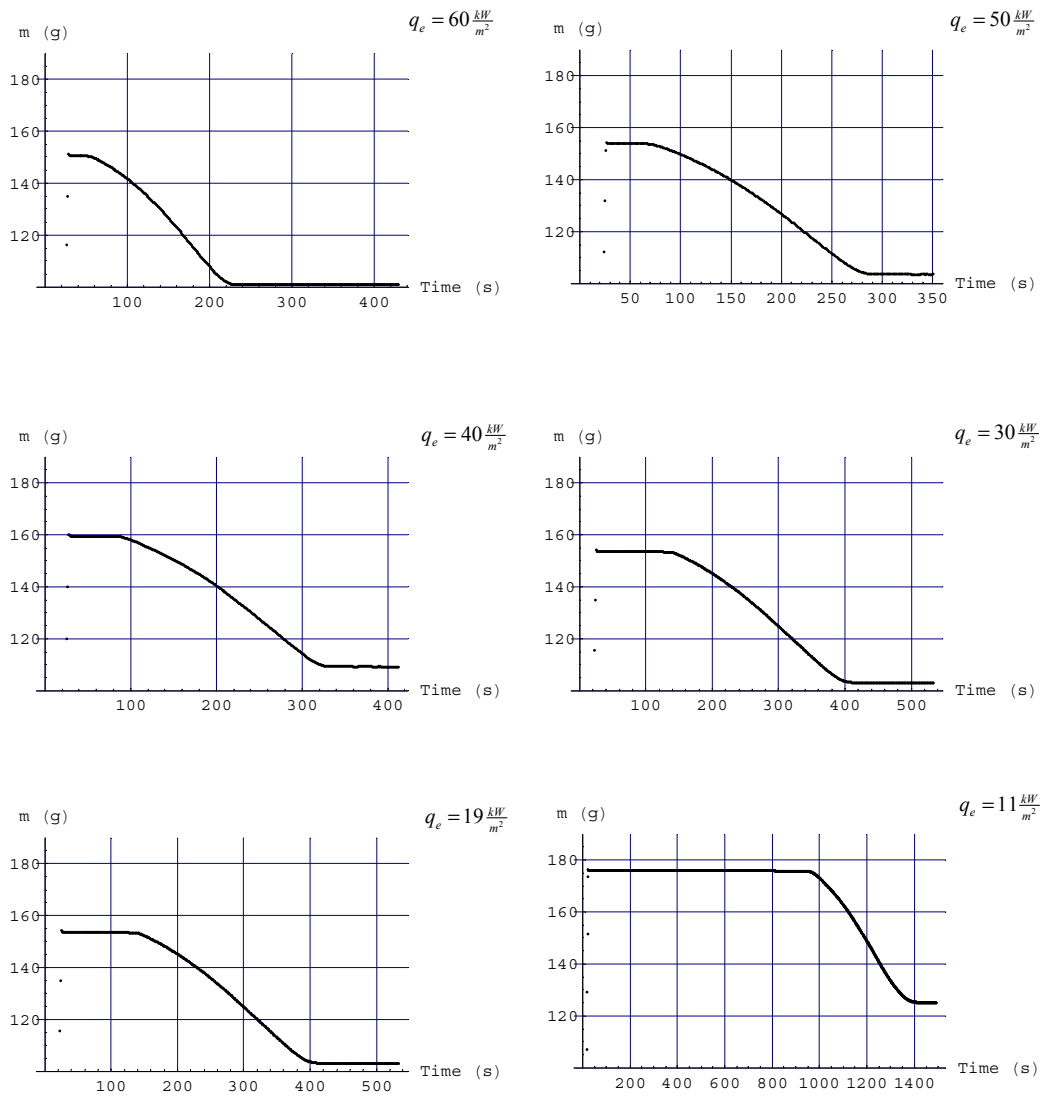


Figure B.17 (Mass Loss results for PMMA)

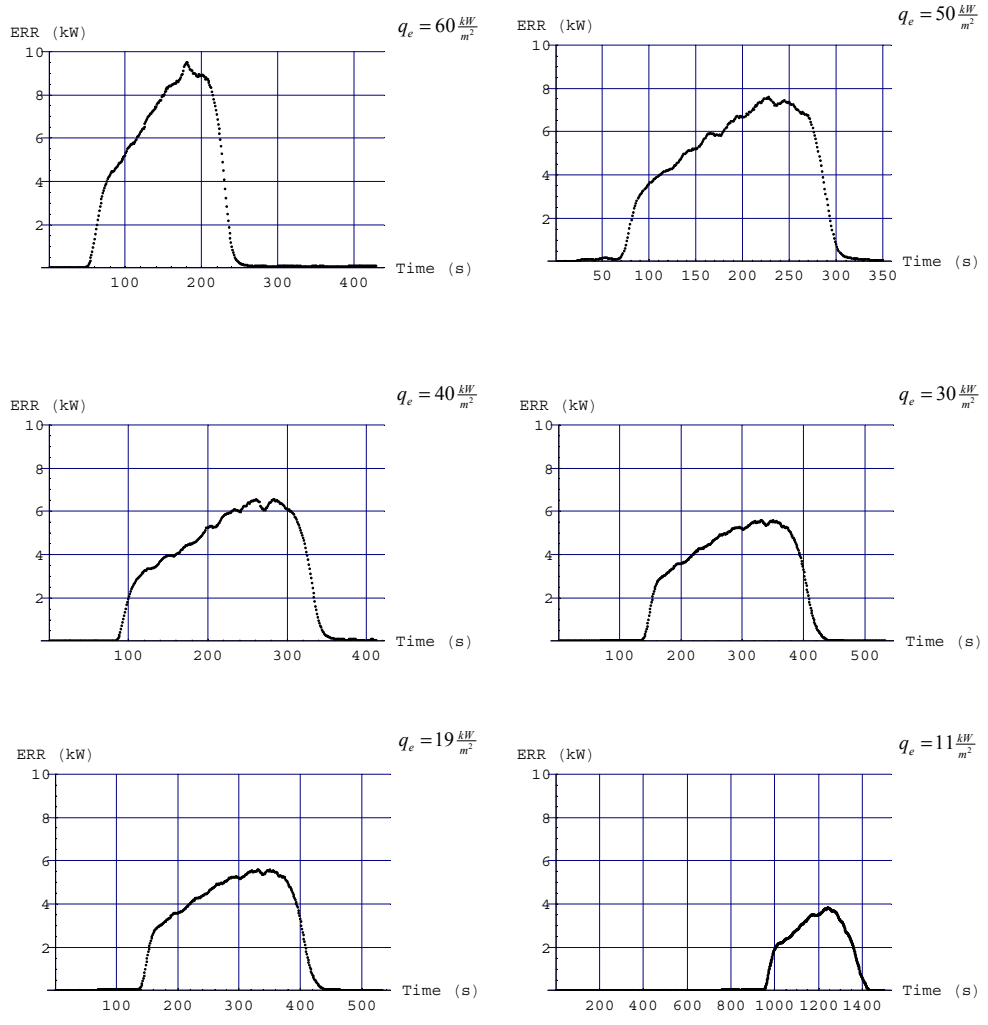


Figure B.18 (Energy Release Rate results for PMMA)

B.7 PVC

Data File Name	Heat Flux $\frac{kW}{m^2}$	Peak ERR $\frac{kW}{m^2}$	80% Peak ERR $\frac{kW}{m^2}$	Peak MLR $\frac{g}{m^2-s}$	80% Peak MLR $\frac{g}{m^2-s}$	Time to Ignition	Heat of Combustion $\frac{kJ}{g}$	Critical Heat Flux $\frac{kW}{m^2}$
PVC1.txt	19					no Ignition		20
PVC8.txt	21.3	64	60	10.9	5.5	690	8.27	
PVC7.txt	23.7	89	70	14	13	480	8.18	
PVC6.txt	26	118	75	13.9	9.7	300	7.8	
PVC2.txt	30	151	90	19.9	9.5	140	9.4	
PVC3.txt	40	194	116	22.9	11.4	65	10.24	
PVC4.txt	50	205	133	26.8	15	40	8.9	
PVC5.txt	60	260	191	41	22	30	8.5	

Table B.7 (PVC Results)

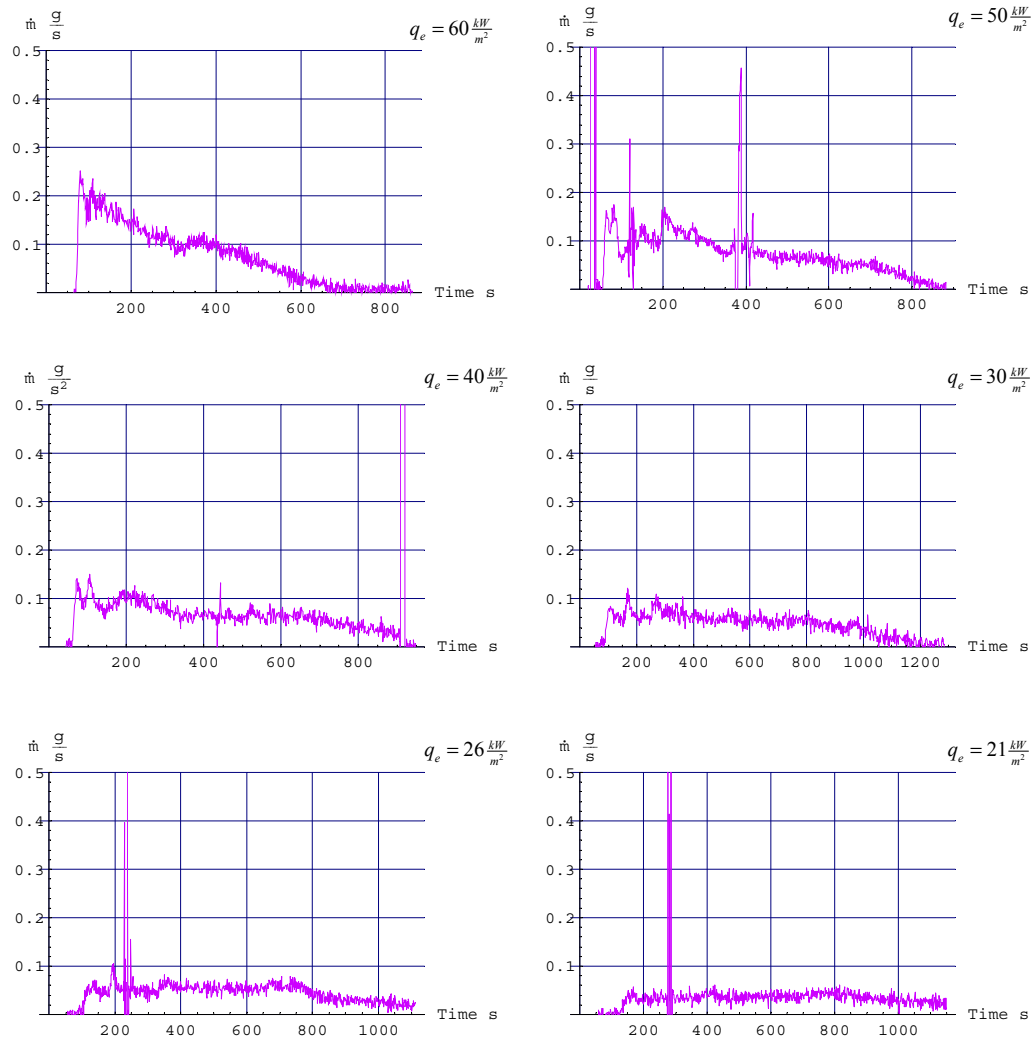


Figure B.19 (Mass Loss Rate results for PVC)

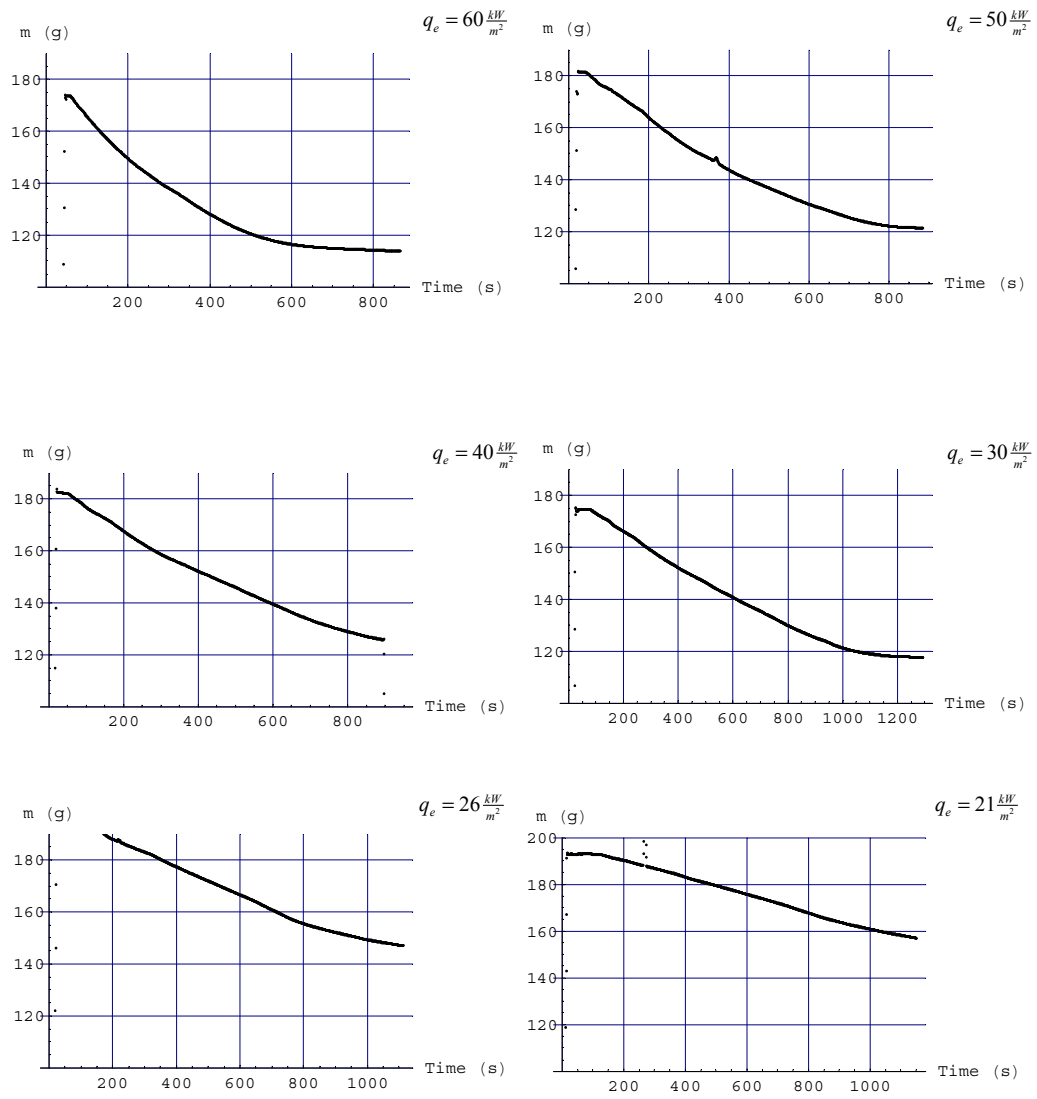


Figure B.20 (Mass Loss results for PVC)

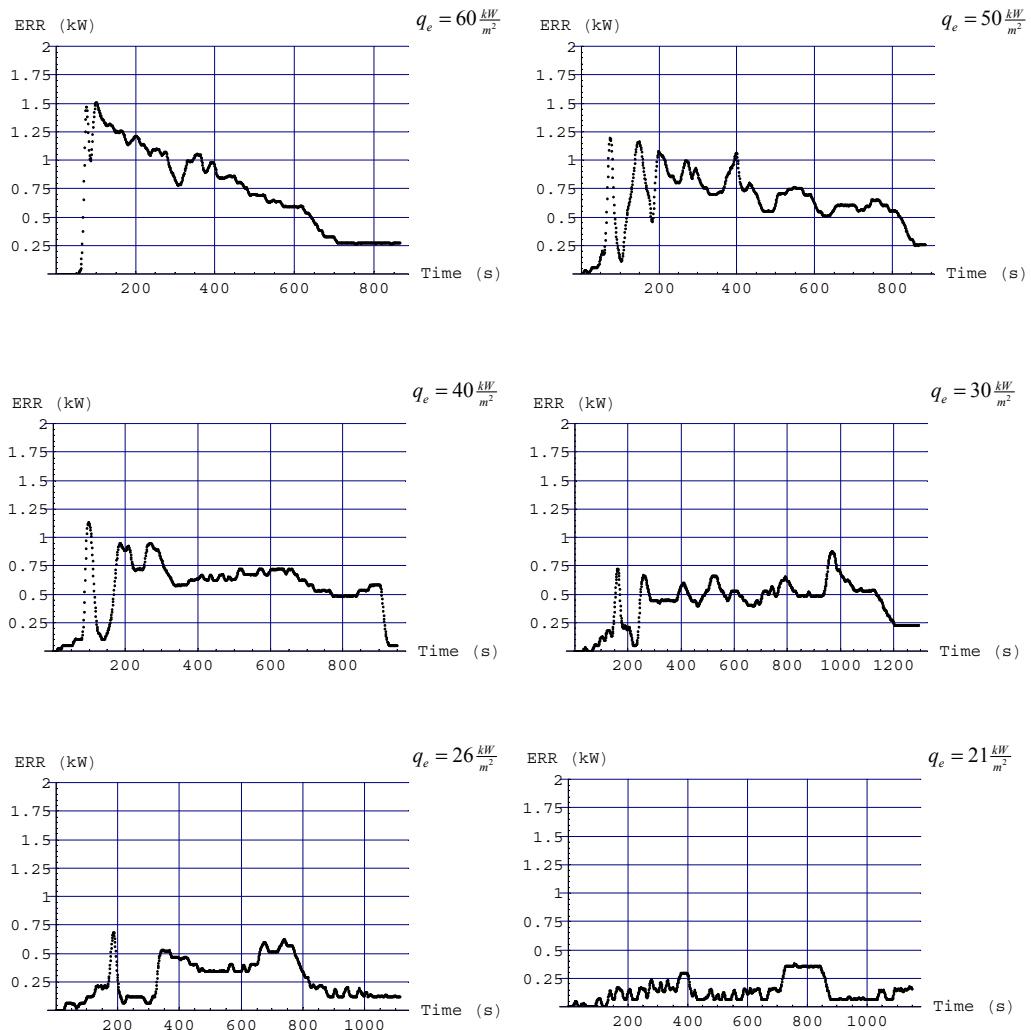


Figure B.21 (Energy Release Rate results for PVC)

B.7 POM

Data File Name	Heat Flux $\frac{kW}{m^2}$	Peak ERR $\frac{kW}{m^2}$	80% Peak ERR $\frac{kW}{m^2}$	Peak MLR $\frac{g}{m^2-s}$	80% Peak MLR $\frac{g}{m^2-s}$	Ignition Mass Flux $\frac{g}{m^2}$	Time to Ignition SEC	Heat of Combustion $\frac{kJ}{g}$	Critical Heat Flux $\frac{kW}{m^2}$
POM_freeburn.txt	0	281	254	22.6	19		forced	14.2	8
POM10.txt	10	350	315	32.8	23.6		1877	13.5	
POM9.txt	11	392	352	31	27.3		1081	13.5	
POM8.txt	13	352	318	30.2	24.5		770	13.6	
POM7.txt	14.8	295	267				668		
POM6.txt	17	393	357	34.2	27.2	0.4	308	13.7	
POM1.txt	19	386	351	32.2	26	2.7	210	13.6	
POM2.txt	30	455	414	38.5	31	1.5	105	13.4	
POM3.txt	40	470	432	40	32	2.5	63	13.3	
POM4.txt	50	571	506	47.5	38.5	0.8	37	13.6	
POM5.txt	60	703	640	57.1	47.2	3.3	32	13.4	

Table B.8 (POM Results)

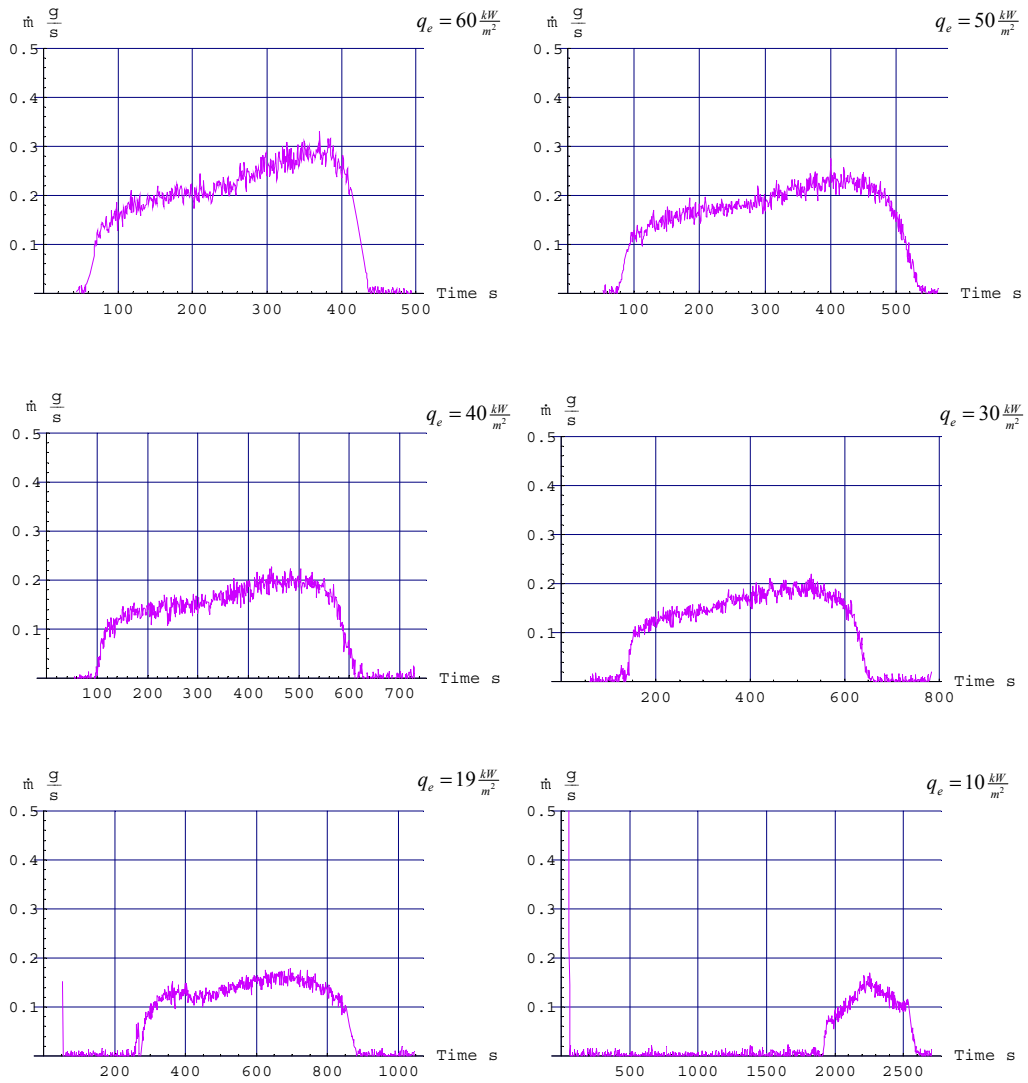


Figure B.22 (Mass Loss Rate results for POM)

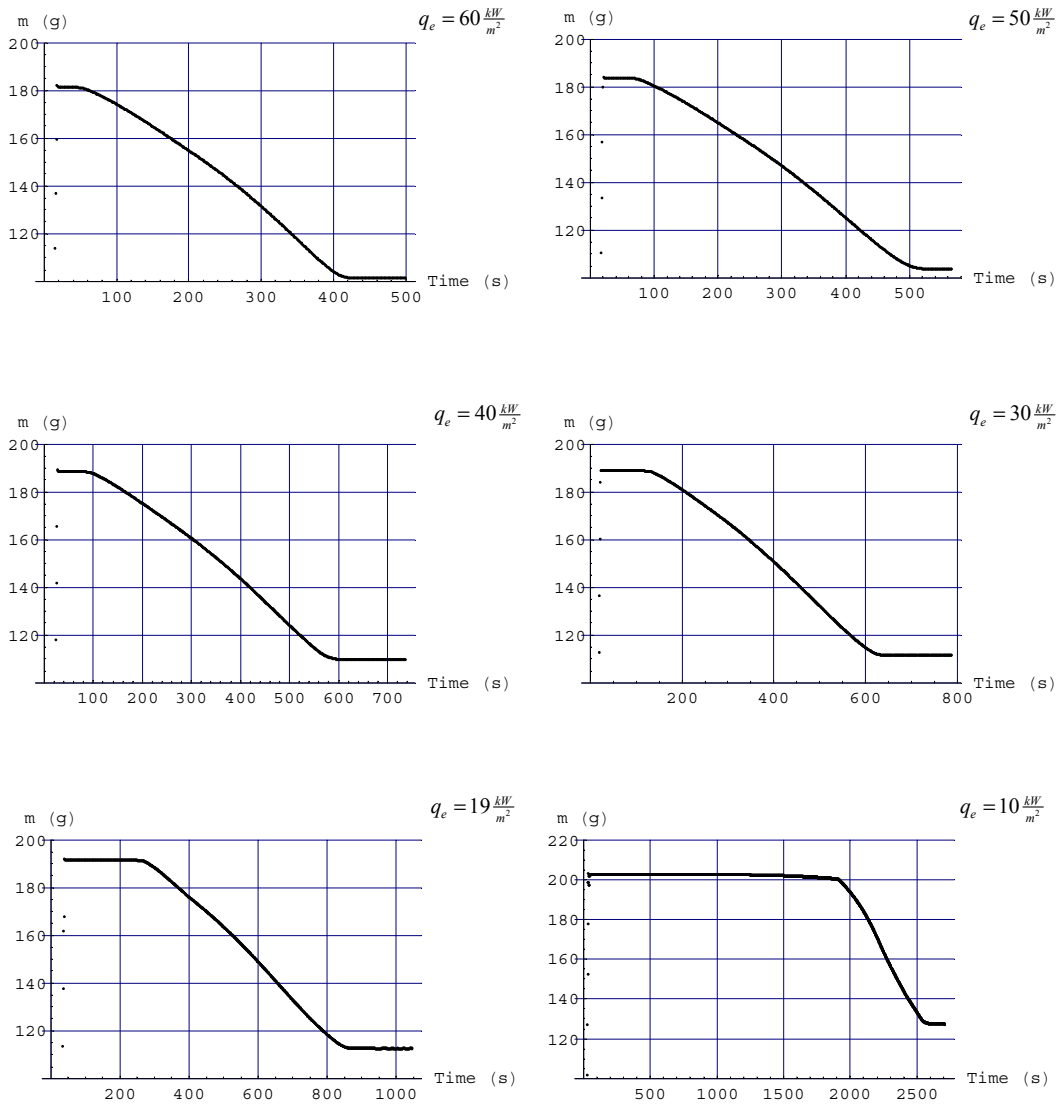


Figure B.23 (Mass Loss results for POM)

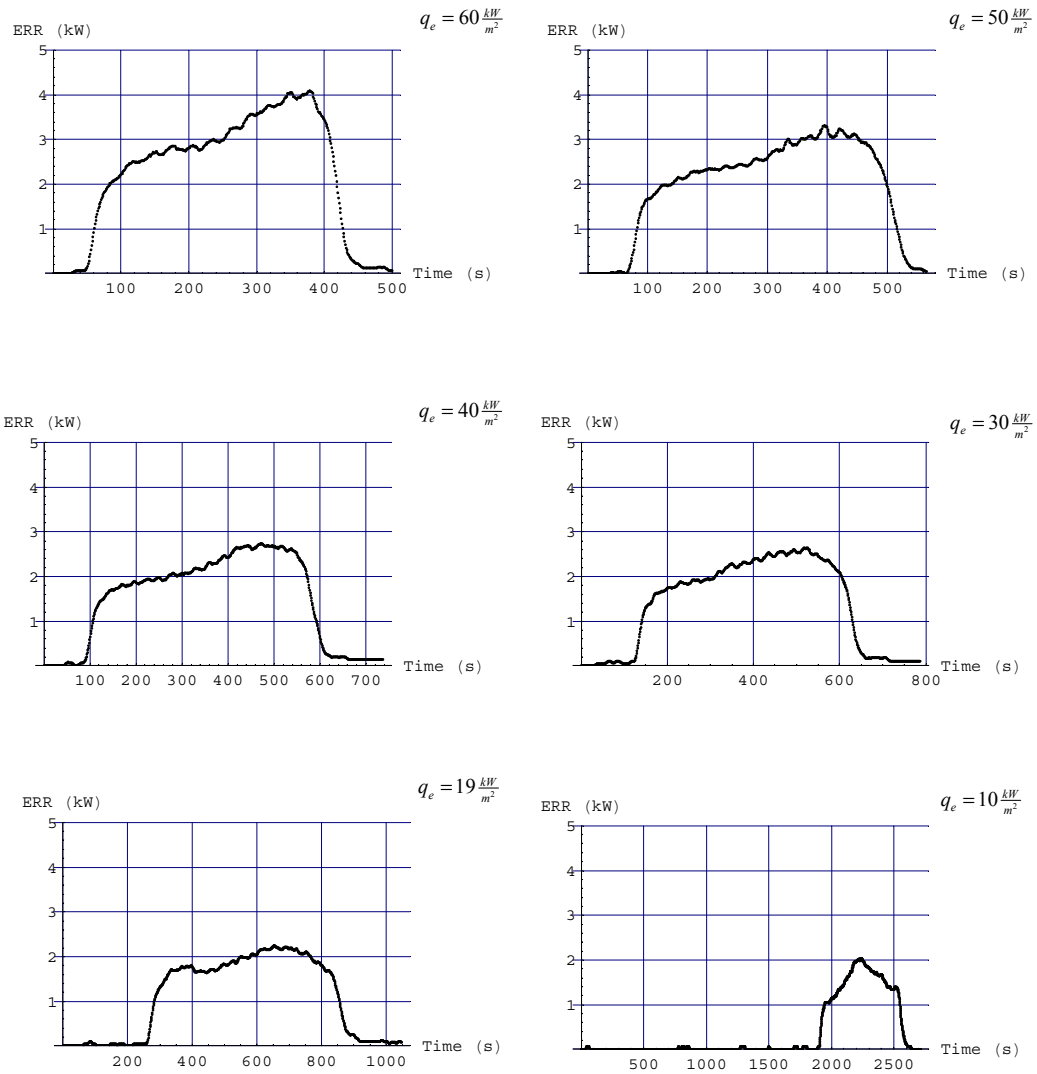


Figure B.24 (Energy Release Rate results for POM)

References

1. Aircraft Materials Fire Test Handbook, DOT/FAA/AR-00/12, Office of Aviation Research Washington, D.C. 20591, April 2002
2. Federal Railroad Administration, 49 CFR part 238 Passenger Equipment Safety Standards. Federal Register, Tuesday, June 25, 2002
3. Federal Transit Administration, Recommended Fire Safety Practices for Transit Bus and Van Materials Selection, Federal Register, Vol. 58, No. 201, Wednesday, October 20, 1993
4. Fire Test Procedures, International Maritime Organization, 1993 Edition
5. Federal Motor Vehicle Safety Standard (FMVSS) Part 571.302, Code of Federal Regulations, 49 Chapter V, October 1, 2003
6. ASTM E-162-98, Standard Test Method for Surface Flammability of Materials Using a Radiant Heat Energy Source, *Annual Book of ASTM Standards, 2003*
7. ASTM E-648-99, Standard Test Method for Critical Radiant Flux of Floor-Covering Systems Using a Radiant Heat Energy Source, *Annual Book of ASTM Standards, 2003*
8. ASTM E-1321-97a, Standard Test Method for Determining Material Ignition and Flame Spread Properties, *Annual Book of ASTM Standards, 2003*
9. ASTM E1354-90, *Standard Test Method for Heat and Visible Smoke Release Rates for Materials and Products Using an Oxygen Consumption Calorimeter*, in *Annual Book of ASTM Standards, 2003*
10. Archibald Tewarson, Generation of Heat and Chemical Compounds in Fires, in SFPE Handbook of Fire Protection Engineering, Section 3, 2nd Edition, 1995
11. Henry Margenau, G.M.M., The Mathematics of Physics and Chemistry
12. Archibald Tewarson, James G. Quintiere, David Purser, Fire Behavior of Materials in Vehicle Crash Fires and Survivability of the Passengers, SAE International, 2004
13. Richard E. Lyon, "Ignition Resistance of Plastics", Draft, 2003

14. Janssens, M., *Calorimetry*, in *SFPE Handbook of Fire Protection Engineering*
15. Marc Janssens, W.J.P., *Oxygen Consumption Calorimetry*, in *Heat Release in Fires*, V.B.a.S.J. Grayson, Editor, Elsevier Applied Science: London, New York.
16. FLOW EFFECTS ON THE FLAMMABILITY DIAGRAMS OF SOLID FUELS: MICROGRAVITY INFLUENCE ON IGNITION DELAY, J. L. Cordova¹, D. C. Walther¹, A. C. Fernandez-Pello¹, T. Steinhaus², J. L. Torero², J. G. Quintiere², and H. D. Ross³